# Coronary Flow Abnormalities in Hypertrophic Cardiomyopathy

Thesis submitted for the degree of *Doctor of Philosophy*

National Heart and Lung Institute

Imperial College London

**Dr Claire E Raphael, BSc (Hons), MA (Hons), MBBS, MRCP**

**CID:** 00324105

National Heart and Lung Institute

Royal Brompton and Harefield NHS Foundation Trust

Sydney Street, London

SW3 6NP

22th June 2016

*To Ee Ling, Sarah, Vass and Steven*

# CONTENTS

**Chapter 6:** Mechanisms of Myocardial Ischaemia in Hypertrophic Cardiomyopathy: Insights from Wave Intensity Analysis and Magnetic Resonance

## Statement of Originality

I declare that this thesis represents my own work except where referenced or acknowledged otherwise

## Copyright

## Acknowledgements

The last three years have been a rollercoaster of a ride and I have a huge number of people to thank who have helped support me and this project throughout this time. It has been extremely humbling to have been blessed with such a huge amount of love, support and academic support.

Firstly, I would like to thank my Primary Supervisor, Dr Sanjay Prasad. Sanjay, you have been a fantastic mentor and friend and have been a huge support to me during the last 3 years. You have helped me advance and become confident as a researcher and have brought out the best in me. I will forever be grateful for all that you have done for me.

I would like to thank Professor Dudley Pennell for his support, particularly while I was ill, excellent feedback on manuscripts and for the facilities of the NIHR Biomedical Research Unit which he made available for this project. Professor Darrel Francis has always been an inspiration to me and has taught me so much about academia and how to write a successful paper and I would like to thank him for his support, unique humour and inspiration.

This project could not have succeeded without the collaboration of Dr Rod Stables and Dr Rob Cooper at Liverpool Heart and Chest Hospital as part of the Imperial College Medical School Collaboration and Professor Carlo Di Mario, Dr Julian Collinson and Dr Ranil de Silva at the Royal Brompton. Recruitment of invasive patients with HCM who are willing to have lengthy research measurements would not have been possible without your help and time and that of the very generous catheter lab staff who went out of their way to be helpful, welcoming and patient in taking research measurements.

Professor Michael Frenneaux and Professor Alun Hughes have gone out of their way to support our work, coming over to the Brompton and taking time to give detailed review

of interim results and papers. I have been extremely lucky that they lent their scientific excellence and wealth of experience to this project.

Dr Justin Davies has been a great support, generously providing his custom program for wave intensity analysis, review of interim results and has been a great personal support in setting up future Fellowships and research collaborations.

Professor Kim Parker has been a real pleasure to work with, and his involvement has not only given me the opportunity to work with the inventor of wave intensity but also to be inspired by his lifelong love of learning, dedication and humour.

I would particularly like to thank Dr Jenny Keegan. Although she was not officially my supervisor, she has taken on that role through a lot of this manuscript, providing scientific review, encouragement and been a great role model as a successful female academic. It has been a real privilege to work with you.

I would like to thank Dr Peter Gatehouse who has taught me a lot about the physics of perfusion and a lot more about how to have scientific integrity and how to support and mentor students. Professor David Firmin has been a real pleasure to work with and learn from. I would also like to thank Dr Iain Pierce for his kind help with matlab and extraction of dicom files, something that would otherwise have taken me several months.

I would like to thank Rick Wage and Peter Drivas for all their hard work in acquiring the CMR data, keeping patients (and me) calm during 2 hour scans and for helping navigate the highly temperamental perfusion pump. Your support when things were hard and your encouragement mean more to me than you know.

I would also like to thank Dr Andrew Arai, Dr Li-Yueh Hsu and Anders Greve of the National Institutes of Health for their hard work and kind support for the perfusion work for this thesis. Their analyses are internationally recognized for their high quality and this is as a result of the huge amount of time and care they put into their work.

I would like to thank the British Heart Foundation who awarded the Fellowship which supported this work, the Wellcome Trust who provided the starter grant that allowed us to collect pilot data and the National Institute of Health Research for the Biomedical Research Unit, which has provided amazing facilities for this complex work.

My greatest thanks goes to the patients who took part in this study. They gave up their time and were extremely patient with the lengthy measurements we took. Without them, there would have been no thesis. Thank you so much for your kindness and generosity.

I would finally like to thank my fellow PhD students for their support, friendship and loyalty during the last 3 years. We have laughed together, cried together – and finally - succeeded together. I have been so lucky to have had such a fantastic group of friends that have made this process infinitely more enjoyable. I thank you for your friendship and look forward to many more years with you.

## Abstracts and Publications related to this Thesis

Raphael CE, Keegan J, Parker KH, Simpson R, Strain S, de Silva R, Di Mario C, Collinson J, Stables RH, Wage R, Sugathapala M, Prasad SK, Firmin D. Validation of high temporal resolution spiral phase velocity mapping of temporal patterns of left and right coronary artery blood flow against Doppler guidewire. *JCMR* 2015:17:85-91

Raphael CE, Cooper R, Parker KH, Collinson J, Vassiliou V, Pennell DJ, de Silva R, Hsu PhD LY, Greve AM, Nijjer S, Broyd C, Ali A, Keegan J, Francis DP, Davies JE, Hughes AD, Arai AE, Frenneaux M, Stables RH, Di Mario C, Prasad SK. Mechanisms of Myocardial Ischaemia in Hypertrophic Cardiomyopathy: Insights from Wave Intensity Analysis and Magnetic Resonance. Under review at *JACC*

Raphael CE, Cooper R, Parker KH, Collinson J, Vassiliou V, Pennell DJ, de Silva R, Hsu PhD LY, Greve AM, Nijjer S, Broyd C, Ali A, Keegan J, Francis DP, Davies JE, Hughes AD, Arai AE, Frenneaux M, Stables RH, Di Mario C, Prasad SK. Impact of left ventricular outflow tract obstruction and microcirculatory dysfunction on coronary haemodynamics in hypertrophic cardiomyopathy. ACC, San Diego, 2015

Raphael CE, Cooper R, Parker KH, Collinson J, Vassiliou V, Pennell DJ, de Silva R, Hsu PhD LY, Greve AM, Nijjer S, Broyd C, Ali A, Keegan J, Francis DP, Davies JE, Hughes AD, Arai AE, Frenneaux M, Stables RH, Di Mario C, Prasad SK. Wave intensity analysis and assessment of myocardial perfusion abnormalities in patients with hypertrophic cardiomyopathy, SCMR Nice, 2015.

Raphael CE, Mitchell F, Petryka J, Vassiliou V, Ali A, Pennell DP, Daubeney PE, Prasad SK. Use of cardiovascular magnetic resonance in measurement of left ventricular wall thicknesses in paediatric patients with known or suspected hypertrophic cardiomyopathy. ESC. Barcelona, August 2014

# Preamble

This thesis examines abnormalities in coronary flow in hypertrophic cardiomyopathy (HCM). I used wave intensity analysis of the coronary arteries and cardiovascular magnetic resonance to better understand the underlying mechanisms of abnormal coronary flow in HCM.

**Chapter 1** reviews the natural history of HCM, its key features, diagnosis and management priorities and options.

**Chapter 2** reviews the literature regarding myocardial perfusion and coronary flow abnormalities in hypertrophic cardiomyopathy and current understanding of the disease processes contributing to each of these.

**Chapter 3** is an overview of wave intensity analysis, the principles and underlying assumptions, application in the coronary arteries and impact of key studies in this area to advances in understanding of coronary physiology and myocardial mechanics.

**Chapter 4** provides a brief review of the role of CMR in HCM, its utility in diagnosis, tissue characterisation and quantification of myocardial perfusion.

**Chapter 5** is a description of the material and methods used in this thesis

For **Chapter 6**, I applied wave intensity analysis and myocardial perfusion analysis to HCM. I review the results and discuss the impact of these findings on contemporary understanding of perfusion abnormalities

**Chapter 7** documents the development of coronary flow velocity measurement using CMR, in-vivo testing and validation against the invasive gold standard

**Chapter 8** uses CMR derived coronary flow velocity and pressure measurements to develop CMR wave intensity analysis and tests it against invasive coronary flow velocity and pressure measurements in our cohort of patients.

# Abbreviations

| | |
|---|---|
| AS | aortic stenosis |
| ASA | alcohol septal ablation |
| ASH | asymmetrical septal hypertrophy |
| bSSFP | balanced steady state free precession |
| CBF | coronary blood flow |
| CFR | coronary flow reserve |
| CMR | cardiovascular magnetic resonance |
| CT | computerised tomography |
| CVR | coronary vasodilator reserve |
| EDV | end diastolic volume |
| EF | ejection fraction |
| ESV | end systolic volume |
| FE | fat-excitation |
| FPR | first-pass reserve index |
| GRE | gradient echo (a type of CMR sequence) |
| LAD | left anterior descending artery |
| LBBB | left bundle branch block |
| LGE | Late gadolinium enhancement |
| LMS | left main stem |
| LVEDP | left ventricular end diastolic pressure |
| LVH | left ventricular hypertrophy |

| | |
|---|---|
| LVOT | left ventricular outflow tract |
| HASTE | half-Fourier spin echo |
| HCM | hypertrophic cardiomyopathy |
| MBF | myocardial blood flow |
| MCE | myocardial contrast echocardiography |
| MPR | myocardial perfusion reserve |
| PET | positron emission tomography |
| PDV | peak diastolic velocity |
| PSV | peak systolic velocity |
| $R^2$ | coefficient of determination |
| RCA | right coronary artery |
| ROI | region of interest |
| SAM | systolic anterior motion of the mitral valve |
| SDD | standard deviation of the difference |
| SD | standard deviation |
| SPECT | Single Photon Emission Computed Tomography |
| SV | stroke volume |
| TE | echo time |
| TI | inversion time |
| TPDV | time to peak diastolic velocity |
| TPSV | time to peak systolic velocity |
| TR | repeat time |
| VTI | velocity time integral |
| WIA | wave intensity analysis |

# List of Tables

# List of Figures

**Figure 1.4**: Small vessel disease in HCM. Left panel – dysplastic small vessel with no surrounding fibrosis. Right panel – small vessel disease with extensive adjacent fibrosis (Varnava *et al.* 2000).

**Figure 1.5**: ESC guidelines for risk stratification in HCM: Patients should be risk stratified for potential of sudden cardiac death and this value used to help the clinician decide whether the patient should be offered an implantable cardioverter defibrillator (ICD).

**Figure 2.1**: Microcirculatory disease in hypertrophic cardiomyopathy. (A) Native heart of a patient with HCM demonstrating areas of macroscopic scarring (arrowed). (B) Cross sectional preparation of an intramural coronary artery showing thickening of the intimal and medial layers of the vessel. (C) Myocardial specimen from a patient with HCM demonstrating multiple abnormal intramural coronary arteries and scarring of the myocardium (original magnification x55). (reproduced from (Camici *et al.* 2012)

**Figure 2.2:** The coronary microcirculation in a healthy heart. While the epicardial coronary arteries are well studied at the time of diagnostic coronary angiography, the majority of the blood vessels in the heart are comprised of the microcirculation (Herrmann et al. 2012).

**Figure 2.3**: Schematic representation of the sequential decrease in coronary perfusion pressure in a physiological heart. The greatest drop in perfusion pressure occurs across the coronary resistance arterioles (Dimitrow *et al.* 2005).

**Figure 2.4**: Left ventricular pressure during two complete cardiac cycles. The pressure changes from approximately 5-15mmHg (the end diastolic pressure) up to 120-140mmHg (the peak systolic pressure) in a healthy heart.

**Figure 2.5**: As the myocardium contracts, individual myocytes shorten and increase in diameter, causing compression of the intramyocardial vasculature.

**Figure 3.1**: A complex pressure waveform may be decomposed by Fourier analysis (left panel) or wave intensity analysis (right panel). In Fourier analysis, the wave is decomposed into sinusoidal wavetrains, whereas in wave intensity, successive wavefronts are described over time.

**Figure 3.2**: Effects of compression and expansion on waves travelling along a "slinky" spring. Energy may be transmitted even though each end of the spring remains stationary

**Figure 3.3:** Wave intensity throughout the cardiac cycle in a normal patient. The top graph shows the separated (black outline) and net wave intensity (filled shapes) for a cardiac cycle. The bottom panel displays the pressure and coronary flow velocity curves over time that were used to derive the wave intensity data.

**Figure 3.4** Wave intensity analysis in the healthy heart. There are 6 principal waves that occur sequentially during the cardiac cycle and which result in acceleration or deceleration of coronary flow within the coronary arteries.

**Figure 3.5** Schematic representation of coronary waves underlying the changes in coronary filling, taken from Davies 2006a

**Figure 3.6:** Effect of left ventricular hypertrophy on coronary WIA: there is attenuation of the BEW due to impaired myocardial relaxation.

**Figure 3.7**: The action of the main waves on coronary flow. During systole, the forward compression and backward compression waves act in opposing directions. During diastole, the BEW acts to accelerate blood flow in the coronary arteries

**Figure 3.8:** Comparison of coronary wave intensity in a patient with a normal heart and in a patient with severe aortic stenosis. In aortic stenosis, the forward travelling pushing wave (B) and backward travelling suction wave (E) are attenuated and there is an

increased backward travelling decompression wave (C) due to microcirculatory compression and increased LV cavity pressures

**Figure 3.9**: Wave intensity in the aorta is comprised of three predominant waves: the forward compression wave, the backward compression wave and the forward expansion wave.

**Figure 4.1**: Cardiovascular magnetic resonance imaging of the heart in HCM (left and middle panels) and of a normal heart (right panels). In HCM, the left ventricle becomes thickened. Late gadolinium imaging (middle panels) demonstrate scarring of the ventricle (white areas).

**Figure 4.2**: Visual analysis of myocardial perfusion using CMR. The heart is imaged at three short axis levels, base (left panel), mid ventricle (middle panel) and apex (right panel). Images are recorded at rest (bottom row) and with peak adenosine stress perfusion (top row). Abnormalities of perfusion are often revealed at peak adenosine stress perfusion. These abnormalities appear as a darker area of the myocardium (arrowed).

**Figure 5.1**: The Combowire system: A pressure and flow transducer is present on the tip of a steerable guidewire, allowing intracoronary measurements (taken from Volcano website).

**Figure 5.2**: Use of the Doppler flowire for assessment of coronary flow velocity

**Figure 5.3**: Although the wire position may move slightly during data acquisition, the wide sampling volume of the Doppler flowire tip will typically continue to record an accurate flow velocity profile

**Figure 5.4**: How to measure the LVEDP. The aortic valve is crossed, typically with a pigtail catheter through the aortic valve and then positioned into the left ventricle such that the pressure trace is stable and the catheter does not induce rhythm abnormalities

**Figure 5.5**: Siemans Skyra 3T scanner in the Cardiovascular Biomedical Research Unit at the Royal Brompton Hospital.

**Figure 5.6** Localisation of the coronary arteries using CMR was performed using scout images of the aortic root to localise the origin and course of the left anterior descending and right coronary artery. These were then cross-cut until a clear cross sectional image of artery was obtained.

**Figure 5.7**: Cross sectional imaging of LAD (top panels) and RCA using phase encoded (A and C), velocity encoded (B and D) and fat excitation imaging (E).

**Figure 5.7.1**: Measurement of LV volumes using CMR tools (screenshot from programme). The semi-automated programme was used to calculate the left ventricular end diastolic and end systolic volumes and measure the left ventricular mass.

**Figure 5.8**: Early diastolic cross sectional imaging of LAD (top panel) and RCA (middle panel) using breath-hold spiral phase velocity mapping. For derivation of pressure data, a cross sectional plane was identified 35mm above the aortic valve plane (bottom panel), a high temporal resolution gradient echo sequence was used to acquire aortic areas throughout the cardiac cycle and these were used to derive the central aortic pressure during the cardiac cycle.

**Figure 5.9**: Using the epicardial and endocardial borders traced at each slice, a model with no geometric assumptions is created for the LV and the RV (screenshot from programme) and used to calculate the LV volumes and mass.

**Figure 5.10**: Quantification of LGE using CMR 42 and the full width-half maximum method. A region of interest within the diseased myocardium is defined and regions with similar signal intensity are automatically identified as LGE.

**Figure 5.11** Post processing of first pass CMR perfusion to generate quantitative perfusion values

**Figure 6.1:** Example traces for separated wave intensity in a control and an HCM patient with LVOT obstruction at rest. The top panels show the WIA pattern. Proximally originating waves are displayed above the axis and distally originating waves below the axis. The bottom panel shows the ensemble averaged pressure (solid line) and flow velocity (dashed line) during the cardiac cycle. Note the difference in the wave intensity and velocity scales. In controls, the dominant wave is the BEW but in HCM, the BCW is dominant. With severe LVOT obstruction, there is an additional forward deceleration wave ($FEW_a$).

**Figure 6.2**: Obstruction of the LVOT due to SAM of the mitral valve (top panel, M mode through mitral valve) results in a transient reduction in outflow at the point of most severe obstruction (middle panel, continuous wave Doppler) and a decelerating wave ($FEW_a$) which is transmitted into the coronary arteries, causing deceleration of coronary flow and a reduction in coronary pressure (bottom panel). The panels were aligned by the ECG R wave with a minimal time delay to account for distance between measurement sites.

**Figure 6.3:** Comparison of the separated cumulative wave intensity (%) for the BEW and $BCW_{tot}$ at rest and following an ectopic beat in HCM patients.

**Figure 6.4**: Comparison of resting coronary resistance in HCM patients with and without LVOT obstruction and control patients. Comparison between groups was performed using ANOVA. A p-value of $<0.05$ was considered to be significant.

**Figure 6.5**: There was a significant correlation between the myocardial perfusion reserve (MPR) and the proportionate increase in percentage of accelerating waves during hyperemia in patients with HCM. Correlation was assessed using Pearson's correlation coefficient (r).

**Figure 6.6**: The relative changes in each wave dictate myocardial perfusion downstream. The two patients above have similar wall thicknesses (22-24mm), no resting LVOT obstruction and normal epicardial coronary arteries. Patient 1 (top) had severe, typical angina whereas patient 2 (bottom) was asymptomatic. The left panel shows net wave intensity at rest, the middle panel net wave intensity during hyperemia (at the same scale) and the right panel a CMR short axis first pass myocardial perfusion image during hyperemia. The top patient has an increase in the BEW but a proportionately greater increase in the BCW during hyperemia which is associated with a large inducible circumferential myocardial perfusion defect during hyperemia (arrowed). The bottom patient has a small increase in the BCW and a large increase in the BEW, resulting in normal myocardial perfusion during hyperemia.

**Figure 7.1**: Cross sectional imaging of LAD (top panels) and RCA using phase encoded (A and C), velocity encoded (B and D) and fat excitation imaging (E)

**Figure 7.2:** Velocity signal output from Volcano console showing a subject with coronary flow velocity reversal during systole that was not well detected by the automatic detection algorithm

**Figure 7.4:** MR velocity-time curves assessed with the semi-automatic technique for repeated breath-holds in 5 right coronary arteries (top) and 10 left anterior descending arteries (middle and bottom).

**Figure 7.5**: MR measurement of mean velocity (a), peak diastolic velocity (b) and peak systolic velocity (c) against Doppler values in 24 vessels, scaled to adjust for differences in heart rate between the two acquisitions. The top panels show comparison between

Doppler and CMR values while the bottom panels are Bland-Altman plots. As expected, the velocities measured with Doppler were higher than those measured using CMR but with a moderate-strong correlation between the two.

**Figure 7.6** MR versus Doppler values of PDV/PSV for the RCA and LAD vessels (top panels) and Bland Altman Plots for agreement (bottom panels). The relationships are linear with slopes close to unity (RCA: slope 1.05, LAD: slope 0.98) and high coefficients of determination. Coefficient of determination was calculated using Pearson's correlation co-efficient.

**Figure 7.7** MR measured velocities at all time points in the cardiac cycle plotted against corresponding Doppler velocities for all 24 vessels. Linear regressions are superimposed on each plot. The slopes of the regression plots vary from vessel to vessel (mean 0.66 ± 0.21, range 0.36 – 0.98) which results in the scatter in MV, PSV and PDV seen in Figure 7.6. Higher regression slopes are seen in patients in whom the heart rate during the MR study was higher than that during the invasive study. Although the slope varies, the relationships between the MR and Doppler velocities for each patient are linear with high coefficients of determination (R = 0.9± 0.12).

**Figure 7.8:** Slope of MR velocity versus Doppler velocity regression lines of Figure 7.7 against the ratio of the heart rate during the MR study ($HR_{MR}$) to that in the invasive study ($HR_{INV}$).

**Figure 8.1**: Early diastolic cross sectional imaging of LAD (top panel) and RCA (middle panel) using breath-hold spiral phase velocity mapping. For derivation of pressure data, a cross sectional plane was identified 35mm above the aortic valve plane (bottom panel), a high temporal resolution gradient echo sequence was used to acquire aortic areas throughout the cardiac cycle and these were used to derive the central aortic pressure during the cardiac cycle.

**Figure 8.2**: Comparison of invasive and CMR-derived wave intensity analysis. All 5 waves are displayed on a single plot, assessed for agreement with invasive data as the gold standard using Bland Altman analysis (top left panel) and using the Pearson correlation coefficient (top right panel). The bottom panels display a visual comparison of WIA using invasive (left) and CMR derived (right) data in the same patient, with the corresponding pressure and flow velocity data shown below. While the absolute values for each wave were greater for CMR compared to invasive measures, the pattern of wave intensity and relative size of each wave was similar between the two traces

**Figure 8.3:** Reproducibility of invasive (top panels) versus CMR-derived (bottom panels) wave intensity values using Bland Altman plots (left) and Pearson correlation coefficient (right).

# CHAPTER 1

## Hypertrophic Cardiomyopathy

Hypertrophic cardiomyopathy (HCM) is the most common genetic disorder affecting the heart and is characterised by left ventricular hypertrophy, interstitial fibrosis (scarring) and myocardial disarray. HCM was first described by Brock (Brock 1957) and Teare (Teare 1958) in 1958 and affects 1 in 500 of the general population (Maron *et al.* 1995). Disease severity is highly variable, with many patients surviving to a near-normal life expectancy, but with an annual risk of sudden cardiac death in the general population of 1% (Maron 2002).

### 1.1 Diagnosis and presentation

The presentation and natural course of the disease is heterogenous. Patients may present with symptoms, including chest pain, shortness of breath, syncope, pre syncope and palpitations. HCM patients typically have an abnormal electrocardiogram (ECG) (Lakdawala *et al.* 2011). Typically, ECGs show evidence of left ventricular hypertrophy or widespread T wave abnormalities and these findings at a routine ECG may also prompt a diagnosis. Tragically, presentation may be with sudden death or aborted sudden

death and HCM remains the leading cause of sudden cardiac death in young adults (Maron 2002).

Diagnosis is usually made using transthoracic echocardiography, with typical findings of a hypertrophied left ventricle which is not dilated in the absence of another cause capable of producing that degree of left ventricular hypertrophy, for example aortic stenosis or hypertension. The magnitude of hypertrophy is typically 15mm or greater, although 13mm or greater is diagnostic in a patient with a first degree relative with HCM (Gersh *et al.* 2011).

Once the diagnosis has been made, patients are typically investigated with ambulatory ECG monitoring to assess for arrhythmias and will usually also undergo exercise testing, to assess for blood pressure response to exercise. Cardiovascular magnetic resonance (CMR) is helpful to quantify left ventricular volumes and mass as well as to assess for presence and extent of myocardial fibrosis.

### 1.2 Genetic inheritance of HCM

HCM is autosomal dominantly inherited but with incomplete penetrance. The disease is commonly caused by mutations in proteins encoding the cardiac sarcomere and its associated proteins, either components of the thick or thin filaments (Maron 2002). The most common mutations are in the beta myosin heavy chain, myosin binding protein C and cardiac troponin T. Other less common mutations may affect troponin I, regulatory and essential myosin light chains, α-actin, α-tropomyosin, α-myosin heavy chain and titin

(Elliott *et al.* 2014). Approximately 40-60% of patients have a known mutation (Bos *et al.* 2010; Ho 2011). These mutations lead to alterations in the contractile and relaxation properties of the myocytes. The sensitivity of contractile proteins to calcium is altered and it is thought there are alterations in the efficiency of energy use from ATP (Spindler *et al.* 1998).

There is considerable intra-genetic heterogeneity, with over 1000 mutations identified to date (Ho 2011). Many of these are missense. Private mutations localised to a family are common. Patients are increasingly diagnosed as a result of family screening, with screening of first degree family members recommended (Gersh *et al.* 2011). Screening has also increased the pickup of patients with gene mutations known to associate with HCM but with no phenotypic evidence of the disease.

### 1.3 Imaging findings in HCM

Patients with HCM typically have a hypercontractile, non dilated ventricle with vigorous systolic function but with impairment of diastolic function demonstrated on echocardiogram (Nagueh *et al.* 2001). The pattern of hypertrophy can vary widely. Most commonly, HCM affects the ventricular septum with a finding of asymmetrical septal hypertrophy. A distinct subset of HCM has apical hypertrophy, known as apical HCM. Apical HCM is most common in Japanese populations and is typically associated with a better prognosis (Maron 2002). HCM patients may have a normal LV mass despite hypertrophy (Olivotto *et al.* 2008).

### 1.3.1 Left ventricular outflow tract obstruction

Approximately one third of patients will have left ventricular outflow tract (LVOT) obstruction at rest, with increased velocities through the outflow tract on continuous wave Doppler echocardiography. This dynamic obstruction occurs due to systolic anterior motion of the mitral valve, causing transient obstruction of blood from the left ventricle and typically results in an increased intra-ventricular pressure. Latent LVOT obstruction was present in a further 1/3 of patients with HCM (Shah *et al.* 2008). In this population, LVOT obstruction was not present at rest but may be provoked by a variety of mechanisms, including pharmacological (amyl nitrate, isoprenolol) and physiologic manoeuvres (e.g. Valsalva or exercise).

LVOT obstruction is thought to occur as a result of unfavourable anatomy, with LVH of the ventricular septum and abnormal mitral valve anatomy as well as an unfavourable shape of the septum rather than simply its absolute size. Systolic anterior motion of the mitral valve (SAM) occurs as the anterior mitral valve apparatus moves into the outflow tract (Figure 1). Factors predisposing to SAM include elongated anterior mitral valve with excess tissue, the angle between the LVOT and the septum and the size of the LVOT and ventricular septum. Drag forces, similar to a hydrofoil, also exacerbate this. SAM of the mitral valve typically results in posteriorly directed mitral regurgitation (Ommen *et al.* 2008).

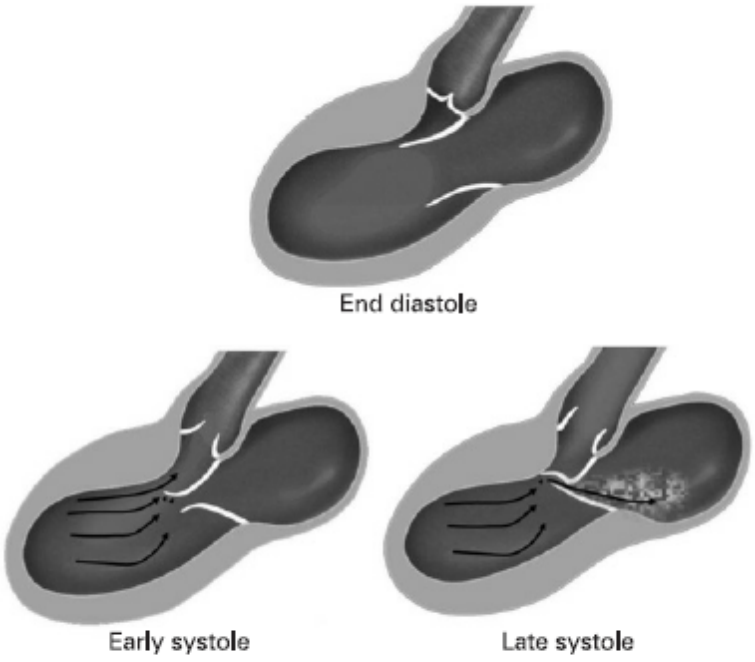


**Figure 1.1**: Left ventricular outflow tract obstruction in HCM is now thought to result from abnormal flow patterns around the hypertrophied septum in early systole, resulting in the mitral valve being pushed into the LVOT and causing obstruction of the LVOT and mitral regurgitation (Ommen *et al.* 2008).

### 1.3.2 Cardiovascular magnetic resonance in HCM

CMR typically demonstrates a hypercontractile ventricle with small left ventricular volumes and a raised left ventricular mass. A CMR study demonstrated that the most common areas of hypertrophy in HCM are the basal anteroseptum and the anterior wall (Maron 2009). LVOT obstruction may be imaged using flow velocity mapping, although recorded velocities are typically lower than that found using echocardiography. CMR allows excellent imaging of the right ventricle, which is hypertrophied in approximately 1/3 of patients (Maron *et al.* 2007). Microvascular obstruction may be seen in patients

with active disease and this is well imaged on early gadolinium sequences. Finally, the presence of replacement fibrosis is closely correlated with areas of late gadolinium enhancement (LGE) (O'Hanlon *et al.* 2010). LGE is typically midwall and patchy in distribution (Figure 2).

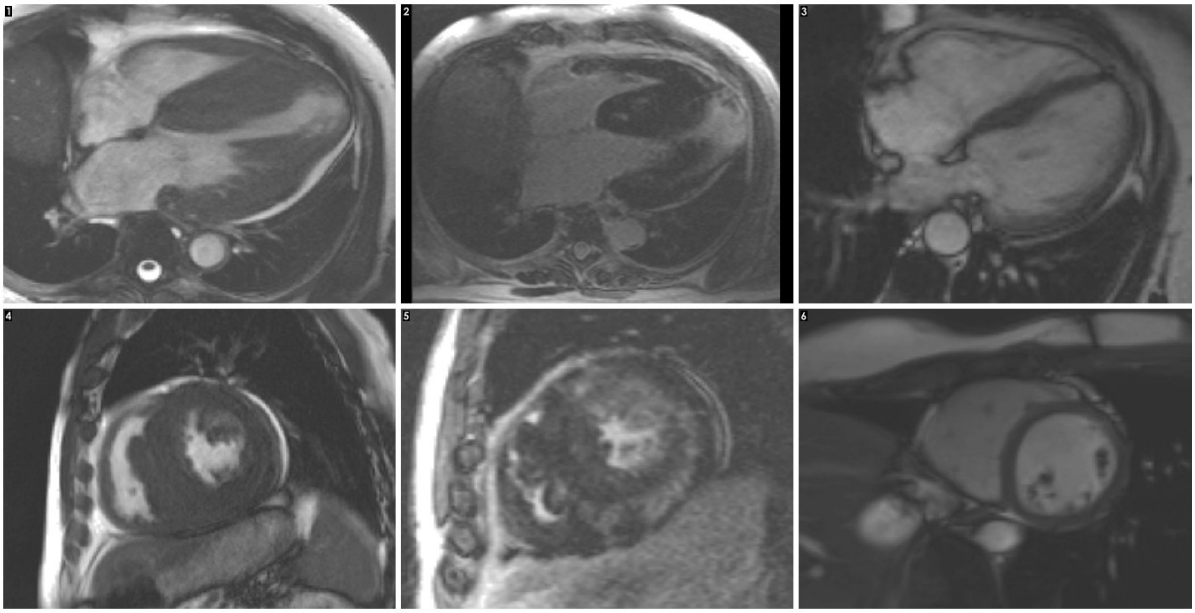

**Figure 1.2**: Cardiovascular magnetic resonance imaging of the heart in HCM (left and middle panels) and of a normal heart (right panels). In HCM, the left ventricle becomes thickened. Late gadolinium imaging (middle panels) demonstrates scarring of the ventricle (white areas).

### 1.4 Histological findings in HCM

The classical description of HCM from autopsy studies is of a hypertrophied ventricle with disorganised myocardial architecture comprised of hypertrophied myocytes, with haphazard alignment (Figure 3). This myocardial disarray appeared to be more prevalent in young sudden death patients (Maron *et al.* 1979; Varnava *et al.* 2001). The ventricle is

frequently fibrosed, with patchy myocardial scarring and an increase in interstitial collagen. Fibrosis may be interstitial, replacement or perivascular (Hughes 2004). There is an increase in the interstitial space and an increase in collagen. This is most commonly seen in the midwall of the ventricle (Shirani *et al.* 2000).

Finally, the small vessels of the heart are also abnormal with decreased luminal diameter of the intramural arterioles and wall thickening (Maron *et al.* 1986; Tanaka *et al.* 1987) (Figure 4).

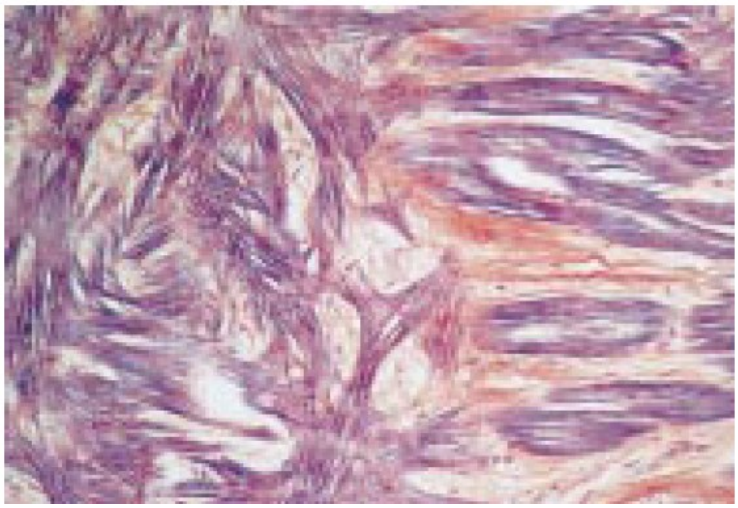

**Figure 1.3**: Myocyte disarray in hypertrophic cardiomyopathy seen using microscopy (taken from (Varnava *et al.* 2000)

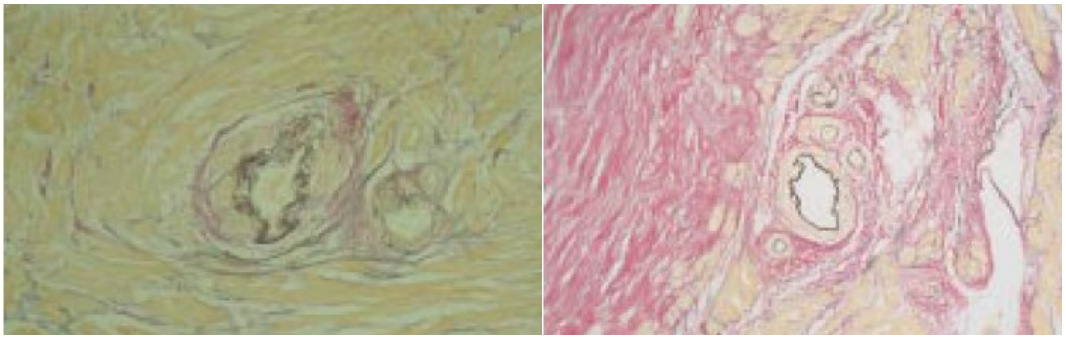

**Figure 1.4**: Small vessel disease in HCM. Left panel – dysplastic small vessel with no surrounding fibrosis. Right panel – small vessel disease with extensive adjacent fibrosis (Varnava *et al.* 2000).

Varnava et al (Varnava *et al.* 2000) performed macroscopic and histological exanimation of 72 patients with HCM and sudden death or end stage disease. The degree of hypertrophy correlated significantly with severity of hypertrophy and disarray. There was no relationship between disarray, small vessel disease and myocardial fibrosis. The magnitude of small vessel disease was not related to age, however there was a weak correlation between small vessel disease and maximum left ventricular wall thickness a well as heart weight. However, severely dysplastic small vessels were seen in some hearts with no widespread fibrosis. Abnormal thickening of the arteriolar wall and reduced capillary density was demonstrated on post mortem examination (Krams *et al.* 1998; Maron *et al.* 1979), Figure 4).

## 1.5 Long term prognosis and risk prediction in HCM

### 1.5.1 Sudden cardiac death

While patients with HCM commonly have a near-normal life expectancy, a subset of patients will be at higher risk for sudden cardiac death and ventricular arrhythmia. The mode of death in these patients is development of ventricular fibrillation, most commonly as a result of degeneration of ventricular tachycardia. The presence of increased fibrosis in the ventricle is thought to provide a substrate for ventricular arrhythmia. Identification of the population at greatest risk for ventricular arrhythmia and sudden death is difficult.

Research in HCM is commonly observational and retrospective in design, with the difficulties of heterogenous in expression of disease and a relatively low event rate, making randomised trials with prospective follow up challenging (Maron 2002). However, certain risk factors that are associated with greater rates of sudden death have been identified and are used for risk stratification in HCM.

The presence of prior cardiac arrest or sustained ventricular tachycardia, left ventricular wall thickness of 30mm or greater (Maki *et al.* 1998; Spirito *et al.* 2000), recent unexplained syncope (Kofflard *et al.* 2003), family history of sudden death and lack of blood pressure response during exercise (Maki *et al.* 1998) have been shown to increase the likelihood of sudden death in HCM.

The presence of LVOT obstruction is known to predict progression to heart failure and death (Elliott *et al.* 2006; Maron *et al.* 2003), although is not used for risk stratification for ICD implantation. Fibrosis, as measured by late gadolinium enhancement on cardiovascular magnetic resonance (CMR) has more recently been shown to predict prognosis (Chan *et al.* 2014; O'Hanlon *et al.* 2010), although is yet to be included into risk stratification models for SCD.

Patients with a higher risk of sudden death are offered implantation of an implantable cardioverter defibrillator (ICD), which will shock the heart in the event of ventricular fibrillation and can use anti-tachycardia pacing or shock therapy to terminate ventricular tachycardia. Device implantation in HCM is a careful decision as the majority of devices

are implanted for primary prevention and the potential risk of inappropriate shocks and the need for repeated generator replacement in a population with a near-normal projected life expectancy (Lin *et al.* 2009; Maron 2010) need to be weighted up against the likelihood of sustained or life threatening ventricular arrhythmias.

Prediction of who will benefit from an ICD is difficult as predictors of sudden death all have low positive predictive value when considered individually (Maron 2010; Zipes *et al.* 2006). In an observational study, patients with an ICD implanted for secondary prevention following cardiac arrest had an 11% annual incidence of appropriate ICD shock with a 5% annual risk in patients with an ICD for primary prevention (Bos *et al.* 2010).

The European Society of Cardiology (ESC) recommends ICD implantation in survivors of cardiac arrest due to VT or VF and in patients with spontaneous sustained VT with syncope or haemodynamic compromise as a 1B recommendation (Elliott *et al.* 2014). ICD implantation should also be considered in patients with a 5-year estimated sudden cardiac death risk of 6% as a IIA recommendation (Figure 5). With a 5 year risk of 4-6% an ICD may be considered and with less than 4%, it is not recommended unless there are features of clinical concern (Elliott *et al.* 2014).

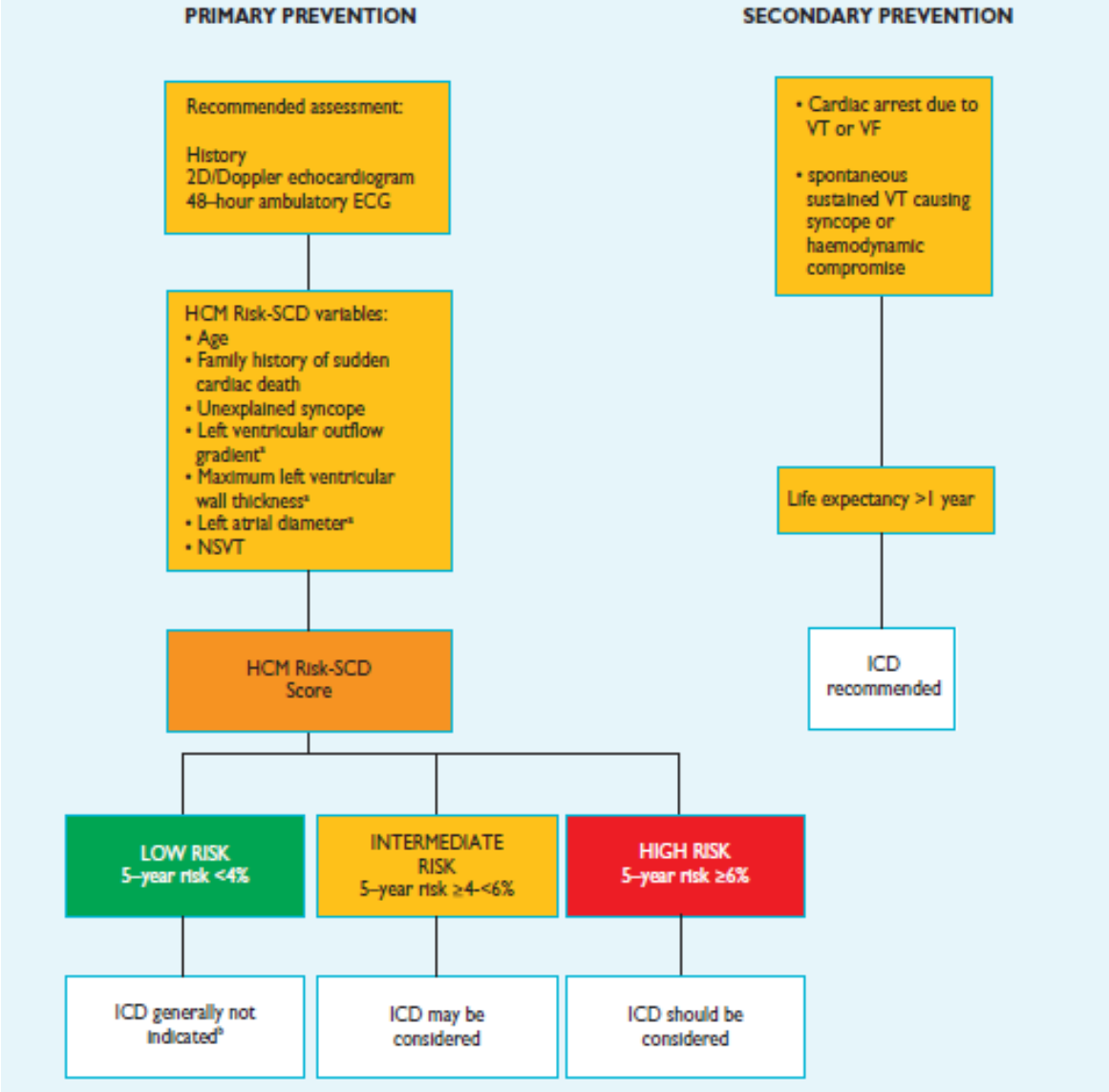


**Figure 1.5**: ESC guidelines for risk stratification in HCM: Patients should be risk stratified for potential of sudden cardiac death and this value used to help the clinician decide whether the patient should be offered an implantable cardioverter defibrillator (ICD).

The 5 year risk is calculated using a risk score validated in a population of 3675 patients from 6 centres and was shown to be comparable with other risk scores such as $CHA_2DS_2$-VASc (O'Mahony *et al.* 2014).

The risk of sudden cardiac death is calculated as follows:

$$Probability\ of\ SCD\ at\ 5\ years = 1 - 0.998^{Prognostic\ index}$$

where the Prognostic index = [0.15939858 x maximal wall thickness(mm)] - [0.00294271 x maximal wall thickness$^2$ (mm$^2$)] + [0.0259082 x left atrial diameter (mm)] + [0.00446131 x maximal (during rest or Valsalva) left ventricular outflow tract gradient (mm Hg)] + [0.4583082 x family history SCD] + [0.82639195 x NSVT] + [0.71650361 x unexplained syncope] 2 [0.01799934 x age at clinical evaluation (years)] (O'Mahony *et al.* 2014).

### 1.5.2 Heart failure

While risk prediction of sudden death has traditionally been the main focus of management within this patient population, the burden of heart failure is increasingly recognised (Maron 2010; O'Hanlon *et al.* 2010). Approximately 5-10% of patients progress to an end stage phenotype of HCM with LV cavity enlargement, wall thinning and systolic dysfunction (Shirani *et al.* 1993; Spirito *et al.* 1997). Patients with heart failure secondary to HCM represent a high risk population. The annual mortality rate is 11% and a substantial increase in sudden cardiac death (Kawarai *et al.* 2011).

Heart failure symptoms may also develop in patients with preserved ejection fraction, with 15-20% of patients developing congestive symptoms and marked shortness of breath on exertion likely due to increased ventricular stiffness and diastolic dysfunction (Maron 2002).

### 1.6 Management of HCM

The aims of treatment in HCM are to manage symptoms such as chest pain, shortness of breath and syncope and secondly, to manage risk and attempt to prevent sudden cardiac death as described previously. New symptoms of shortness of breath and signs of heart failure may result from development of left ventricular impairment and therefore repeat imaging of ventricular function, including diastolic function, is required. Development of atrial fibrillation may also worsen symptoms, particularly in combination with a ventricle with impaired relaxation and therefore resting or ambulatory ECG monitoring may be appropriate.

Chest pain is common in patients with HCM. This may result from either the disease itself or potentially from co-existent atherosclerotic coronary artery disease. Patients with both hypertrophic cardiomyopathy and atherosclerotic coronary artery disease have a particularly poor outcome with a 46% 10 year survival in patients with severe epicardial coronary disease compared to 77.1% in the population with no coronary disease (Sorajja *et al.* 2003).

### 1.6.1 Lifestyle advice in HCM

Lifestyle advice is an important part of HCM management. Patients are advised to avoid becoming dehydrated, particularly in the case of LVOT obstruction, as this will worsen the gradient across the LVOT. They should also avoid vasodilators such as angiotensin converting enzyme inhibitors and drugs which cause dehydration such as diuretics. Similarly, they are advised to avoid conditions which cause significant peripheral vasodilatation such as saunas or steam rooms (Ommen *et al.* 2008). Intense physical exertion is considered to be a potential trigger for sudden death in susceptible patients (Maron *et al.* 1996) and patients with HCM are therefore typically advised not to complete in most competitive sports.

### 1.6.2 Management of atrial fibrillation and stroke

Approximately 20% of patients with HCM develop atrial fibrillation (AF). This is more common in patients with left atrial enlargement and in older patients (Olivotto *et al.* 2001) (Robinson *et al.* 1990). Patients with HCM and AF have a greater risk of embolic stroke than in the general population with AF (Guttmann *et al.* 2014). AF is also more likely to lead to development of heart failure and episodes of acute decompensation. Treatment is typically with beta blockers or amiodarone if the aim is to restore sinus rhythm and direct current cardioversion may be used as with AF in the general population. If a rate control strategy is employed, beta blockers and calcium channel blockers may be used to control the heart rate. Because of the increased risk of stroke, patients with HCM and AF should be anti-coagulated, typically with warfarin (Gersh *et al.* 2011).

### 1.6.3 Family screening

Long term management in HCM also involves taking a family history and where appropriate, the recommendation of family screening of first degree relatives. Genetic screening may be appropriate in this cohort if the index patient is found to carry a pathogenic mutation and this may allow patients who do not carry the mutation to be reassured and discharged from follow up. Patients considering starting a family should be counselled appropriately about the risk of passing on the condition and the need for regular screening of their children.

### 1.6.4 Pharmacological treatment in HCM

Pharmacological treatment in HCM is usually for management of symptoms or to reduce the gradient through the left ventricular outflow tract. Treatment of shortness of breath and congestive symptoms in the presence of preserved ejection fraction is typically with beta blockers or calcium channel blockers. In the case of systolic impairment, ACE inhibitors, spironolactone and diuretics may also be used (Gersh *et al.* 2011; Maron 2002). Disopyramide, usually prescribed with a beta blocker, may be highly efficacious in treatment of symptomatic patients with outflow tract obstruction.

### 1.6.5 Management of chest pain in HCM

Chest pain typically requires the exclusion of coronary artery disease via an appropriate test such as CT coronary angiography. Chest pain is present in up to 40-50% of patients with HCM (Elliott *et al.* 1996). This is commonly prolonged and atypical and may often occur at rest, unlike classical angina pectoris due to epicardial coronary artery disease

(Pasternac *et al.* 1982). Less commonly, patients describe a more classical, exertional pain. However, while both microvascular ischaemia and chest pain are both common in HCM, there is no consistent association between the two (Cannon *et al.* 1991; Udelson *et al.* 1989).

Treatment of chest pain in HCM is often challenging. Typically older anti anginals are used, such as beta blockers and calcium channel blockers. The mechanism of action of these is thought to relate to reduction in heart rate and oxygen consumption in the case of beta blockers, with potential additional effects of improved diastolic filling seen with verapamil. This may improve myocardial perfusion, particularly of the subendocardial layer (Gistri *et al.* 1994). In patients with LVOT obstruction, surgical or percutaneous relief of the obstruction may also improve perfusion (Timmer *et al.* 2011) and reduce symptoms of chest pain and shortness of breath.

Beta blockers may reduce or eliminate the LVOT gradient through reduction in ventricular contractility and heart rate, particularly on exercise. This allows greater coronary filling during diastole and maintains ventricular preload (Vaglio *et al.* 2008). Calcium channel blockers such as Verapamil may also be used, usually as a second line agent and act through their negatively ionotropic and chronotropic effects. Both verapamil and diltiazem have previously been shown to reduce the LVEDP and the pulmonary capillary wedge pressure in patients with HCM (Bonow *et al.* 1981; Rosing *et al.* 1979). The mechanism is likely to be due to a reduction in intra-cellular calcium. Disopyramide, a less commonly prescribed agent is a class 1A anti arrhythmic. The

mechanism of action is not clear but it does reduce gradients through the left ventricular outflow tract (Ommen *et al.* 2008). Finally, non pharmacological treatments such as alcohol septal ablation and myectomy are effective at altering the ventricular geometry and increasing the width of the outflow tract.

### 1.6.6 Management of LVOT obstruction

The presence of LVOT obstruction has important effects on haemodynamics. The dynamic obstruction may result in reduced stroke volume and this may result in syncope. It will also result in an increased pressures within the LV cavity, which may increase compression of the microcirculation, resulting in angina. Finally, mitral regurgitation increases the workload of the ventricle and may result in shortness of breath on exertion. Symptoms typically worsen on exertion as the ventricular contraction becomes more vigorous and the systemic vascular resistance is reduced (Maron 2002). LVOT obstruction is associated with reduced survival: Elliott studied a population of 917 patients with HCM and followed them for a median of 61 months. 31% of patients had LVOT obstruction at rest (defined as a gradient of 30mmHg or greater). These patients had a lower 5 year survival free from death or transplantation, although most events occurred in patients who were symptomatic, with a 91% 5 year survival rate in NYHA I patients with LVOT obstruction. The severity of LVOT obstruction was associated with a higher rate of sudden death and ICD discharge (Elliott *et al.* 2006).

Patients with latent LVOT obstruction, i.e. an outflow tract gradient of less than 30mmHg at rest, rising to greater than 30mmHg with provocation, also have a trend towards

decreased survival compared to age and sec matched controls. Their average annual mortality rate was estimated at 2% per year (Vaglio *et al.* 2008).

### 1.6.7 Septal reduction therapy

For symptomatic patients with a significant gradient across the LVOT (50mmHg or greater) who do not respond to pharmacological therapy, invasive septal reduction therapy may be appropriate. There are two main ways this may be performed: alcohol septal ablation (ASA) involves the injection of medical pure alcohol into a septal perforator branch using percutaneous angiographic access. This induces a targeted infarction of the myocardium, ideally at the contact point of systolic anterior motion of the mitral valve.

Myectomy involves surgical removal of a small portion of the septum in the area of SAM contact. The classical Morrow procedure involved two parallel longitudinal incisions in the basal septum at a level below the aortic valve. The two incisions are then joined distally and the tissue excised to produce a trough in the septum and reduction in outflow tract obstruction (Ommen *et al.* 2008). The technique has been adapted to extend the trough beyond the SAM contact point to alter flow vectors around the hypertrophied septum and these have improved operative success. Abnormalities of the mitral valve, for example redundant mitral valve tissue or abnormal papillary insertion may be repaired at the same time. Operative mortality has been quoted at approximately 1% in an experienced centre (Ommen *et al.* 2008).

Improvement of symptoms after myectomy and ASA are reported, however survival benefit as a result of these interventions is less clearly established (Ball *et al.* 2011; Woo *et al.* 2005). Finally, pacing of the right ventricle to induce deliberate dyssynchrony may be used to reduce the gradient across the LVOT and improve symptoms, although evidence from a randomised controlled trial suggested this did not improve prognosis (Maron *et al.* 1999).

### 1.6.8 Novel therapies in HCM

While older agents such as beta blockers and calcium channel blockers remain the mainstay of pharmacotherapy in current management of HCM, there is much interest in newer agents that may act more directly on pathophysiological pathways in the disease process, with the aim of slowing or attenuating disease progression. Various agents have been trialled.

Cibenzoline, a class 1a antiarrhythmic agent has been shown to attenuate the gradient across the LVOT in HCM. It also improved diastolic function in HCM with and without outflow obstruction. This was hypothesised to occur via two main mechanisms. Firstly, cibenzoline acts to block sodium channels within the myocytes which, through the sodium/calcium exchange pump, therefore leads to a reduction in intracellular calcium. This is thought to improve relaxation during diastole. Secondly, the reduction in outflow tract obstruction may lead to a reduced cardiac afterload. A high afterload is known to be associated with slowed and impaired ventricular relaxation (Saito *et al.* 2011).

Trials are ongoing using Ranolazine, an inhibitor of the late sodium channel. Studies performed in vitro using cardiomyoctes from myectomy patients demonstrated that administration of ranolazine partially reversed the HCM-related cellular abnormalities via inhibition of the late sodium channel. In HCM, the action potential is normally prolonged and ranolazine led to a reduction in action potential duration in HCM cardiomyocytes, with resultant reduction in the occurrence of early and delayed afterdepolarizations. Finally, as a result of the faster kinetics of calcium transients and the lower diastolic calcium (Coppini *et al.* 2013) concentration, ranolazine accelerated the contraction-relaxation cycle of HCM trabeculae, improving diastolic function.

Drugs that inhibit the renin-angiotensin-aldosterone system have also been proposed as having potential to improve myocardial perfusion and animal data has suggested some evidence of beneficial remodelling of the microcirculation and improved diastolic function following administration of these agents (Tsybouleva *et al.* 2004).

### 1.7 Conclusions

HCM is the most common cause of sudden cardiac death in young adults and affects 1 in 500 of the general population. It is characterised by unexplained left ventricular hypertrophy, myocardial fibrosis and myocyte disarray. Patients with HCM have a heterogenous disease course, ranging from asymptomatic with a normal life expectancy to a more malignant course with an increased rate of sudden cardiac death and heart failure. Symptoms of shortness of breath and chest pain are common and present in approximately 40% of patients. Management is centred around risk stratification and

decision to implant an ICD, treatment of symptoms, lifestyle advice and family screening. Treatment can be pharmacological or consideration of septal reduction therapy in patients with LVOT obstruction. Pharmacological treatment is commonly with older medications, such as beta blockers and calcium channel blockers, although more recently novel agents are being evaluated for more disease-specific therapy.

# CHAPTER 2

## Myocardial perfusion and coronary flow abnormalities in HCM

Myocardial ischaemia is likely to play a pivotal role in the pathophysiology of HCM. Recurrent bouts of ischaemia are hypothesised to lead to the development of fibrosis, adverse remodelling of the left ventricle and development of systolic dysfunction (Cecchi *et al.* 2003; Olivotto *et al.* 2006). Myocardial ischaemia is perhaps an underappreciated disease process within HCM with much attention focussed on LV outflow tract obstruction (Maron *et al.* 2003; Olivotto *et al.* 2008), diastolic dysfunction (Geske *et al.* 2007) and replacement fibrosis (Chan *et al.* 2014; O'Hanlon *et al.* 2010). In this chapter I will review the current understanding of myocardial perfusion in HCM and the effects of the disease on coronary flow patterns within the epicardial coronary arteries.

### 2.1.1 Microvascular Disease and Myocardial Ischaemia in HCM

Interest in myocardial ischaemia in HCM began with the finding of ischaemic injury on post mortem studies. Coagulative necrosis and neutrophilic infiltrate have both been identified following sudden death, in the absence of epicardial coronary artery disease. There was also evidence of more chronic ischaemia, with replacement fibrosis suggesting recurrent ischaemia (Basso *et al.* 2000) (Figure 6). The intra-mural arterioles themselves

are abnormal, with a thickened intimal and medial layer and reduced luminal area (Maron *et al.* 1986). Patients with HCM have also been shown to have a reduction in capillary density (Mundhenke M, Schwartzkopff B 1997), potentially occurring due to repeated ischaemic insults, although a genetic predisposition to decreased vascular density cannot be excluded. More recently, evidence of ongoing cardiac injury has been demonstrated with persistently raised troponin in some HCM patients (Sato *et al.* 2003).

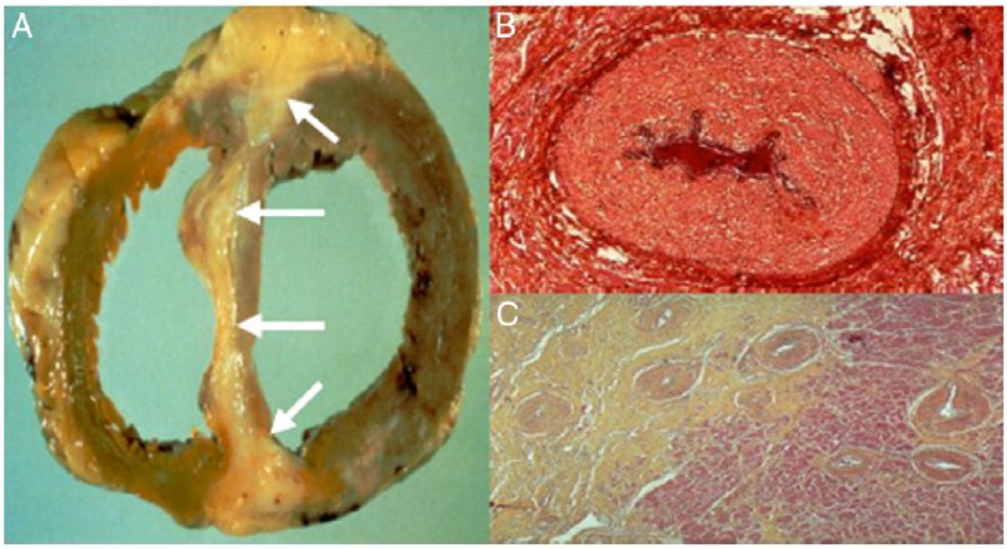


**Figure 2.1**: Microcirculatory disease in hypertrophic cardiomyopathy. (A) Native heart of a patient with HCM demonstrating areas of macroscopic scarring (arrowed). (B) Cross sectional preparation of an intramural coronary artery showing thickening of the intimal and medial layers of the vessel. (C) Myocardial specimen from a patient with HCM demonstrating multiple abnormal intramural coronary arteries and scarring of the myocardium (original magnification x55). (reproduced from Camici *et al.* 2012)

Myocardial ischaemia occurs as a result of an imbalance between the oxygen consumption of the myocytes and the oxygen supply to these myocytes. This may result from increased metabolic demand, for example due to increased muscle mass (hypertrophy), increased heart rate, increased contractility and increased systolic wall tension. In addition, there may be direct metabolic effects from excessive catecholamines (Daly & Kwong 2013). In HCM, the hypercontractile ventricle and increased left ventricular intra cavity pressures may increase extravascular compression of the intra-mural arterioles and further increase the workload of the ventricle (Krams *et al.* 2004; Maron *et al.* 2009).

### 2.1.2 Assessment of myocardial ischaemia and dysfunction in HCM

The majority of patients with HCM have abnormal perfusion as assessed using nuclear or other non-invasive techniques (Maron *et al.* 2009). These perfusion abnormalities are thought to represent microvascular dysfunction, i.e. disease of the microcirculation. Perfusion may be assessed using nuclear techniques such as PET or, more recently, techniques that do not require the use of ionising radiation such as CMR. Previous work using PET has suggested a similar resting myocardial blood flow compared to healthy controls but with a blunted perfusion index (Camici *et al.* 1991). Vasodilator stresses such as dipyridamole or adenosine may be used to measure peak hyperaemic myocardial perfusion and, when compared to resting perfusion, provide a measure of the perfusion reserve.

While perfusion defects are often greatest in the hypertrophied wall, studies have also shown perfusion abnormalities in the non hypertrophied myocardium (Camici *et al.* 1991). This suggests that impaired perfusion is not simply due to LVH but likely to represent a primary disease process. Both PET (Cecchi *et al.* 2003) and CMR studies (Petersen *et al.* 2007) have demonstrated a greater perfusion abnormality in the subendocardium compared to the subepicardium.

Thallium imaging may provide an assessment of perfusion. Defects are compared between stress and rest imaging as with other perfusion techniques, however absolute perfusion quantification is not possible: all perfusion is assessed relative to the rest of the myocardium. Fixed perfusion defects on thallium are thought to represent areas of myocardial scarring (O'Gara *et al.* 1987), while reversible defects are thought to represent areas of ischaemia. Stress induced transient dilatation of the left ventricular cavity may also occur in HCM, suggesting diffuse subendocardial ischaemia.

### 2.1.3 Prognostic significance of perfusion abnormalities in HCM

It is over 20 years since the landmark studies by Cecchi *et al* that demonstrated the prognostic importance of perfusion defects using PET in a cohort of 51 patients with HCM followed for a total of 8 years (Cecchi *et al.* 2003). In this study, myocardial blood flow measured by PET was shown to be a powerful independent predictor of outcome with a 10 fold increase in relative risk of death and a 20 fold increase in development of heart failure, cardiac transplantation and death.

Olivotto assessed the predictive value of myocardial perfusion on development of left ventricular systolic dysfunction in HCM in the same cohort. At baseline, patients had measurement of rest and dipyridamole-induced hyperaemic myocardial blood flow. While there was no significant different in myocardial blood flow at rest between HCMs and controls (0.84±0.31 vs 1.0±0.23ml/min/g, the dipyridamole myocardial blood flow (Dip-MBF) was significantly reduced in HCM compared to healthy controls (1.5±0.69 vs 2.71±0.69 ml/min/g) (Olivotto *et al.* 2006).

A total of 11 patients had heart failure at follow up, defined as an ejection fraction of 50% or less, 3 of whom had had impaired EF at baseline. On multivariate analysis, the two independent predictors of the development of systolic LV impairment were a Dip-MBF in the lowest tertile (<1.1ml/min/g) and an end diastolic LV dimensions in the highest tertile. At 8 year follow up, patients in the lowest tertile of Dip-MBF had a 7.5 fold higher risk of development of systolic dysfunction (defined as EF<50%) compared to the other tertiles. No patients with a preserved vasodilator capacity in the highest tertile developed heart failure.

The authors suggested this may support microvascular dysfunction as a necessary condition for the development of systolic dysfunction. They hypothesised that the reduced Dip-MBF was likely to result in recurrent ischaemic damage of the myocardium, with development of replacement fibrosis and LV remodelling, chamber dilatation and reduction in contractile function. This was similar to the mechanisms thought to underlie development of heart failure following acute myocardial infarction.

Studies by other groups, using other modalities to assess perfusion, have failed to show prognostic significance. Yamada studied 216 patients with HCM who underwent Thallium SPECT using dipyridamole stress. 25% of these exhibited fixed perfusion defects and an additional 22% had reversible defects. 7% had both forms of perfusion defects. Patients with fixed perfusion defects were more likely to have a history of syncope, larger left ventricular dimensions, larger left atrial dimensions and lower maximal peak oxygen consumption on exercise. Reversible perfusion defects did not relate to symptomatic status or known clinical risk markers although these were associated with a greater maximal wall thickness of the left ventricle and a larger left atrium. There was no relationship between reversible defects and the presence of a resting LVOT gradient of 30mmHg or greater. There was no relation between the presence of a reversible defect and peak exercise oxygen consumption or ST depression. Over 41 month follow up, there was no association between any form of perfusion effect and disease related death (Yamada *et al.* 1998).

Ambulatory ECG monitoring may also allow an indirect measure of myocardial ischaemia, through detection of dynamic ECG changes. In patients under 30, ST segment depression on ambulatory monitoring was predictive of exertional chest pain and shortness of breath. However there was no relationship between ST segment depression and conventional markers of sudden death (syncope, family history of sudden death and non sustained ventricular tachycardia) and overall the correlation between symptomatic status and ambulatory ST segment depression was poor. Reversible thallium-201 defects were present in 30% of the patients included in the study and these were not associated

with symptoms, risk factors for sudden death or ambulatory ST segment depression (Elliott *et al.* 1996).

The significance of myocardial ischaemia using non invasive testing in HCM therefore remains controversial (Argulian & Chaudhry 2012) and perfusion imaging is not considered a clinical diagnostic technique in HCM, nor is it used in risk stratification or to aid management (Gersh *et al.* 2011). This may relate to availability of nuclear imaging as the landmark studies demonstrating prognostic significant utilised positron emission tomography (PET).

### 2.1.4 Effects of treatment on perfusion in HCM

Abnormalities of perfusion have been shown to improve with treatment in small series of HCM patients. Patients with reversible perfusion defects on SPECT improved following diltiazem in a small study of 20 patients with HCM (Sugihara *et al.* 1998). The transient dilatation index showed significant improvement with normalisation of perfusion after diltiazem in 13/20 patients. A significant improvement in myocardial flow velocity was also seen with myocardial contrast echocardiography following alcohol septal ablation in patients with HCM (Pedone *et al.* 2006).

### 2.1.5 Association between myocardial fibrosis and myocardial perfusion defects: insights from CMR

Bravo (Bravo *et al.* 2013) assessed a population of 47 patients with HCM who underwent both CMR, to assess for delayed enhancement and PET, to quantify myocardial blood flow and coronary flow reserve. While patients with delayed enhancement typically had a lower MBF at stress and a lower coronary flow reserve compared to patients without delayed enhancement, these patients also had a greater LV wall thickness, indicating more severe disease. There was concordance between areas of delayed enhancement and regional myocardial perfusion defects in the majority of patients. 4/47 patients had normal regional myocardial perfusion but had areas of LGE and 3 patients with no LGE had apical regional myocardial perfusion abnormalities, suggesting that microvascular dysfunction and myocardial ischaemia are not the only causes of delayed enhancement in HCM.

## 2.2 Assessment of the coronary circulation in health and disease

In normal coronary anatomy, three main epicardial coronary arteries, the left anterior descending (LAD), circumflex and right coronary artery (RCA), originate from the aortic root. These run along the epicardial surface of the heart and supply the coronary vasculature. Each divides into progressively smaller branches. Epicardial coronary stenoses are a common cause of chest pain and are studied at the time of angiography. Epicardial coronary artery disease may be assessed using multiple techniques. Invasive coronary angiography was the first technique to allow direct imaging of the coronary arteries by placement of a catheter into the coronary artery. Injection of radio-opaque

contrast into the coronary arteries allows clear delineation of the coronary arteries, their branches and assessment of any coronary artery stenoses.

Coronary artery dominance may also be assessed at the time of angiography. This is variable between individuals and is defined by the vessel from which the posterior descending artery (PDA) originates. Approximately 80% of individuals have a right dominant circulation where the PDA originates from the right coronary artery, 10-15% have left dominance, where the PDA originates from the circumflex artery and the remainder of patients have a co-dominant system, with branches supplied from both the right and left coronary arteries.

### 2.2.1 Assessment of the microcirculation in vivo in hypertrophic cardiomyopathy

Although the epicardial coronary arteries are well studied, it is the small vessels of the microcirculation that comprise the majority of the myocardial circulation (Figure 2.2). Direct visualisation of the microcirculation may only occur ex vivo due to the small size of the individual vessels (typically less than 300μm diameter). However, the effect of impaired perfusion may be indirectly measured using quantitative perfusion analysis.

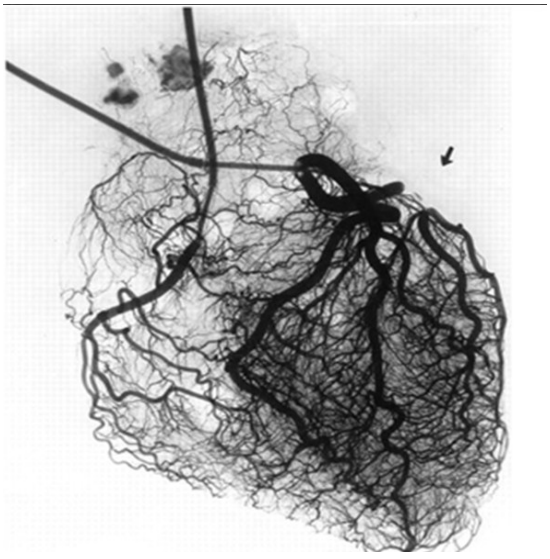

**Figure 2.2:** The coronary microcirculation in a healthy heart. While the epicardial coronary arteries are well studied at the time of diagnostic coronary angiography, the majority of the blood vessels in the heart are comprised of the microcirculation (Herrmann et al. 2012).

## 2.3 Importance of the coronary microcirculation

In the absence of significant coronary artery stenoses, the epicardial coronary arteries create minimal resistance to blood flow (Chilian *et al.* 1989) and there is minimal pressure difference between the central aorta and the distal coronary vessels (Pijls *et al.* 1995). The pre-arterioles and arterioles represent the majority of the pressure drop across the coronary circulation and can constrict or dilate to match supply to varying myocardial demand (Chilian *et al.* 1989). These vessels are much smaller in calibre (100-500 μm). Vessel dilatation is related to the coronary flow, the distending pressure and the myogenic tone. This is thought to be mediated by the autonomic nervous system and the endothelium. In the physiological range, coronary flow is largely independent of perfusion pressure. Auto-regulation controls blood flow dependent on the myocardial oxygen demand via changes in the size of the resistance arterioles, allowing relatively rapid adjustment as metabolic demand increases, typically occurring within a few seconds (Sipkema *et al.* 1997)

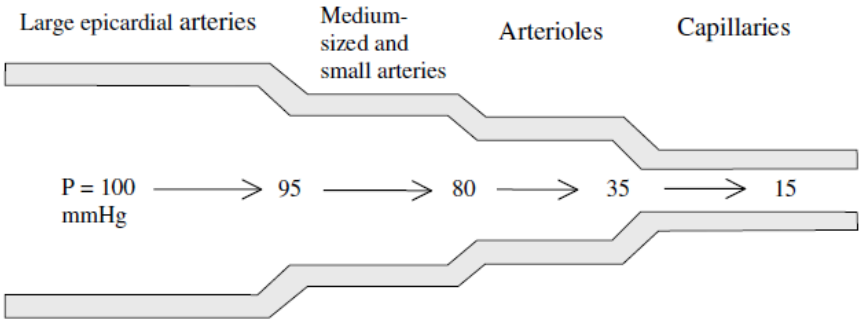


**Figure 1**
Sequential decrease of coronary perfusion pressure in consecutive segments of coronary vasculature. The largest fall in perfusion pressure occurs in coronary resistance arterioles.

**Figure 2.3**: Schematic representation of the sequential decrease in coronary perfusion pressure in a physiological heart. The greatest drop in perfusion pressure occurs across the coronary resistance arterioles (Dimitrow *et al.* 2005).

### 2.3.1 Microcirculatory disease and Cardiac Syndrome X

Patients with classical angina but a normal coronary angiogram provided a diagnostic conundrum prior to improved understanding of the coronary microcirculation. Measurement of the impact of small vessel disease using either myocardial perfusion imaging or assessment of coronary flow reserve allowed cardiologists to identify a subset of this population with evidence of downstream microcirculatory disease, despite the normal epicardial coronary arteries. These patients have been described as having "cardiac syndrome X" (Herrmann *et al.* 2012). Microvascular disease may also co-exist with epicardial coronary artery disease and this is thought to be the reason why at least 20% of patients with angina continue to experience symptoms even after complete revascularisation (Tonino *et al.* 2009).

### 2.3.2 Coronary flow reserve: assessment of both the epicardial vessels and the microcirculation

In the healthy heart, 5% of the cardiac output enters the coronary circulation at rest (Camici *et al.* 1989). Since resting myocardial oxygen extraction is relatively high, increased myocardial demand, for example during exercise, is largely met by increased coronary blood flow. This is mediated by the size of the resistance vessels (the vascular resistance) and the extravascular compression of these vessels by the myocardium itself (the extravascular resistance). Coronary flow may therefore be measured at rest and after a vasodilatory pharmacological stress agent, allowing calculation of the coronary flow reserve, a measure of the step-up in coronary flow in response to increased demand.

Coronary flow reserve (CFR) is defined as the ratio of coronary flow at hyperaemia to coronary flow at rest. This may either use the mean coronary flow across the whole cardiac cycle, as is typical in invasive measurement or the peak maximal blood flow in diastole, as is more commonly measured in echocardiographic assessment of CFR. For epicardial coronary disease, a CFR of less than 2 is considered to imply a functionally significant stenosis (Westerhof *et al.* 2006).

Coronary flow reserve (CFR) measures the flow of blood through both the epicardial coronary arteries and the small vessels (the microcirculation), providing measure of the coronary circulation as a whole (Jörg-Ciopor *et al.* 2004), comparing flow at rest and at hyperaemia. Abnormal CFR may therefore result from disease of the epicardial coronary arteries (atheroma) and/or disease of the microcirculation.

Stenoses in the epicardial coronary arteries causes increased resistance to coronary flow. Autoregulatory dilation of the resistance vessels attempts to compensate for reduction in perfusion pressure distal to the stenosis (Kwong & Korlakunta 2008). This usually results in a coronary flow at rest sufficient to meet the metabolic demand. However, increased demand due to physical activity may result in myocardial ischaemia of the tissues distal to the coronary stenosis (Kwong & Korlakunta 2008).

CFR may also be reduced in microvascular disease, including diabetic patients (Akasaka *et al.* 1997) and aortic stenosis (Rajappan *et al.* 2002). As CFR is a ratio, reduction in CFR may result either from reduced stress coronary flow or an increase in basal coronary flow. Increased basal coronary flow may occur due to increased basal heart rate. McGinn demonstrated that an increase in heart rate of 15 beats per minute resulted in a 15% decrease in the CFR (McGinn *et al.* 1990) and that CFR was therefore dependent on the basal resting conditions.

In the normal heart, there is a gradient of CFR across the myocardial wall, with the highest CFR in the subepicardial layer, closest to the epicardial coronary arteries, and the lowest CFR in the subendocardial layer, where the microcirculation is most sensitive to extravascular compressive forces. CFR abnormalities therefore manifest first in the subendocardial layer. Due to limitations of spatial resolution, PET can only be used to detect subendocardial versus subepicardial abnormalities in the hypertrophied myocardium. The subendocardial/subepicardial flow ratio allows assessment of transmural steal: a hyperaemic value of subendocardial/subepicardial flow ratio of less

than 0.8 has been suggested as a marker of subendocardial hyoperfusion and this has been documented previously in HCM (Choudhury *et al.* 1999; Lorenzoni *et al.* 1998). Studies using CMR at our institution, with improved spatial resolution, has also demonstrated subendocardial hyoperfusion in patients with syndrome X following adenosine infusion (Panting *et al.* 2002).

In an attempt to compensate for the greater sensitivity of the subendocardium to ischaemia, there is a greater density of vessels of the microcirculation in this layer compared to the subepicardium and therefore during diastole, coronary flow is approximately 10% higher in the subendocardial compared to the subepicardial layers (Westerhof *et al.* 2006).

**2.4 Regulation of coronary flow**

Regulation of coronary blood flow occurs as a result of both intrinsic and extrinsic effects. The extrinsic (external from the heart) effects relate to changes in the sympathetic and sympathetic nervous systems and neurohormonal changes. Myogenic autoregulation is an intrinsic effect that allows maintenance of myocardial oxygen supply despite changes in the perfusion pressure. Therefore, if the coronary perfusion pressure increases, there will be a transient increase in coronary flow before it returns to its original level, providing there has been no change in myocardial demand. Similarly, if the perfusion pressure falls, there will be a transient fall in coronary flow before return to baseline (Dole 1987). This was shown to be true up to a perfusion pressure of 40mmHg in a canine conscious model (Canty 1988; Spaan *et al.* 1981b). Changes in the

myocardial oxygen consumption will also result in a change in the coronary flow to keep the myocardial oxygen supply constant. Again this is thought to be mediated due to local release of metabolites such as adenosine or carbon dioxide (Westerhof *et al.* 2006) . Alteration in the vascular resistance therefore occur via changes in the coronary arterial smooth muscle tone, modulated by autoregulatory mechanisms and vasoactive metabolites such as adenosine and carbon dioxide (Westerhof *et al.* 2006). To study alterations in coronary flow as a result of extravascular compression, one must ideally eliminate changes due to alterations in the vascular resistance. This is largely achieved by study of the coronary circulation at maximum hyperaemia, achieved with a continuous intravenous adenosine infusion.

### 2.4.1 Effect of ventricular contraction on coronary flow

There are two key mechanisms by which contraction of the myocardium leads to changes in the vasculature supplying the myocardium. Firstly, cardiac contraction will lead to an increase in pressure in the ventricular lumen, exerting intra-myocardial and therefore vascular transmural pressure. This is the underlying principle of both the waterfall model and the intra myocardial pump model (discussed below). Secondly, contraction of the ventricle will lead to changes in the diameter and tortuosity of vessels making up the microcirculation. This is described in the varying elastance and vascular deformation model (Westerhof *et al.* 2006).

### 2.4.2 Increased intraventricular pressure during ventricular contraction

The intraventricular pressure increases significantly during contraction of the ventricle (Figure 8).

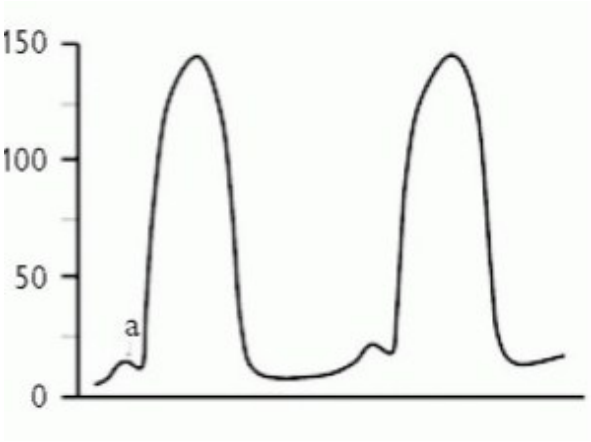


**Figure 2.4**: Left ventricular pressure during two complete cardiac cycles. The pressure changes from approximately 5-15mmHg (the end diastolic pressure) up to 120-140mmHg (the peak systolic pressure) in a healthy heart.

The increase in intraventricular pressure during systole results in a decrease in the vascular transmural pressure. The myocardial architecture is designed to operate in these varying pressure conditions.

### 2.4.3 Deformation of the microcirculation during ventricular contraction

Changes in coronary resistance will result from the effect of contraction of the myocardium causing deformation of the resistance vessels within the myocardium. In a

healthy person, this is seen as a reduction in coronary flow during systole, resulting from compression of the microcirculation as the myocardium contracts causing impedence to blood flow (Figure 9). Isolated heart studies have demonstrated systolic reversal of flow in situations where the coronary bed is vasodilated and the myocardium is hypercontractile. The degree of vascular deformation that occurs is likely to relate to the wall layer (i.e epicardial or endocardial) and whether contraction is isovolaemic (minimal effect) or shortening (greater effect) (Westerhof *et al.* 2006).

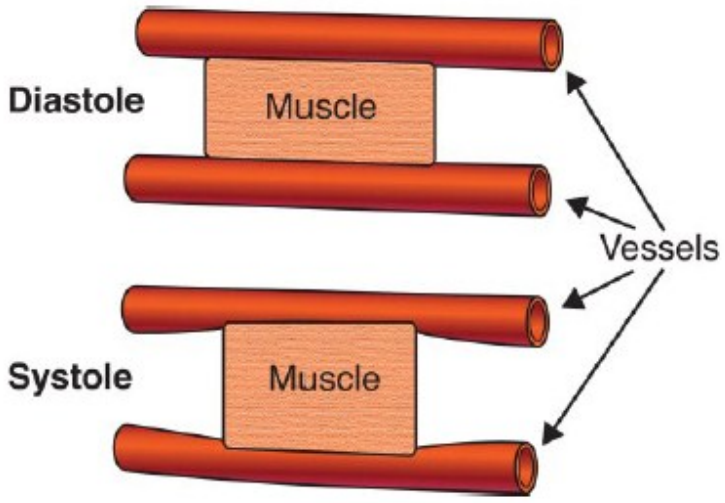


**Figure 2.5**: As the myocardium contracts, individual myocytes shorten and increase in diameter, causing compression of the intramyocardial vasculature (Westerhof *et al.* 2006).

## 2.5 Models proposed to explain differential coronary flow in systole and diastole

### 2.5.1 The vascular waterfall model

The vascular waterfall model was proposed as a mechanism to describe the impediment of coronary flow during systole. The intra-ventricular pressure exerts a pressure on the vascular lumen of the small blood vessels contained within the myocardium, such that the intramyocardial pressure is assumed to be equal to the ventricular pressure in the subendocardial layer and negligible in the subepicardial layer. Therefore calculation of resistance is more complex than simply assessment of the arterial – venous pressure difference. The "waterfall pressure" occurs as there is an interstitial pressure during ventricular contraction, transmitted to the vascular lumen. However, the waterfall model assumes that the coronary resistance is not affected by cardiac contraction and does not allow for systolic reversal of flow or changes in vascular resistance or volume (Westerhof *et al.* 2006).

### 2.5.2 The intramyocardial pump model

The intramyocardial pump model (Spaan *et al.* 1981a) was a progression of the waterfall model that allowed for changes in vascular volume and resistance. Vascular compliance, however, was assumed to remain constant. This was not thought to be sufficient, leading to the time varying elastance model.

### 2.5.3 The time varying elastance model

Vascular compliance is likely to be important as the increased thickening and stiffness of the ventricle in systole will have an impact both on the vascular volume and the elastance

of the vasculature itself. Elastance is defined as the ratio of the ventricular pressure to the left ventricular volume. Elastance will therefore change throughout the cardiac cycle independently of the ventricular preload and afterload. As discussed above, thickening of the myocardium in ventricular systole leads to an increase in muscle diameter and this may impinge on small vessels running through the myocardium as well as increasing the wall tension of these vessels. The pressure-area relationship for a small vessel embedded in the myocardium is therefore different in systole to diastole (Westerhof *et al.* 2006). The time varying elastance model describes coronary flow impediment during systole as a result of the contractility of the left ventricle rather than the pressure within the ventricle (Krams *et al.* 1989).

### 2.5.4 The vascular deformation model

Finally, as well as reducing the diameter of vessel, ventricular contraction may also deform the microvasculature, causing distortion of the vessel path and tortuosity. This will additionally change the resistance of the microvasculature (Pries *et al.* 1997). There is heterogeneity in the composition of the microcirculation across the myocardium. During systole, flow is lower in the subendocardial layers compared to the subepicardium. The effects of ventricular contractility were investigated by use of dobutamine to increase cardiac contractility. With dobutamine, the reduction in systolic subepicardial flow was greatest compared to subendocardial systolic flow (Iwanaga *et al.* 1995). This may occur as vascular deformation and shortening of the muscle fibres is greatest in the subendocardium (Westerhof *et al.* 2006).

Work by Toyota (Toyota *et al.* 2005) demonstrated flow reversal in the subendocardial arterioles during systole with the diameter of these vessels approaching zero at the point of maximal compression. However, the subepicardial arterioles showed no reversal of flow and diameter was largely unchanged during systole compared to diastole. The fact that the vessels do not completely collapse suggests that, in contrast to the waterfall model, that the intramyocardial pressure is not equal to the lumen pressure as one would expect complete collapse if the arterioles were subject to the systolic pressures within the LV cavity. The interaction between the intramyocardial pressure and the interstitial pressure is likely to also be affected by the ease at which interstitial fluid can move as well as mechanical cross talk (Westerhof *et al.* 2006). When the intramyocardial pump is unable to displace intravascular fluid, muscle contraction will be reduced.

### 2.5.5 Wave intensity analysis

Davies et al (Davies *et al.* 2006a) employed coronary wave intensity analysis to explain the variations in coronary flow during the cardiac cycle. At the start of the cardiac cycle, myocardial contraction begins. This generates a proximally originating wave, the forward compression wave due to ejection of blood from the ventricle into the aorta. As the ventricle contracts, it also produces a distally originating wave due to compression of the microcirculation by the contracting myocardium. This distally originating wave decelerates flow in the coronary artery and is termed the early backward travelling compression wave. In the healthy circulation, the opposing effects of these two waves results in a plateau of coronary blood flow. After the early backward travelling

compression wave is a second distally occurring wave, the late backward travelling compression wave. This results from passive reflection of the forward travelling pushing wave and also continued compression of the microcirculation.

As the ventricle begins to relax at the start of diastole, a further two waves produced, again one proximally originating and one distally originating. The proximal wave is a forward travelling expansion wave, causing deceleration of blood flow. This wave results from slowing of ventricular contraction, causing a "suction" effect at the aortic end of the coronary artery and decelerating blood travelling down the coronary artery. Distally, the late backward travelling decompression wave, resulting from relief of pressure on the microcirculation, causes blood to accelerate down the coronary artery. This wave dominates over the proximal wave and so the net effect is of increased flow velocity within the coronary artery and a falling intra coronary pressure. Finally, a late forward travelling pushing wave results from closure of the aortic valve, accelerating blood down the coronary artery (Davies *et al.* 2006a).

Davies found that 94% of wave energy that resulted in acceleration of blood down the coronary artery came from two waves: the proximally originating forward compression wave and the distally originating backward decompression wave. There was less change in coronary velocity as a result of the forward compression wave compared to the change in velocity resulting from the backward decompression wave. This is because the forward compression wave is rapidly opposed by the early and late backward travelling pushing waves which occur due to compression of the microcirculation as well as

reflection of the forward travelling pushing wave. The dominant backward travelling decompression wave has a larger effect on coronary blood flow velocity. This is because this wave, unlike the forward compression wave, is not opposed by its own reflections and the opposing waves at the same time are smaller and more short lived.

## 2.6 Assessment of coronary flow in HCM

Coronary flow has been measured both invasively and non invasively in several studies of small populations of hypertrophic cardiomyopathy patients in comparison with control populations. Coronary flow velocities are typically higher at rest in HCM compared to controls, with systolic flow reversal commonly seen.

### 2.6.1 Invasive studies: measurement of coronary flow and coronary resistance

Yang (Yang *et al.* 2004) assessed coronary haemodynamics in 8 symptomatic HCM patients and compared them with 8 matched controls. They demonstrated a higher coronary flow, lower coronary resistance and lower CFR in HCM compared to control patients. The study population all had unobstructed epicardial coronary arteries confirmed on invasive angiography. The control population had atypical chest pain and a normal coronary flow reserve. LVOT gradient was assessed using simultaneous measurements of ascending aorta and LV inflow pressures. Two patients had apical hypertrophy and 6 hypertrophy affecting predominantly the septum and lateral wall. The coronary arteries were significantly larger in HCM patients compared to normal controls (LAD of 3.1+/- 0.4 in HCM and 2.6+/-0.3mm in control patients). Coronary flow in the LAD was greater in HCM patients compared to control patients. The coronary

resistance, however, was lower in HCM patients than controls. CFR was lower in HCM than controls (2.1+/-0.7 versus 3.4+/-1.0). There was a direct correlation between the CFR and coronary resistance but no correlation between CFR and LVOT gradient. Coronary flow during systole was significantly lower in HCM compared to controls and reversal of flow during systole was commonly seen (63% of cases with reversal of flow, 25% with zero coronary flow in mid systole. This was thought to relate to the degree of LVH as there was a significant inverse correlation between systolic VTI and septal wall thickness. Perhaps as an attempt to compensate, the diastolic VTI was higher in HCM compared to controls, however this was insufficient to produce a normal CRF.
The direct relationship between CFR and coronary resistance was therefore thought to provide evidence that HCM patients have near-maximal vasodilatation of the microcirculation in an attempt to compensate for the increased LV mass. The authors hypothesise that the previously described compression of microcirculation and narrowing of intramyocardial small arteries and arterioles is unlikely to be the predominant cause of the reduced CFR as if this were the case, an increased coronary resistance would be expected.

Cannon et al assessed a cohort of 20 patients with HCM compared to 28 control subjects. They measured coronary flow in the great cardiac vein, the left ventricular filling pressure, the lactate and the oxygen content. HCM patients had a higher blood flow in the great cardiac vein at rest compared to controls and a lower coronary resistance. The LVEDP was higher and pulmonary artery wedge pressure was lower. Pacing of the coronary sinus was performed at paced heart rates up to a maximal heart rate of 150bpm.

In the control patients, there was a steady increase in coronary flow with increased heart rate. In the HCM patients, there was an initial increase in coronary flow, but then fell after a heart rate of 150bpm, associated with chest pain in the majority of the patients (Cannon *et al.* 1991).

Patients with LVOT obstruction had a higher resting flow in the great cardiac vein and lower coronary resistance than those without resting obstruction. The LVEDP was similar between patients with and without resting LVOT obstruction. This increased by a small amount with pacing (from 16±6mmHg at rest to 20±6 with pacing). Pacing resulted in a reduction of LVOT gradient (75±37mmHg at peak pacing compared to 37±25mmHg at rest). There was a significant increase in LVEDP with pacing in the HCM patients but not the control patients. Those with the greatest increase in LVEDP had a fall in cardiac vein flow when pacing was performed from a moderate to peak level of pacing. At the higher pacing rate, 18/20 of the HCM patients experienced their typical chest pain.

Control subjects showed increased lactate consumption from rest to peak pacing. Patients with HCM had decreased lactate consumption with 6/20 patients producing lactate at peak pacing. There was no difference between the LVOT obstruction and no LVOT obstruction groups. However, use of lactate as a marker of ischaemia must be cautious as abnormal lactate metabolism has been reported in animals with no myocardial hypoxia or ischaemia and angiographically normal coronary arteries (Jackson *et al.* 1978).

### 2.6.2 Measurement of coronary flow using echocardiography

Ahn (Ahn *et al.* 2013) assessed a population of patients with asymmetrical septal hypertrophy (ASH) and compared them to a population with apical HCM (ApHCM) using transthoracic echocardiography to assess the mean diastolic coronary flow at rest and following adenosine infusion in the mid to distal LAD. The coronary flow reserve was defined as the ratio of the mean diastolic coronary flow velocity after adenosine compared to that at rest. They found the basal mean diastolic coronary flow to be higher in patients with ASH than in healthy controls, with similar mean diastolic coronary flow in ApHCM and healthy controls. After adenosine, the coronary flow was significantly lower in both subtypes of HCM compared to the control population. The coronary flow was compared to abnormalities on stress myocardial perfusion using CMR. Patients with abnormal stress myocardial perfusion tended to have a lower coronary flow reserve than those with a normal perfusion scan. Patients with a CFR of 2 or less had a higher E/E' ratio, a higher baseline mean diastolic coronary flow velocity and a higher rate pressure product before and after adenosine infusion.

## 2.8 Summary

In summary, abnormalities in perfusion and coronary flow have both been commonly reported in series of patients with HCM. Abnormal perfusion is thought to result from (1) increased demand from the hypertrophied myocardium (2) impaired relaxation of the fibrosed ventricle and (3) abnormalities of the small blood vessels within the heart (microcirculatory dysfunction). PET and, more recently, CMR studies, have shown that perfusion is often normal at rest but there is a failure to increase perfusion sufficiently

with stress vasodilators. Coronary flow abnormalities are commonly seen in HCM, with flow that is typically increased at rest and with a reduced coronary flow reserve. Abnormalities are most pronounced during ventricular systole, where coronary flow may be absent or even reversed. However, the exact mechanisms behind these abnormalities have not been clearly described, nor have the abnormalities of flow been directly related to the abnormalities of perfusion observed downstream in the myocardium.

# CHAPTER 3

## Wave Intensity Analysis

I have previously described the contribution of coronary wave intensity analysis (WIA) in improving understanding of the mechanisms underlying the temporal changes in coronary flow within the coronary arteries in the healthy circulation. In this chapter I will review the development of WIA and the mathematical concepts and assumptions that underlie the technique.

### 3.1 What is wave intensity analysis?

Unlike the systemic arteries, the coronary arteries have circulatory pressure generated from both the proximal and the distal end of the artery. In the systemic arteries, blood flow can be conceptualised more easily, as a pressure gradient occurs along the artery, driving blood towards the capillaries. The situation in the coronary circulation is more complex. Proximally, pressure is generated from contraction of the left ventricle into the aorta and distally, compression of the microcirculation causes distally generated pressure. The relative contribution of the proximally and distally occurring forces determine the speed and direction of blood flow within the coronary arteries.

Wave intensity analysis allows separation of the relative contribution of these proximal and distal forces on the coronary circulation throughout the cardiac cycle. A wave is defined as "a disturbance that propagates from one place to another over time"(Sen *et al.* 2013c) and in the circulation, waves are used to represent the conversion of elastic energy within the arteries to kinetic energy of the blood. Therefore a "waveform" of pressure $P$ and velocity $U$ may be described as the summation of successive wavefronts propagating forwards or backwards in the artery with magnitudes $dP_{\pm}$ and $dU_{\pm}$ (Parker 2009). "Wave intensity" refers to a measure of the instantaneous energy flux due to waves within a system. It is important to emphasise that in arterial waves, $P$ and $U$ are not independent, but that any change in $P$ must be accompanied by a change in $U$.

Wave intensity analysis (WIA) is an alternative to Fourier analysis. It uses methods first used to describe gas dynamics and applies the principles of conservation of mass and momentum in elastic vessels to the cardiovascular system. While Fourier analysis allows a complex waveform to be defined as the composite of a series of sine waves of different frequencies, WIA defines waves in the time domain (e.g. during the cardiac cycle), rather than the frequency domain. This has several advantages. It does not assume that the circulation is always in a steady state, nor does it assume that the period of a cardiac cycle is regular.

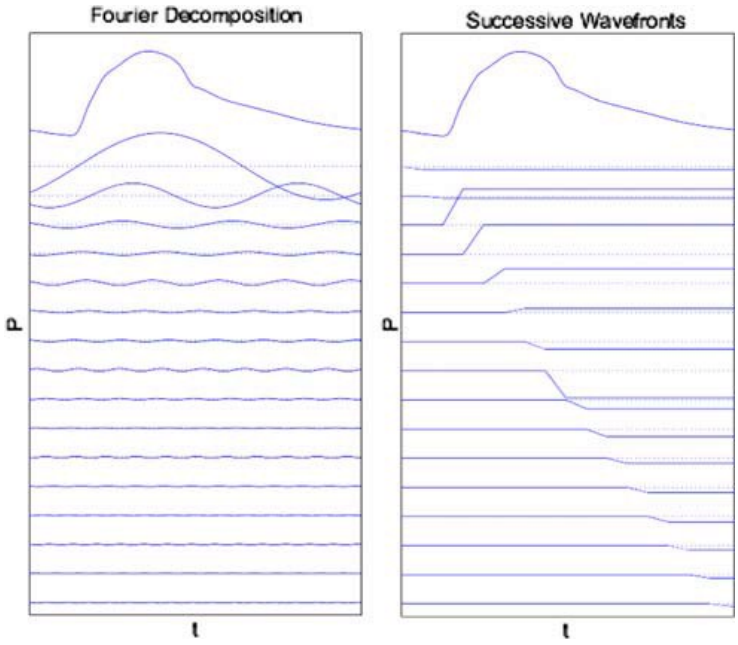


**Figure 3.1**: A complex pressure waveform may be decomposed by Fourier analysis (left panel) or wave intensity analysis (right panel). In Fourier analysis, the wave is decomposed into sinusoidal wavetrains, whereas in wave intensity, successive wavefronts are described over time (Parker 2009).

Wave intensity is derived from pressure and flow changes measured simultaneously in the vessel of interest, traditionally measured invasively at the time of angiography (Sen *et al.* 2013b). It is important to clarify a few key points in terminology at this point. Firstly, a wavefront is defined as a series of propagating waves in a given direction. The waveform refers to the shape and magnitude of a signal, for example the shape of the pressure or coronary flow velocity signals recorded at cardiac catheterisation. While in some instances, a wave is associated with the bulk movement of blood along the vessel, this is not always true. In WIA, a wave may result from the transmission of energy in a

longitudinal direction, in the same way as energy may be transmitted along a "slinky" spring while each end of the slinky remains stationary.

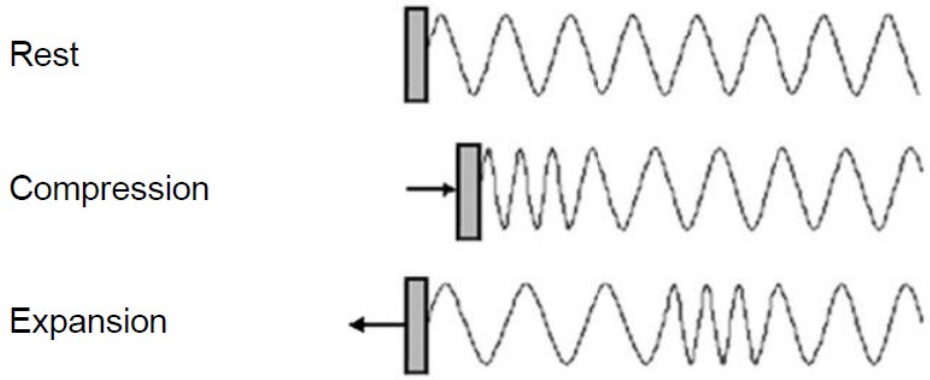


**Figure 3.2**: Effects of compression and expansion on waves travelling along a "slinky" spring. Energy may be transmitted even though each end of the spring remains stationary (Hughes *et al.* 2008).

### 3.2 Use of WIA to understand coronary haemodynamics in health and disease

Inspection of the changes in pressure and velocity allow determination of the major waves responsible for changes in coronary haemodynamics at each given point in the cardiac cycle. Table 1 demonstrates the four possible combinations of pressure and flow. If pressure increases and flow increases, this indicates a proximally occurring wave that accelerates flow into the coronary artery. When pressure increases but coronary flow velocity decreases, this represents a decelerating, distally occurring wave. A decrease in pressure but an increase in velocity indicates a distally occurring, accelerating wave and a decrease in pressure with a decrease in velocity a proximally occurring deceleration wave (Davies *et al.* 2006a).

| Pressure | Velocity | Wave Origin | Wave Nature |
|---|---|---|---|
| ↗ | ↗ | Aortic end (proximal origin) | Accelerating |
| ↖ | ↙ | Microcirculatory end (distal origin) | Decelerating |
| ↘ | ↖ | Microcirculatory end (distal origin) | Accelerating |
| ↙ | ↙ | Aortic end (proximal origin) | Decelerating |

**Table 3.1**: The potential combinations of pressure and velocity changes measured within a coronary artery and the information about the nature of the underlying wave that can be derived (Davies *et al.* 2006a).

Waves can be classified according to their origin and their effect on pressure and flow. In forward waves, pressure and flow change in the same direction. In backward waves, pressure and flow change in opposite directions. Compression waves will increase pressure while an expansion wave results in a decrease in pressure. Therefore, waves can be classified into 4 types: a forward expansion wave, a forward compression wave, a backward compression wave and a backward expansion wave. The FCW and BEW cause acceleration of flow while the BCW and FEW cause deceleration of flow. So, for example, a BEW resulting from relaxation of the ventricle will decrease pressure and accelerate flow along the coronary artery (Rolandi *et al.* 2012).

### 3.3 Separated and net wave intensity

For consideration of coronary haemodynamics, waves can either be separated and described as the proximal components separately to the distal components, separated wave intensity, or the overall effect of both proximal and distal waves can be combined to give the net wave intensity. For net wave intensity, the direction of the net wave will

be the same as the dominant wave between the distal and proximal effects. Whether distal or proximal waves predominate will be determined by the timepoint within the cardiac cycle and any cardiac pathology present. These waves may be derived by measurement of the rate of change in flow velocity and the rate of change in pressure simultaneously at a single point (Hadjiloizou *et al.* 2008). An example of separated and net wave intensity in the coronary arteries is given below (Figure 13).

The change in pressure as a result of a wave may be described either as compression or decompression. Waves associated with an increased pressure may be described as compression (or pushing) waves and waves associated with a decrease in pressure are described as expansion (or pulling/suction) waves.

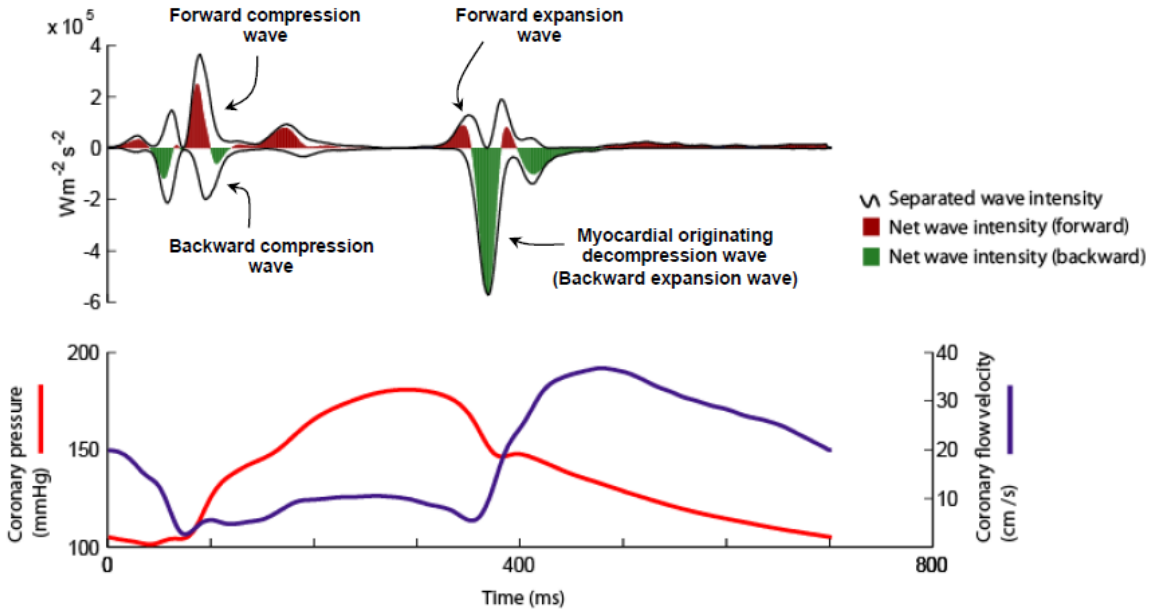


**Figure 3.3:** Wave intensity throughout the cardiac cycle in a normal patient. The top graph shows the separated (black outline) and net wave intensity (filled shapes) for a

cardiac cycle. The bottom panel displays the pressure and coronary flow velocity curves over time that were used to derive the wave intensity data (Sen *et al.* 2013b).

### 3.3.1 Net and separated wave intensity analysis

The *net wave intensity*, measured in $Ws^{-2}m^{-2}$, is defined as the product of the pressure change (dP) and the flow velocity change (dU) at each point during the cardiac cycle. Wave originating from the proximal end of the vessel have positive values and those originating distally have negative values.

*Net wave intensity*:

$$WI\ net = WI_+ + WI_- = \left(\frac{dP}{dt}\right)\left(\frac{dU}{dt}\right)$$

The net wave intensity does not require knowledge of the local wave speed and therefore is a robust measure of net wave properties. Separated wave intensity allows separation of waves into proximally originating and distally originating waves. This is particularly useful in the coronary arteries, where separate distal and proximal effects are in play, however requires estimation of the local wave speed.

*Proximally originating wave intensity:*

$$WI_+ = \frac{1}{4\rho c}\left(\frac{dP}{dt} + \rho c\frac{dU}{dt}\right)^2$$

*Distally originating wave intensity:*

$$WI_- = -\frac{1}{4\rho c}\left(\frac{dP}{dt} - \rho c\frac{dU}{dt}\right)^2$$

Where ρ is the blood density (taken as 1050kg/m$^3$, *c* is the local wave speed, *dU* is the incremental change in coronary flow velocity and *dP* is the incremental change in coronary artery pressure

The data may be presented as the peak wave intensity, a measure of the magnitude of the wave, or the area under the curve for a single wave, the cumulative wave intensity, calculated as follows:

$$I = \int_{t(start)}^{t(end)} dIdt.$$

Here, *I* represents the wave energy i.e. the energy flux carried by the wave and has units of J/m$^2$. The advantage of the integral approach is that a weaker wave of longer duration may be equally as important as a wave of greater magnitude but shorter duration. Integration allows a more direct comparison than the magnitude of the wave only.

### 3.4 Assumptions of the WIA technique

WIA uses a 1 dimensional approximation of arteries and therefore an artery is considered to be a long thin tube. The increase in velocity towards the centre of the artery and the no slip condition at the wall are not accounted for in WIA.

The single point measure of local wave speed (Davies *et al.* 2006b) is assumed to be constant. Local wave speed is estimated using measurements of pressure and flow at a single point in the coronary vessel. This has been shown to be correct when taken over at least one complete cardiac cycle (Sen *et al.* 2013b). The units of wave intensity may be Wm$^{-2}$s$^{-2}$ or Wm$^{-2}$. The latter was commonly used in earlier WIA publications, where the definition of wave intensity was equal to *dPdU*. However, more recent publications

refined the definition to $\left(\frac{dP}{dt}\right)\left(\frac{dU}{dt}\right)$ and this is the definition used within this thesis. This has the advantage that it allows direct comparisons of wave intensity taken at different sampling frequencies. Since wave intensity is measured in the time domain, an increase in the sampling frequency will increase the wave intensity. Use of the later equation allows measurement of wave intensity independent of time and sampling frequency.

### 3.5 Estimation of local wave speed

The wave speed varies between arteries and changes from the proximal to the distal aorta. An estimate of the local arterial wave speed is required to be able to separate wave intensity into proximally originating and distally originating waves. The local arterial wave speed may be determined by measurement of the transit time of a wave from one site to another. Alternatively, it may be calculated if the elastic properties of the vessel and the dimensions of the artery wall are known, however this would require invasive measurement of properties of the arterial wall which typically cannot be performed in vivo.

While the water hammer equations may be used to calculate the wave speed in the systemic arteries, an alternative technique was required for estimation of wave speed in the coronary arteries as this would require the assumption that there is a sufficient period of the cardiac cycle free of reflected waves. Therefore Davies *et al* validated a new technique for use in the coronary arteries, validated in the aorta against the foot to foot pullback method in the aorta (Davies *et al.* 2006b).

### 3.5.1 Methods of calculation of the local wave speed

Two approaches may be used to calculate the local wave speed: the *PU* loop method and the sum of squares. The *PU* loop method involves plotting *P* against *U*. This plot will be linear when only forward travelling waves are present ,with a gradient of $\rho c$. This is a robust and reliable method to determine the local wave speed, however it requires a sufficient period of the cardiac cycle that exhibits this linear relationship with wave only occurring from either the proximal or distal end. In the systemic and pulmonary arteries, such a period occurs in early systole, however such an assumption cannot be made in the coronary arteries. A practical difficulty of this approach is that small time lags, even of only 5ms between measurement of *P* and *U* may have significant impact on the calculated local wave speed.

The sum of squares method may be used when it cannot be assumed that there is a period where only forward waves are present in the artery. This method is based on the observation that the use of an incorrect wave speed will result in the calculation of self cancelling forward and backward wave intensity. Since the sum of the separate wave intensities must be equal to the net wave intensity, minimising the magnitude of the separated wave intensities may be used to determine the wave speed. The following equations may be used to minimise the sum of the absolute values of the separated wave intensities as a function of *c*, the local wave speed (Parker 2009).

$$W = \sum |dI_+(t)| + \sum |dI_-(t)| = \frac{1}{2}\sum \left(\frac{\mathrm{d}P^2}{\rho c} + \rho \mathrm{d}U^2\right)$$

when the sum is taken over the cardiac cycle. To minimise with respect to *c*, this equation may be simplified as follows:

$$c = \frac{1}{\rho}\sqrt{\frac{\sum dP^2}{\sum dU^2}}$$

Both the PU loop and sum of squares methods work well in in vitro experiments, however the sum of squares method has not been well validated in the coronary arteries. Measurements made in the coronary arteries before and after percutaneous coronary intervention resulted in non physiological results (Kolyva *et al.* 2008). This may be due to large reflection sites close to the measurement site or neglect of the reservoir pressure in calculations, however further data is needed.

Since wave intensity is affected by the gradient of the pressure and coronary flow velocity waveforms, it is very sensitive to noise in measurement. Therefore, a Savitzky-Golay filter is typically employed which will allow smoothing of noisy data without erosion of peaks in the data (Savitzky & Golay 1964). This filter will fit a polynomial of a chosen order to a chosen number of points around the centre point using the least squares method.

### 3.6 Wave intensity: studies in cardiovascular physiology

WIA has been used to study cardiovascular physiology in a number of situations to date, including the aorta (Parker & Jones 1990), the coronary arteries (Davies *et al.* 2006a) and the carotid, brachial and radial arteries (Zambanini *et al.* 2005).

When a wave encounters a discontinuity in conditions, reflection of the wave occurs. A discontinuity occurs when there is a physical change in boundaries, for example, when there is a bifurcation of a coronary artery, when there is a change in local wave speed or a change in cross sectional area of the vessel (Parker 2009). At a bifurcation, the size of reflected waves is dependent on the area and wave speed of the parent and daughter vessels. Waves propagating from parent to daughter vessels are considered to occur under well matched conditions. However, waves travelling from daughter back into parent vessels are poorly matched. This results in "wave trapping", where wave reflection is significant. This is analogous to sound absorption: the multiple wave reflections results in considerable damping in the arterial tree (Parker 2009).

### 3.6.1 Coronary haemodynamics in the healthy heart

As described in the previous chapter, Davies *et al* (Davies *et al.* 2006a) studied 20 patients with a clinical indication for coronary angiography. The pre-test probability for coronary disease in these patients was considered to be low and the exclusion criteria include previous coronary intervention, left ventricular impairment, valvular disease, regional wall motion abnormalities on echocardiography, rhythms other than sinus and the use of nitrates in the 24 hours preceding angiography. While the history of chest pain was generally atypical, subjects did have risk factors for coronary artery disease (including microvascular disease) with 12/20 having hypertension, 9/20 current smokers, 13/20 with total cholesterol >5mmol/L. No patients had diabetes.

Davies took care to minimise physiological variation in coronary flow as a result of physical, psychological and pharmacological factors. Therefore patients rested in bed for at least an hour before angiography, smokers were asked to refrain from smoking for 24 hours prior to the study and all patients were asked to avoid caffeine containing beverages and alcohol for at least 12 hours prior to study. As patients were nil by mouth for the procedure, patients had not eaten for at least 9 hours prior to angiography. To minimise psychological stress, patients were reassured and had careful explanation of the procedure prior to study. Finally, drugs that were thought most likely to impact on coronary haemodynamics, namely nitrates, were withheld for at least 24 hours prior to the procedure.

Using WIA, Davies *et al* identified six waves within the cardiac cycle. These waves allowed explanation of the coronary flow profile seen in the healthy heart. During ventricular systole, myocardial contraction generates the forward compression wave due to ejection of blood from the ventricle into the aorta, and the early backward compression wave due to compression of the microcirculation. In the healthy circulation, the opposing effects of these two waves results in a plateau of coronary blood flow. After the early backward travelling compression wave comes the late backward travelling compression wave, resulting from passive reflection of the forward travelling pushing wave and continued compression of the microcirculation.

As the ventricle begins to relax, two further waves are generated. Proximally, a forward travelling expansion wave causes deceleration of blood flow, while distally, the dominant backward expansion wave, resulting from relief of pressure on the microcirculation, causes acceleration of coronary flow. Finally, a late forward travelling pushing wave results from closure of the aortic valve, accelerating blood down the coronary artery (Davies *et al.* 2006a).

Davies demonstrated that the dominant backward travelling expansion wave has the largest effect of all the waves on coronary blood flow velocity in the healthy heart. This is because this wave, unlike the forward compression wave, is not opposed by its own reflections and the opposing waves at the same time are smaller and more short lived.

### 3.6.2 Effect of age on coronary haemodynamics

The mean age of patients in the Davies paper was 54±10 years, range 35-75 years. There was a progressive increase in the proportion of total wave intensity made up by the forward travelling expansion wave, while the late travelling compression wave decreased with increasing age. The other waves did not significantly change with age. The increase in forward travelling expansion wave with age may result from an increase in vascular stiffness with an alteration of ventricular-arterial coupling resulting in greater energy delivery into the coronary artery. Another explanation is that the increased wave speed results from increased augmentation of the aortic pressure with age. This would result in a faster decline in pressure (dP/dtmax during relaxation of the ventricle, leading to an increase in magnitude of the forward travelling expansion wave (Davies *et al.* 2006a).

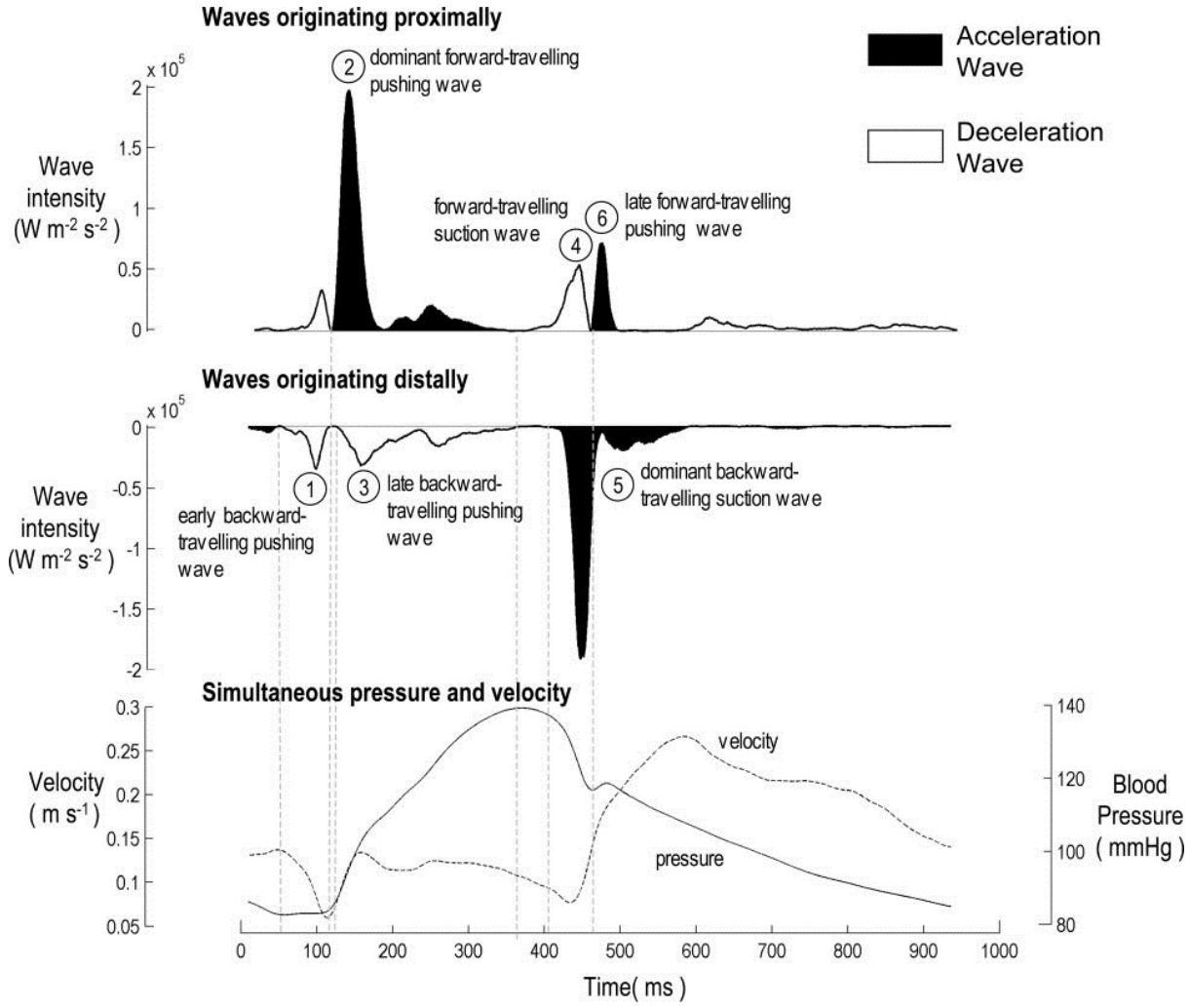


**Figure 3.4 Figure 3.4** Wave intensity analysis in the healthy heart. There are 6 principal waves that occur sequentially during the cardiac cycle and which result in acceleration or deceleration of coronary flow within the coronary arteries.

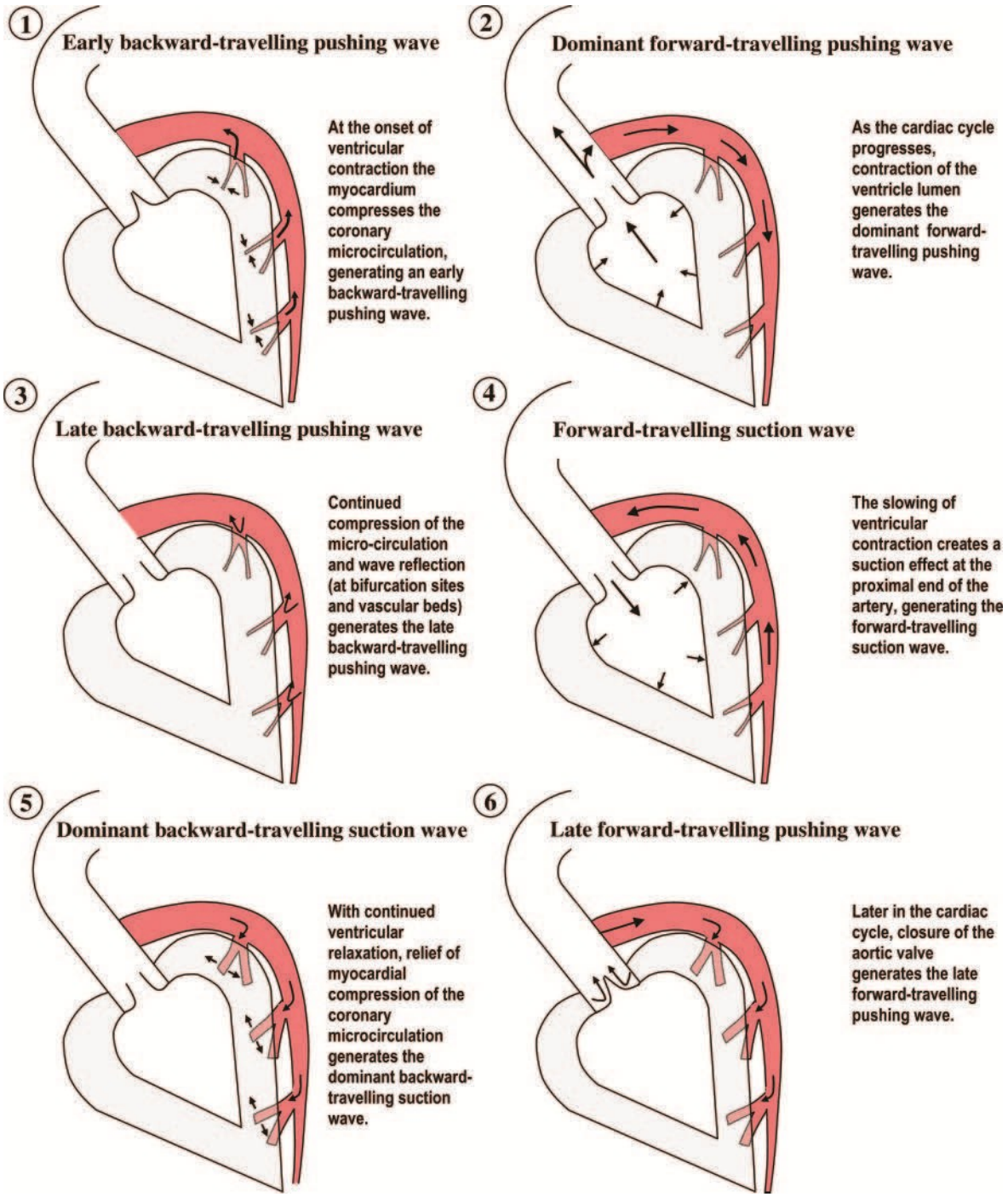


**Figure 3.5** Schematic representation of coronary waves underlying the changes in coronary filling, taken from Davies 2006a

### 3.6.3 Comparison of wave intensity in the LMS and RCA

Hadjiloizou *et al* (Hadjiloizou *et al.* 2008) compared the coronary haemodynamic patterns between the proximal left main stem (LMS) and the proximal right coronary artery (RCA). They studied 20 patients with unobstructed coronary arteries and assessed the coronary flow velocity and performed WIA in the right and left coronary systems. Coronary flow in the proximal RCA was similar in systole and diastole. Coronary flow velocity was lower in the RCA compared to the LMS and this was due to a lower distally originating decompression wave. The distally originating decompression wave in the LMS correlated with the left ventricular pressure and that of the RCA with the estimated right ventricular pressure.

WIA revealed that both the LMS and the RCA showed a pattern of 6 waves, 3 originating from the proximal (aortic) end and 3 from the distal (microcirculatory) end. In both arteries, the first of the proximal waves was a large forward travelling compression wave, causing acceleration of blood down the coronary artery and resulting from ejection of blood from the left ventricle into the aorta and then the coronary arteries. The right coronary artery filling was predominantly from proximally occurring waves, with a smaller backward compression and backward compression wave relative to the LMS. The total cumulative wave intensity was similar between the LMS and the RCA. The authors found that the differences in flow velocity profiles between the RCA and LMS was predominantly due to differences in the distally occurring waves (Hadjiloizou *et al.* 2008).

### 3.7 WIA in disease states

#### 3.7.1 Hypertensive heart disease

WIA has been used to study the effect of different myocardial diseases on coronary haemodynamics. Davies *et al* (Davies *et al.* 2006a) compared a population of hypertensive patients with left ventricular hypertrophy with a healthy population, referred for angiography with atypical chest pain and with a structurally normal heart on echocardiography. Patients with LVH commonly have impaired diastolic function. Davies *et al* demonstrated that a population of 10 patients with LVH had the same pattern of 6 waves as the healthy population, but with a reduced backward travelling decompression wave and a proportionately larger early forward travelling pushing wave. The authors hypothesise that this may result from negative myocardial remodelling with impaired relaxation of the ventricle during diastole (Davies *et al.* 2006a). Sen *et al* suggests that the results provide a mechanism for the common symptoms of shortness of breath in this population, namely that there may be mismatch between perfusion and myocardial mass in the hypertrophied ventricle (Sen *et al.* 2013b). When diastole is shortened, for example, during exercise, there may be further attenuation of the backward travelling decompression wave.

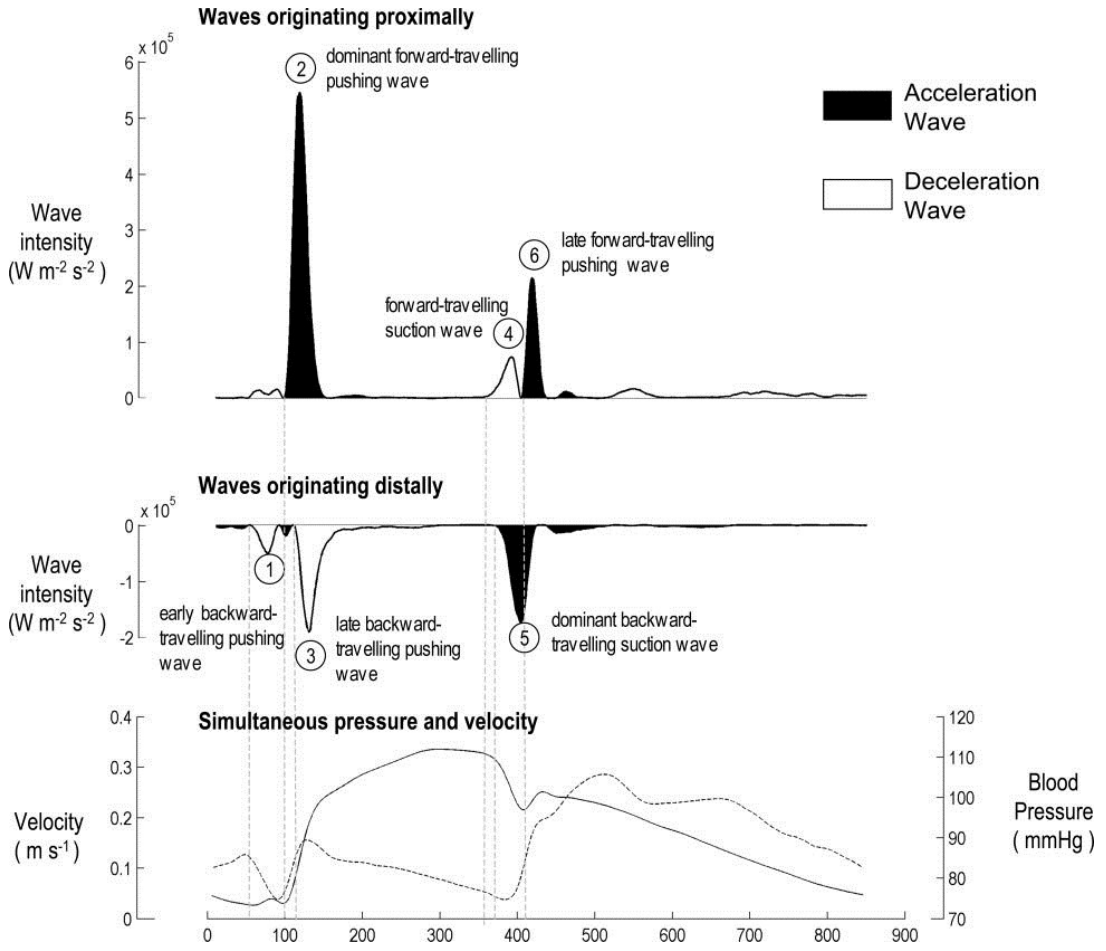


**Figure 3.6:** Effect of left ventricular hypertrophy on coronary WIA: there is attenuation of the BEW due to impaired myocardial relaxation and increase in the BCW due to increased compression of the microcirculation.

### 3.7.2 Measurement of the instantaneous effect of biventricular pacing on coronary filling using WIA

Kyriacou *et al* (Kyriacou *et al.* 2012) assessed a population of patients with chronic heart failure referred for cardiac resynchronisation therapy (CRT). This therapy has been shown to reduce morbidity and mortality in a population with symptomatic heart failure, left bundle branch block (LBBB) and an ejection fraction of less than 35% (Cleland *et al.* 2005). Patients with LBBB and impaired ejection fraction have a less efficient ventricle

as a result of cardiac dyssychrony: as parts of the ventricle contract, others are relaxing. Synchronisation of contraction of the left and right heart is achieved by biventricular pacing. WIA was used to demonstrate the instantaneous effect of this synchronisation on coronary blood flow: there was a significant increase in coronary flow velocity time integral in the left main stem with biventricular pacing at an AV delay of 120ms compared to the baseline intrinsic LBBB pattern. This occurred due to an increase in the backward originating decompression wave. The atrioventricular delay can be altered to improve ventricular filling prior to myocardial contraction. Use of extremes of atrioventricular delay demonstrated reduction in coronary blood flow and WIA was used to describe the mechanism of these changes by the effects on the backward travelling decompression wave.

This study was the first in humans to use WIA to demonstrate the effect of changes in ventricular contraction and relaxation through biventricular pacing on coronary blood flow, resulting in improved coronary haemodynamics, namely an increase in the backward decompression wave.

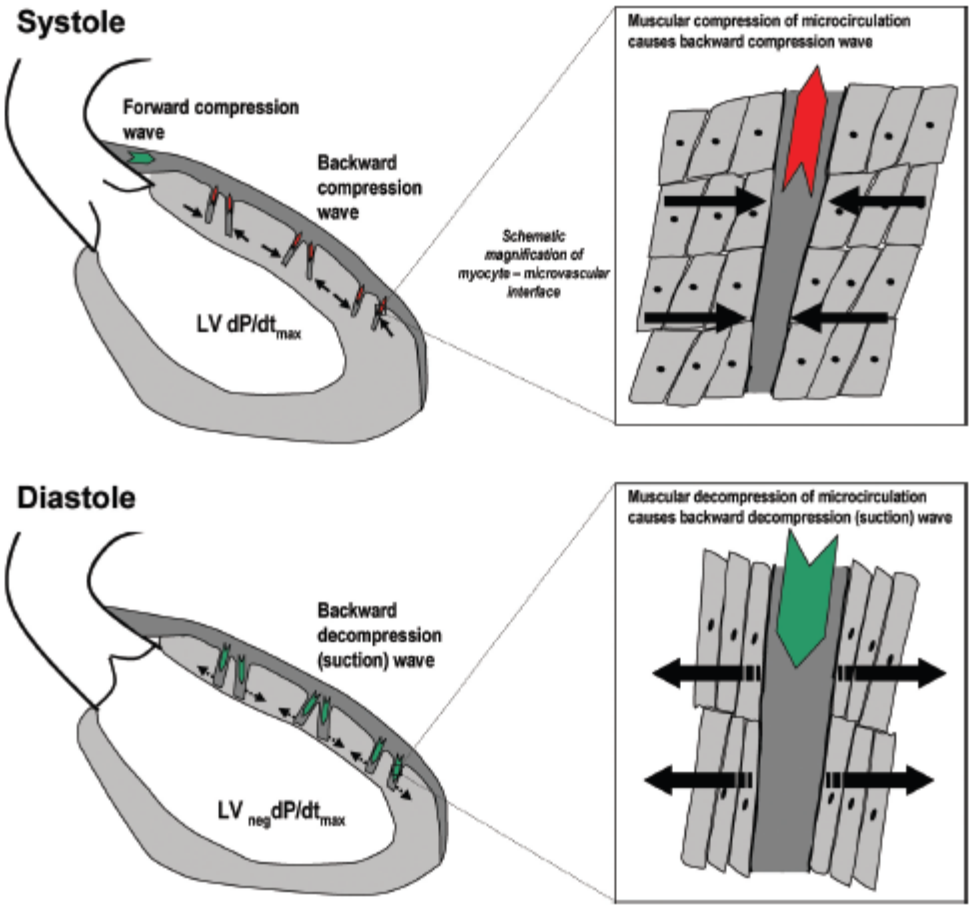


**Figure 3.7**: The action of the main waves on coronary flow. During systole, the forward compression and backward compression waves act in opposing directions. During diastole, the BEW acts to accelerate blood flow in the coronary arteries

### 3.7.3 Aortic stenosis

Aortic stenosis is a fixed obstruction of blood flow from the left ventricle due to disease (most commonly calcific degeneration) of the aortic valve. This increases pressure within the left ventricle and commonly patients develop left ventricular hypertrophy as a result of ventricular contraction against this fixed obstruction. Patients with severe aortic stenosis often complain of shortness of breath or chest pain on exertion and the development of symptoms such as these is a common indication for valve replacement

(Rader *et al.* 2014). This patient group have an impaired coronary flow reserve and increased basal metabolic demand (Eberli *et al.* 1991). There is reduced transcoronary perfusion pressure which has important effects on the coronary haemodynamics.

Davies *et al* assessed the effect of transcatheter aortic valve implantation (TAVI) on coronary haemodynamics in patients with severe aortic stenosis (Davies *et al.* 2011). They demonstrated the immediate effects of relief of aortic stenosis on coronary filling and demonstrated that the backward decompression wave increased following TAVI. Furthermore, they assessed the effect of increasing heart rate (modelled using rapid pacing) on coronary filling. Prior to TAVI, increased heart rate was associated with a reduction in the backward decompression wave. This reversed following the transcatheter valve implantation, with restoration of physiological reserve and an increase in the backward decompression wave at higher heart rates (Davies *et al.* 2011).

The group concluded that the reduction in backward compression wave at increased heart rate may provide a mechanism to explain the common symptoms of angina and shortness of breath in this population.

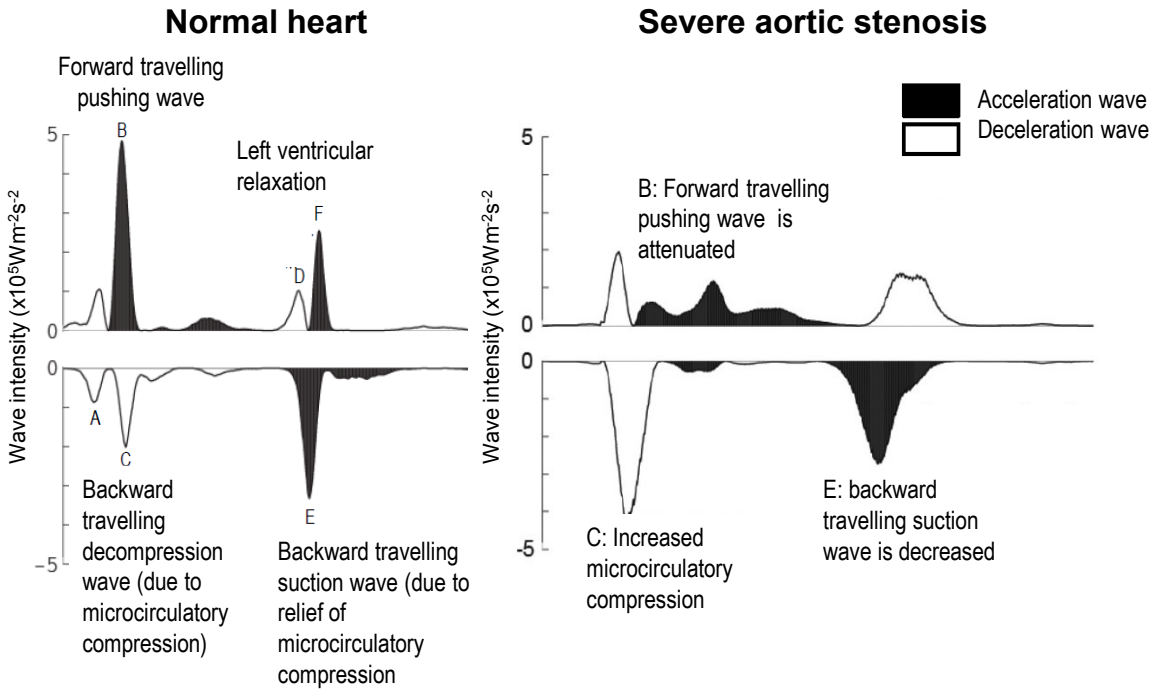


**Figure 3.8:** Comparison of coronary wave intensity in a patient with a normal heart and in a patient with severe aortic stenosis. In aortic stenosis, the forward travelling pushing wave (B) and backward travelling suction wave (E) are attenuated and there is an increased backward travelling decompression wave (C) due to microcirculatory compression and increased LV cavity pressures (Davies *et al.* 2006a, 2011)

### 3.7.4 Coronary haemodynamics in assessment of severity of coronary stenoses

The severity of a stenosis within a coronary artery may be assessed either by measurement of flow proximal and distal to the stenosis or, more commonly, by measurement of pressure proximally and distally. Cardiac catheterisation allows for the simultaneous measurement of pressure both proximal to and distal to a stenosis (Cape *et al.* 1996). The best time in the cardiac cycle to assess these changes is in a "wave free"

period within the cardiac cycle when there are no accelerating or decelerating forces either proximally or distally. At this timepoint, there is a steady decrease in coronary pressure and flow and the microvascular resistance is stable. Resting measurements may be taken at this point to assess the functional significance of a coronary stenosis without the need for adenosine. The instantaneous wave free ratio (iFR) has been shown to have excellent correlation with fractional flow reserve (FFR) (Sen *et al.* 2013a) and ongoing trials will establish whether this measure predicts event free survival.

### 3.7.5 WIA in the aorta

Data collected in the ascending aorta has demonstrated filling patterns within the vessel. Firstly, a forward travelling compression wave accelerates blood, resulting from ventricular contraction. This is followed by a smaller backward traveling compression wave, resulting from reflection from the distal circulation. This reflection of the forward travelling compression wave occurs at sites of impedence mismatch in the distal circulation. Khir and Parker studied the effect of arterial occlusion on this backward travelling compression wave (Khir & Parker 2002). Towards the end of systole, a forward travelling expansion wave occurs, resulting from the deceleration of ventricular contraction prior to aortic valve closure. WIA performed in the carotid arteries, radial and femoral arteries have demonstrated these three predominant waves with additional reflected waves.

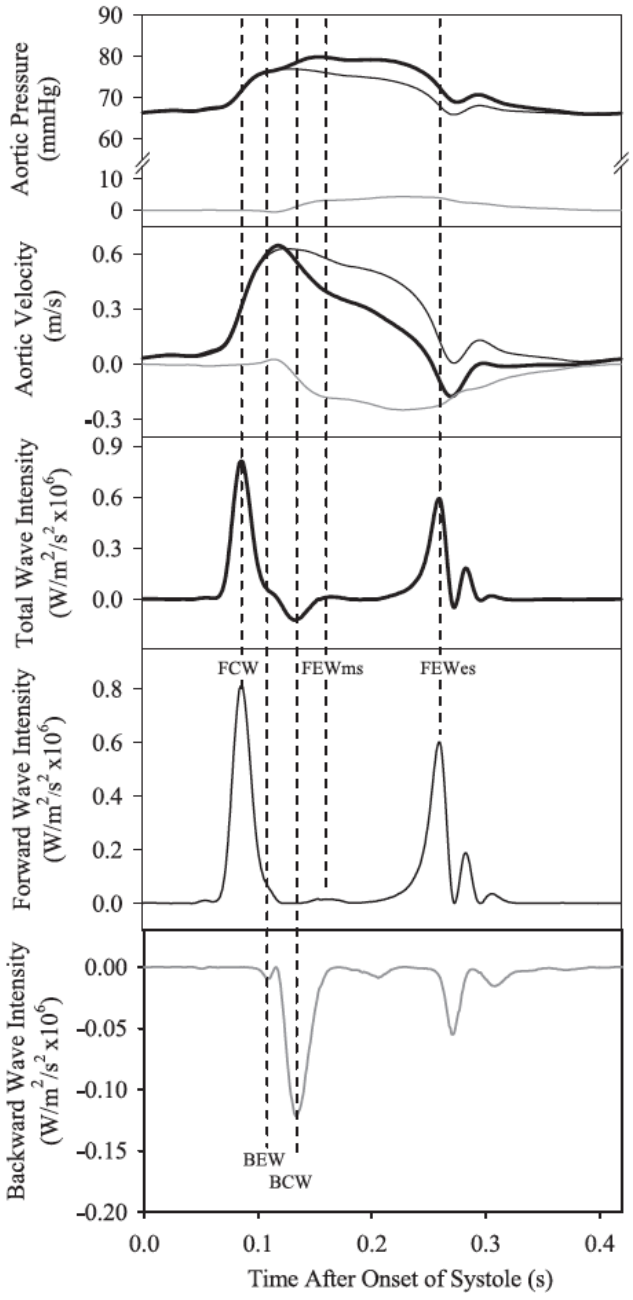


**Figure 3.9**: Wave intensity in the aorta is comprised of three predominant waves: the forward compression wave, the backward compression wave and the forward expansion wave. Taken from (Penny *et al.* 2008)

### 3.8 Summary

Wave intensity analysis allows understanding of the myocardial mechanics that underlie pressure and flow changes in systemic arteries and coronary arteries. Measurement of WIA has improved understanding of the effect of aortic stenosis and left ventricular hypertrophy on coronary artery flow velocity. Application to HCM, where both proximal and distal factors are in play during the majority of the cardiac cycle, is likely to also improve understanding of the factors contributing to both coronary flow and myocardial perfusion abnormalities.

# CHAPTER 4

## Cardiovascular magnetic resonance in HCM

CMR is a valuable tool in HCM in diagnosis, tissue characterisation with late gadolinium assessment and with first pass myocardial perfusion. In this chapter I will review each of these.

### 4.1 Cardiovascular magnetic resonance assessment of HCM

CMR provides useful diagnostic and prognostic information in the assessment of hypertrophic cardiomyopathy. CMR may be used in diagnosis in patients where echocardiography is of insufficient quality for diagnosis and has been shown to identify regions of hypertrophy that may be missed on transthoracic echocardiography, for example in the apex and anterolateral wall (Rickers *et al.* 2005). CMR allows accurate and reproducible measurement of left ventricular volumes, ejection fraction and mass (Pennell 2010).

### 4.2 Late gadolinium imaging

CMR allows tissue characterisation, using late gadolinium imaging. Gadolinium chelates are extracellular contrast agents commonly used during CMR. As gadolinium remains

extracellular, it accumulates in areas of acute infarction, scar or areas where the interstitial space is expanded. In healthy myocardium, the myocytes are densely packed with a small interstitial space and with normal capillary density. Gadolinium therefore washes out rapidly. In areas of fibrosis and infarction, gadolinium will persist (Mahrholdt *et al.* 2005; Simonetti *et al.* 2001). Gadolinium acts to shorten both T1 and T2. At low dose (<0.12 mmol/kg) the predominant effect is shortening of T1 and this shortens in proportion to the concentration of gadolinium in the extracellular space.

Imaging is performed using inversion recovery sequences with the T1 time optimised to null the normal myocardium, i.e. image the normal myocardium as dark. Areas with high gadolinium concentration, such as infarction, will have higher signal intensity and are therefore brighter on inversion recovery sequences (Simonetti *et al.* 2001).

Late gadolinium enhancement is common in HCM and has been shown to be related to areas of replacement fibrosis (O'Hanlon *et al.* 2010). This is commonly midwall, diffuse and patchy in distribution and most commonly, although not exclusively, found in the areas of myocardial hypertrophy (Cummings *et al.*; Debl *et al.* 2006). Approximately 60% of patients with HCM have late gadolinium enhancement (Noureldin *et al.* 2012).

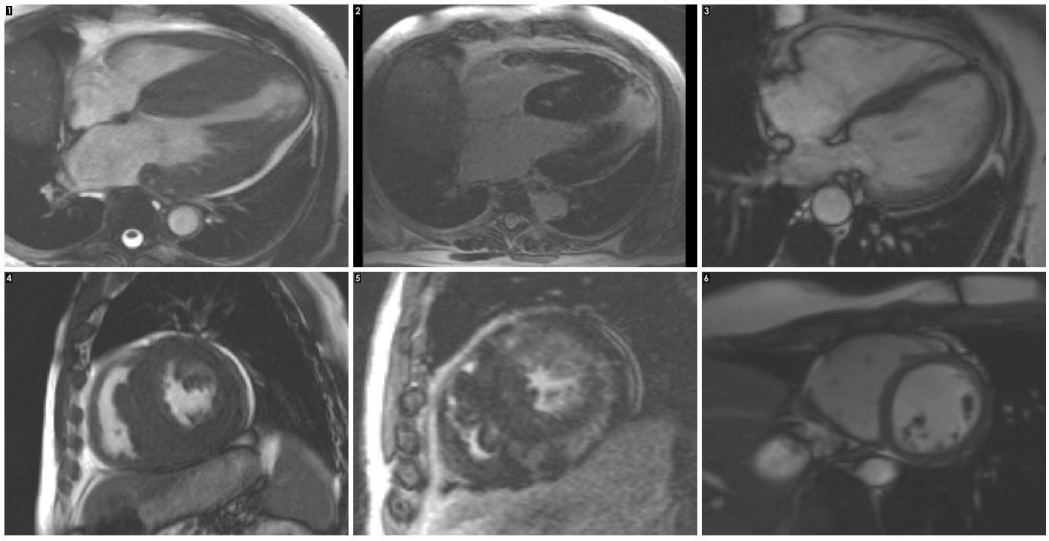

**Figure 4.1**: Cardiovascular magnetic resonance imaging of the heart in HCM (left and middle panels) and of a normal heart (right panels). In HCM, the left ventricle becomes thickened. Late gadolinium imaging (middle panels) demonstrate scarring of the ventricle (white areas).

### 4.3 First pass perfusion CMR

As well as providing a visual assessment of myocardial perfusion, CMR first pass perfusion allows absolute quantification of myocardial perfusion. Perfusion images are acquired at rest and at adenosine stress, following rapid injection of gadolinium contrast. As gadolinium-rich blood is delivered to the myocardium, there is therefore a progressive increase in the signal intensity from dark to brighter (Figure 4.2). Areas with decreased myocardial blood flow (MBF) have a decreased uptake of gadolinium and so appear darker compared to areas of normal perfusion.

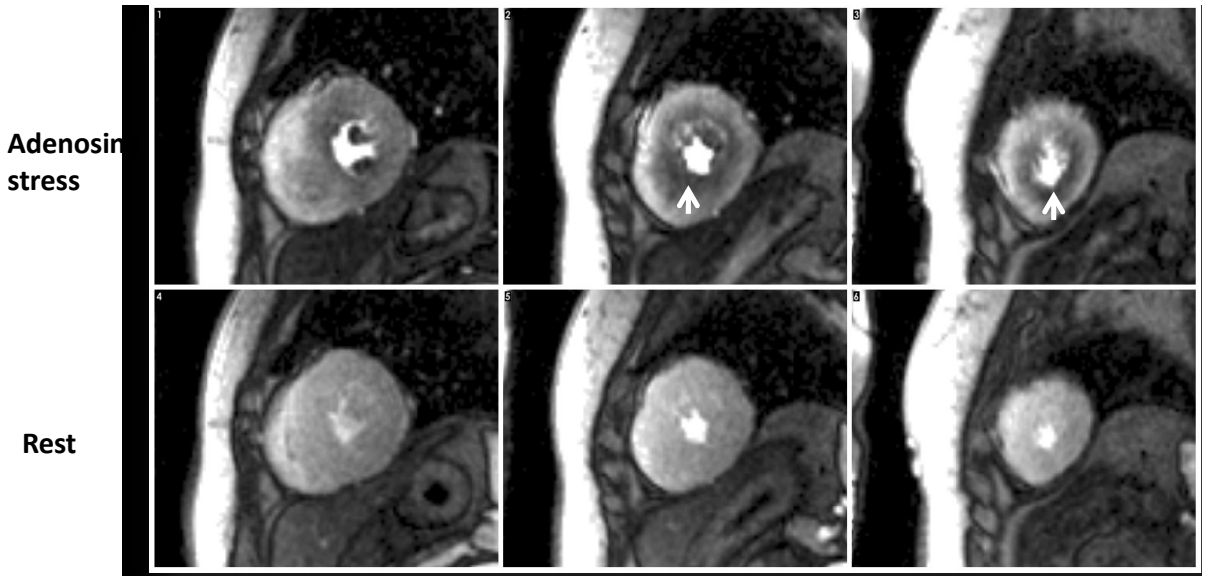


**Figure 4.2**: Visual analysis of myocardial perfusion using CMR. The heart is imaged at three short axis levels, base (left panel), mid ventricle (middle panel) and apex (right panel). Images are recorded at rest (bottom row) and with peak adenosine stress perfusion (top row). Abnormalities of perfusion are often revealed at peak adenosine stress perfusion. These abnormalities appear as a darker area of the myocardium (arrowed).

### 4.4 Quantification of absolute myocardial perfusion by CMR

CMR perfusion is assessed using first pass imaging with gadolinium based extra cellular contrast agents (Gd-DTPA). T1 sensitive pulse sequences with a high temporal resolution allow quantification of the uptake of gadolinium by the myocardium. The change in signal intensity may therefore be measured over time. A compact bolus is rapidly injected via a large peripheral vein and imaging of the myocardium in short axis, typically at three levels over 50-70 frames after injection is acquired. As gadolinium is taken up by the myocardium, the signal intensity increases due to the shortened T1 time.

Up to 50% of the circulating Gd-DTPA diffuses from the intravascular to the extravascular component on first pass through the capillary bed. This is the period of greatest change in signal intensity and may reveal heterogeneity of perfusion in the myocardium as well as allowing sensitive detection of myocardial ischaemia (Daly & Kwong 2013).

**4.5 Stress imaging for ischaemia**

Imaging of ischaemia requires either exercise or pharmacologic stress of the heart, inducing a supply/demand mismatch in the myocardium. Exercise is the most physiological stress, however performance of supine exercise during CMR is challenging, may interfere with image quality and may not achieve a target heart rate. Pharmacological agents such as adenosine or dobutamine are therefore preferred. Dobutamine is a positive ionotrope which causes increased metabolic requirements via an increase in heart rate (chronotrophic response) and an increase in myocardial contractility. It additionally has some vasodilator activity. Adenosine has less of a chronotropic effect and largely acts to induce coronary vasodilation (Daly & Kwong 2013).

### 4.6 Quantification of perfusion abnormalities using CMR

While abnormalities of perfusion may be easy to see on visual inspection in some cases, it is advantageous to also be able to quantify the severity of these abnormalities numerically. If the whole myocardium is under-perfused, this is difficult to assess visually as visual analysis requires reference normal myocardium to allow abnormal myocardium to be identified. Calculation of absolute myocardial perfusion using CMR requires additional imaging so the rate of uptake of gadolinium contrast in the myocardium can be compared to the rate of contrast uptake within the myocardial blood pool. Therefore in addition to the three short axis slices acquired during qualitative perfusion analysis, an additional sequence, the arterial input function is acquired. This is optimised for the left ventricular blood pool, allowing measurement of contrast uptake into the blood pool (Gatehouse *et al.* 2004).

To quantify absolute myocardial blood flow, the signal intensity of the myocardial and left ventricular blood pools are measured. The myocardial time intensity curve (the increase in signal intensity against time) and the arterial input function (the signal intensity of the LV blood pool) are then combined using a Fermi deconvolution function to calculate absolute perfusion of the myocardium. The deconvolution function allows improved signal to noise ratio as it requires the transfer function to take a pre-specified shape, allowing data points due to noise to be discounted. This has been well validated in animal models with labelled microspheres (Hsu *et al.* 2012). The spatial and temporal resolution of this technique is greater than that of nuclear imaging such as positron emission tomography (PET) and CMR offers the additional advantages of (1) assessment

of fibrosis during the same imaging examination (2) no requirement for ionising radiation.

Absolute quantification requires lengthy post-processing and image analysis and so it not used in clinical practice, although has provided important insights into the microcirculation in HCM. Petersen *et al* (Petersen *et al.* 2007), demonstrated significantly impaired hyperaemic myocardial blood flow in HCM (1.84±0.89 mL/min/g compared to healthy controls (3.42±1.76 mL/min/g). The hyperaemic blood flow related to the LV wall thickness, with a greater wall thickness associated with poorer blood flow per unit of myocardium.

**4.7 Summary**

CMR allows measurement of some of the key features of HCM, with accurate measurement of LV dimensions and ejection fraction, tissue characterisation of replacement fibrosis using late gadolinium imaging and assessment of absolute perfusion at rest and hyperaemia, using first pass perfusion imaging.

**Specific Aims of this Thesis**

1. To use coronary wave intensity analysis to better understand the mechanisms of chest pain and perfusion defects in hypertrophic cardiomyopathy

***Rationale***: Although chest pain is very common in HCM, it is not well understood and treatment is difficult. Improved understanding of the underlying mechanisms of chest pain in this complex disease will allow more targeted treatment

2. To develop coronary wave intensity analysis using cardiovascular magnetic resonance

***Rationale***: Coronary WIA allows detailed mechanistic understanding of myocardial mechanics that underlie disease processes. However, invasive data acquisition is associated with a small but significant risk of complications and a non-invasive alternative would be desireable and allow study of a wider population of patients.

**Specific Hypotheses**

***Hypothesis 1***: WIA allows explanation of the observed perfusion abnormalities in hypertrophic cardiomyopathy, with a smaller backward travelling suction wave (due to impaired relaxation) and a larger backward travelling compression wave (due to increased microcirculatory compression) compared to normal subjects.

***Hypothesis 2***: Wave intensity analysis can be performed non-invasively using cardiovascular magnetic resonance in patients with hypertrophic cardiomyopathy.

# METHODS

## 5.1 Invasive haemodynamic study

### 5.1.1 Patient identification

HCM patients studied were identified from the cardiomyopathy service at the Royal Brompton and Harefield NHS Foundation Trust and Liverpool Heart and Chest Hospital. Patients referred had a clinical indication for angiography, typically chest pain, a perfusion defect on non invasive imaging or indications for alcohol septal ablation. Control patients had a clinical indication for angiography and atypical chest pain, recruited from Royal Brompton and Harefield NHS Foundation Trust and Imperial College NHS Foundation Trust.

HCM was defined as the presence of a non dilated and hypertrophied left ventricle in the absence of a systemic or cardiac disease capable of producing the magnitude of LVH seen. All patients had a wall thickness of 15mm or greater on CMR.

For the control population, additionally, patients were required to have a history of atypical chest pain, a normal resting ECG and a structurally normal heart on echocardiography or CMR.

During pre-assessment all patients had a full history and clinical examination. Blood pressure, pulse rate and an electrocardiograph were recorded and blood were taken for full blood count, urea and electrolytes and a group and save.

Ethical approval was granted by Hampshire National research ethics committee (REC ref 12/SC/0732). All patients gave written informed consent for the study. All eligible patients

were sent information about the study and given at least 24 hours to consider whether they wished to participate. They were then contacted by one of the investigators, given opportunity to ask any questions and, if the patient was willing to take part and able to give consent, enrolled in the study.

### 5.1.2 Exclusion Criteria

Patients with known significant epicardial coronary artery disease (defined as >50% narrowing of coronary arteries >2mm), significant hypertension (>140/80 on two successive readings) or other comorbidities such as valvular heart disease that may contribute to left ventricular hypertrophy were excluded.

For control patients, in addition to the exclusions listed above, CMR or echocardiographic evidence of cardiomyopathy, microvascular ischaemia (for example syndrome X) or significant valvular disease (defined as more than mild stenosis or regurgitation of any of the valve) were also excluded.

### 5.1.3 Cardiac catheterisation

Patients enrolled in the study had a clinical indication for cardiac catheterisation for assessment of possible coronary artery disease. This was typically as a result of symptoms of shortness of breath and/or chest pain.

Cardiac catheterisation was performed in the catheter laboratory. Patients were typically pre-assessed with blood taken to assess the renal function and for any unexpected findings which might increase the potential risk of procedural complications, such as anaemia. Patients were consented for diagnostic angiography and quoted a risk of 1 in 1000 for death, stroke, myocardial infarction or need for emergency surgery. All patients had peripheral venous access secured prior to starting the procedure with a 20gauge peripheral cannula.

All patients consented to additional research measurements following completion of diagnostic angiography. They were quoted a small increase in risk as a result of wires placed in the proximal coronary arteries and a small increase in fluoroscopic screening time, equating to the equivalent of about 10 months of background radiation exposure. The potential side effects of an adenosine infusion, including flushing, chest pain and shortness of breath were explained. All patients read the patient information leaflet, had time to ask any questions, discuss with family members and had at least 24 hours to consider inclusion in the study.

Upon entry into the catheter laboratory, patients were asked to lie on the angiography table. The patient was draped using sterile drapes. Peripheral arterial access was established using a 6F sheath and the Seldinger technique. Diagnostic coronary angiography was performed using standard clinical technique. This involved selective intubation of the left and right coronary systems using preformed catheters, typically a Judkins left 4 and Judkins right 4, inserted over an 0,35J guidewire using Seldinger technique.

Fluroscopic images were taken in multiple planes to assess for the presence of coronary artery disease. The left coronary system was engaged using an antero-posterior (AP) projection, and typically imaged in a right anterior oblique (RAO), shallow caudal projection, an RAO cranial projection, a left anterior oblique (LAO) caudal projection, an LAO cranial projection and an AP caudal projection. The right coronary artery was typically engaged in an LAO projection and images taken in LAO, RAO and LAO cranial projections (Mitchell et al. 2008).

### 5.1.4 Invasive pressure and flow measurements

Once diagnostic angiography was completed, the angiographic operator began the study protocol to obtain simultaneous invasive pressure and flow haemodynamic data using the Combomap (Volcano, Europe) system. The console has a continuous ECG feed from the patient, and this was optimised to obtain a good quality ECG signal prior to data acquisition. A pressure transducer from the catheter laboratory table inputted a continuous pressure signal from the manifold which recorded the pressure from the guide catheter.

Data was acquired using a 6800 Combomap console and the 9500 Combowire (Volcano, Europe). The Combowire is a guidewire with a diameter of 0.014" (0.36mm). The wire is a standard length of 185cm. The Combomap system allows simultaneous measurement of pressure and flow velocity data using a specialised wire with a Doppler flow velocity and a pressure transducer mounted at the tip of the guidewire, with a distance of 5mm between the two sensors (Figure 5.1). Although this must result in a slight time delay, this is negligible (estimated as 0.25-1ms for a wave speed between 5-20m/s).

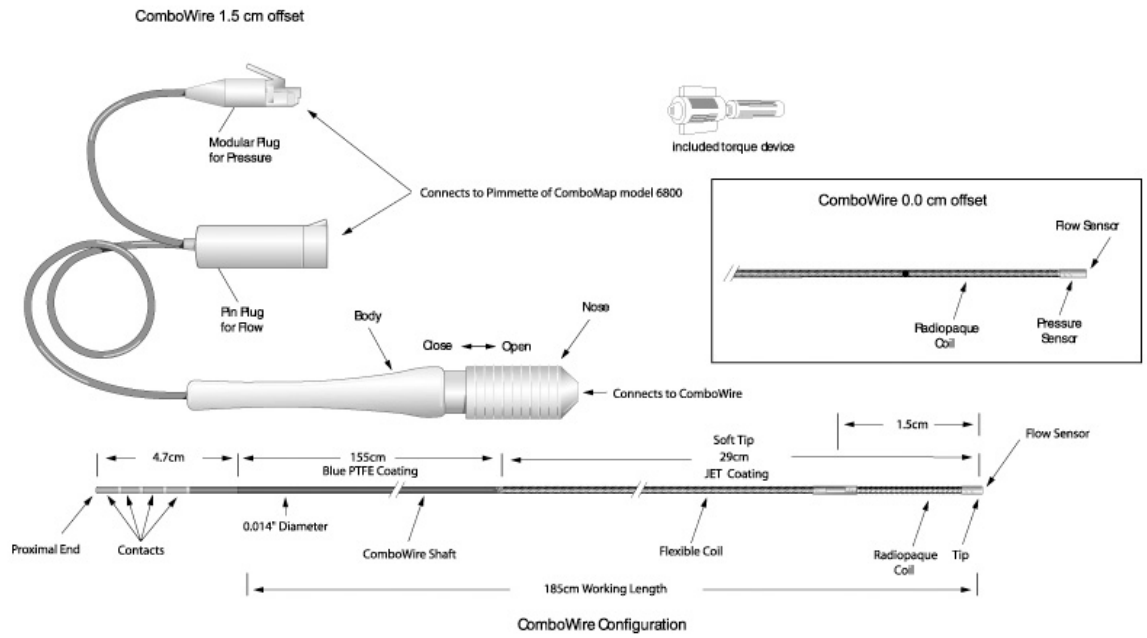


**Figure 5.1**: The Combowire system: A pressure and flow transducer is present on the tip of a steerable guidewire, allowing intracoronary measurements (taken from Volcano website)[1]

The Combomap console displays a live feed of the pressure and coronary flow velocity data. Two pressures are displayed on screen. The aortic pressure, transduced from the hollow catheter and the pressure recorded from the Combowire. The pressure is normalised with the wire in the proximal vessel, i.e. the pressure recorded from the catheter is set to equal the pressure recorded from the wire. The wire is then advanced into the proximal LAD or proximal RCA to record pressure and flow velocity at these positions. The pressure and flow velocity scales were adjusted to ensure optimal recording. Small adjustments were made in the scale to optimise the recording.

[1] http://intl.volcanocorp.com/products/combowire-xt.php#

### 5.1.5 Pressure and Doppler flow velocity sensors

The pressure sensor at the tip is formed of a Micro Electro Mechanical System (MEMS) which is made up to a think silicon diaphragm over a reference pressure chamber. Miniature resistors embedded in the diaphragm change resistance depending on flexion of the diaphragm in response to pressure within the blood vessel. Factory calibration coefficients are used to convert these changes in resistance into changes in blood pressure.

The Doppler sensor is a piezoelectric crystal. These crystals have the property that they will deform with application of an electric current, emitting ultrasound waves. Similarly, the crystal will also deform if ultrasound waves hit the crystals. Use of these properties allows a single transducer to both transmit and detect ultrasound signals in the same wave as a conventional ultrasound probe. The Doppler equation may then be used to convert the crystal deformation signal into a velocity signal.

The Doppler effect describes the finding that the recorded frequency of a wave depends on the relative speed of the source of the wave and the recorder/observer. In the coronary circulation, the Doppler probe is stationary on the tip of the wire and blood flow is detected either moving towards or away from the probe. When blood moves towards the probe, each successive wave takes slightly less time to reach the probe than the previous wave. Therefore there is an apparent increase in frequency detected as the wavefronts appear closer together. When blood is moving away from the probe, the arrival time between waves is increased with an apparent decrease in frequency detected, compared to the emitted frequency.

The Doppler probe can therefore be used to calculate velocity. Ultrasound waves are emitted from the piezoelectric crystal at the tip of the wire at a known frequency. The probe also acts as a detector, measuring the frequency of waves reflected back from red blood cells flowing

past. The difference in frequency between the emitted and received ultrasound waves can be used to calculate the velocity of blood which has reflected the wave using the following equation (Jenni et al. 2000):

$$Flow\ (in\ ml/min) = \Pi r^2(\frac{APV}{2})(0.6)$$

Where APV is the average peak velocity and r is the radius of the coronary vessel

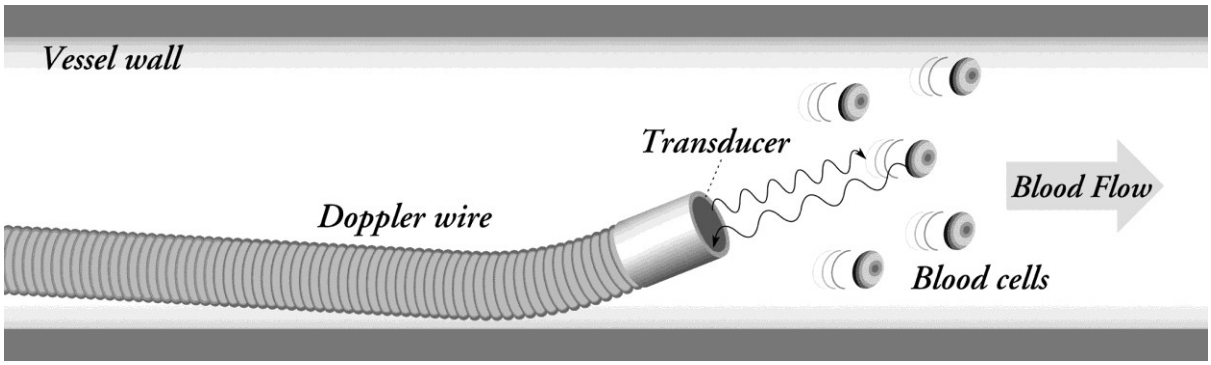


**Figure 5.2**: Use of the Doppler flowire for assessment of coronary flow velocity[2]

Blood flow within a coronary vessel is not uniform, but is greatest at the centre of the vessel. The wire should therefore be positioned in the centre of the vessel lumen to enable measurement of the peak coronary velocity. Although a small bend in the wire may be required in order to direct it into the vessel of interest, this should be avoided if possible. The sample volume is taken from a position approximately 5mm from the tip of the transducer and there is a 2.25mm width due to divergent ultrasound. Therefore, even in the case of eccentric wire position, the majority of the flow velocity profile will be sampled (Figure 5.3). Validation work has previously demonstrated this in vitro and in animal models (Doucette et al. 1992).

[2] Reproduced with permission from Volcano Corp, Europe

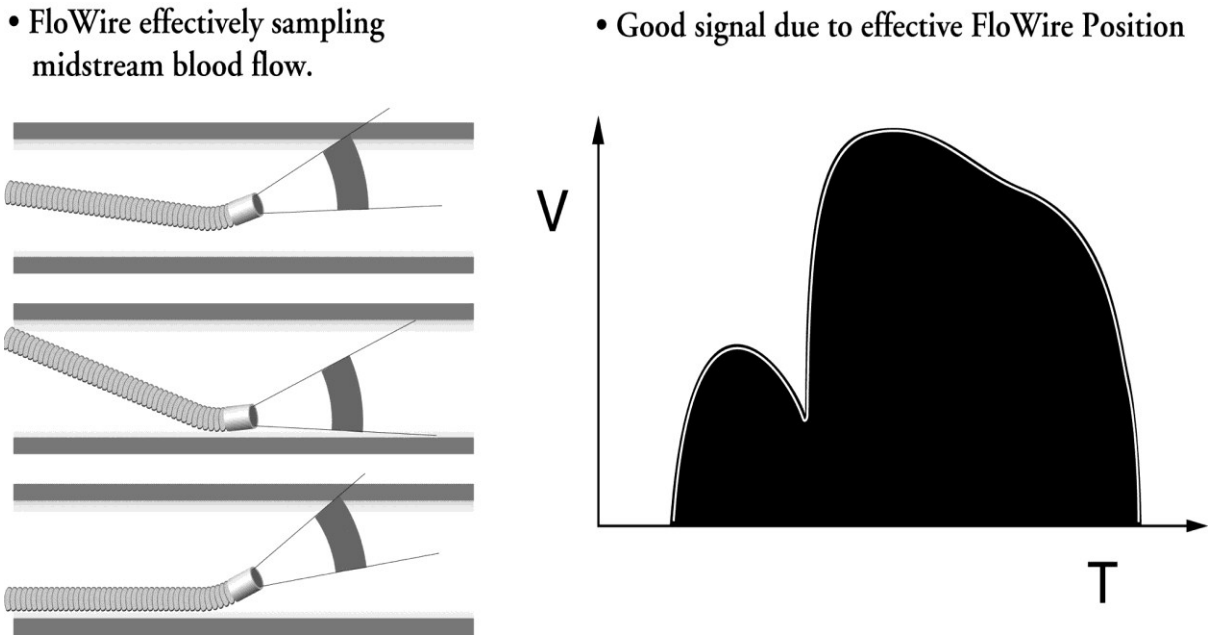


**Figure 5.3**: Although the wire position may move slightly during data acquisition, the wide sampling volume of the Doppler flowire tip will typically continue to record an accurate flow velocity profile[3].

### 5.1.6 Wire insertion and optimisation of signal output

Prior to wire insertion, the patient was administered intravenous heparin at a dose of 70iu/kg, aiming for an activated clotting time of 250-300seconds. This prevented formation of thrombus on the Combowire. Next the Combowire was prepared by flushing with 10ml of heparinised saline. The wire was carefully connected to the Combomap recording system under sterile conditions. It was ensured that the distal pressure on the Combomap (the wire pressure) was recorded as zero while the catheter was outside of the body. If not, the wire was "zeroed", i.e. set to zero pressure using a semi automated adjustment on the Combomap.

Guide catheters were used to establish selective engagement of the left coronary system and the Combowire was then placed into the guide catheter using an introducer needle. It was then advanced into the left main stem (LMS). Once in the LMS, the wire was "normalised",

[3] Reproduced with permission from Volcano Corp, Europe

so that the pressure recorded by the wire was set to be equal to the pressure recorded by the guide catheter.

The Combowire was then carefully advanced into the proximal LAD, proximal to the origin of the first diagonal vessel under fluoroscopy guidance. The introducer needle was removed. The Doppler flow velocity signal was then optimised using small movements of the wire until a clear signal with good density of Doppler signal was obtained (Figure 5.3). The instantaneous pressure velocity (IPV) threshold was then adjusted to ensure good tracking of the Doppler signal. The IPV threshold is a ratio of signal to noise and small adjustments in this threshold allowed improvement in the tracking of the Doppler signal. A range of 1-3 was used for the majority of studies.

One minute of continuous recording of pressure and coronary flow was completed. All recordings of pressure, flow velocity and electrocardiogram were be acquired at 1000Hz, for a period of 60 seconds. A fluoroscopic recording was made to document the location of invasive measurements (Davies et al. 2006).

Once sufficient rest data was collected in the proximal LAD, the adenosine infusion at 140micrograms/kg/min was started. This was continued for three minutes. Blood pressure and heart rate were recorded at rest and at peak hyperaemia. Once peak hyperaemia was obtained (defined as a stable Doppler coronary flow velocity after 3 minutes of adenosine infusion), a further minute of continuous recording was taken. The adenosine infusion was then stopped. The Combowire was removed and angiographic images were taken to ensure there was no damage to the coronary vessel resulting from placement of the Combowire. The guide-catheter was then exchanged for a right guide catheter, typically a Judkins right 4 guide and the Combowire was then placed in the proximal right coronary artery. The pressure was

again normalised in the ostium of the vessel and the wire then carefully placed in the proximal right coronary artery until a clear and stable Doppler flow velocity trace was obtained. One minute of continuous recording was again obtained. Finally, the catheter was withdrawn into the aortic root and a continuous recording of pressure in the aortic root was obtained.

### 5.2 Measurement of left ventricular end diastolic pressure

The left ventricular end diastolic pressure (LVEDP) provides information on left ventricular filling and volume status of the patient. It is measured by placement of a catheter into the left ventricle through the aortic valve (Figure 5.4). This fluid filled hollow catheter is connected to an external pressure transducer and pressure from the left ventricle is transmitted through a continuous fluid column to this transducer to produce a left ventricular waveform. This pressure transducer was adjusted at the start of each case so that zero pressure was set at the level of the right atrium while the patient was supine.

For all study patients, the LVEDP was measured at rest and following adenosine infusion. The LVEDP was measured at the end of diastole just after the a wave. Care was taken in catheter positioning as the placement of a catheter in the left ventricle may often produce abnormal rhythms, with ventricular premature beats or short runs of ventricular tachycardia. The catheter was therefore carefully positioned where a stable trace could be obtained without rhythm disturbance. The catheter was then flushed to ensure that the pressure waveform was accurately obtained, with no damping of the ‘a’ wave which may lead to inaccurate measurement. LVEDP was measured at rest and following adenosine infusion, again using an infusion of 140micrograms/kg/minute for three minutes.

The normal LVEDP is between 3 and12mmHg. High LVEDP is associated with impaired ventricular function, volume overload and conditions of impaired ventricular relaxation such as HCM. A LVEDP above 30mmHg is associated with pulmonary oedema and if this was recorded during cardiac catheterisation, injection of dye was typically minimised to avoid on-table decompensation (Mitchell et al. 2008).

**Figure 5.4**: How to measure the LVEDP. The aortic valve is crossed, typically with a pigtail catheter through the aortic valve and then positioned into the left ventricle such that the pressure trace is stable and the catheter does not induce rhythm abnormalities (Mitchell et al. 2008).

## 5.3 Calculation of coronary haemodynamic measurements

### 5.3.1 Temporal profile of proximal LAD coronary flow

The cycle length, duration of systole and diastole and time between onset of diastole (defined by the dicrotic notch (Kyriakidis et al. 1997)) to peak coronary flow velocity were calculated for each patient. Coronary volume flow rate was calculated from the product of the coronary flow velocity and the coronary diameter as previously described (Timmer et al. 2011)

### 5.3.2 Coronary flow reserve

The coronary flow reserve is defined as the ratio between the mean coronary flow at peak hyperaemia and the mean coronary flow at rest. It is a measure of the ability of the heart to increase coronary flow as a result of a hyperaemic stimulus, commonly adenosine. In a healthy heart, the coronary flow reserve is approximately threefold (Baumgart et al. 1998). If the vessel diameter is not known, the coronary flow velocity reserve (CFVR) may be used. This is defined as the ratio of the mean hyperaemic coronary flow velocity to the mean basal coronary flow velocity.

### 5.3.3 Calculation of coronary flow reserve and coronary resistance

Coronary flow reserve was calculated as the mean coronary flow velocity throughout the cardiac cycle at maximal hyperemia divided by the mean coronary flow velocity at rest. The coronary resistance was calculated as the mean pressure divided by the coronary flow in the LAD.

## 5.4 Measurement of coronary artery dimensions

Measurement of coronary artery diameter was performed in two orthogonal planes. Views were selected to minimise distortion and avoid regions of overlapping branch vessels. The proximal LAD and RCA were zoomed up and measured using calibrated QCA measurements. The guiding catheter was used for scale, filmed while devoid of contrast medium. Care was taken to measure the LAD and RCA at the point where the pressure and flow samples were taken using the Combo wire.

## 5.5 Echocardiography

All patients underwent a full transthoracic echocardiogram, with detailed measurement of left ventricular function, assessment for any valvular pathology and assessment of diastolic function, including mitral inflow traces and tissue Doppler imaging. Studies were performed according to the British Society of Echocardiography guidelines[4].

## 5.6 Data processing for invasive wave intensity analysis

Data analysis was performed using a customised automated Matlab analysis program used for previous wave intensity analysis (Davies et al. 2006; Davies et al. 2011). Data from the Combomap was outputted and segments of 4-5 beats of good quality recording of both pressure and flow identified for the LAD at rest, LAD at peak hyperaemia and RCA at rest. These were saved as text files and inputted into the Matlab program. Each text file included an ECG recording, proximal pressure from the catheter, distal pressure from the Combowire and the instantaneous peak velocity. Each of these was sampled at 5ms intervals. Input of the simultaneous pressure and flow data was processed automatically using the Matlab program. Four to five beats of pressure and flow were ensemble averaged using the automated program, to minimise the effect of noise without loss of data quality. Each beat was overlaid using the R wave to line up the traces and ensemble averaging was performed.

A Savitzky- Golay filter was then used to smooth the data without loss of true peaks and troughs (Savitzky & Golay 1964). This type of filter works by fitting a polynomial to each

[4] www.bseecho.org

data frame using the least squares method. The polynomial order and frame width constants for the Savitzky- Golay filter were set at 3 and 31 for all data analysis.

The derivatives of the pressure and flow at each time-point were used to calculate the net wave intensity, with units $Wm^{-2}s^{-2}$. Waves were categorised in terms of direction (forward for waves of proximal origin, backward for waves of distal origin) and associated pressure change (compression – associated with a rise in pressure, expansion – associated with a fall in pressure). The sum of squares method was used to determine the wave speed and allow calculation of the separated wave intensity at rest (Parker 2009). Since this method has been shown to be less accurate under conditions of low coronary resistance (Rolandi et al. 2014), only the net wave intensity was used to compare rest and hyperemia. The wave intensity against time was outputted graphically.

### 5.7 CMR data acquisition

#### 5.7.1 Patient preparation

Data for CMR perfusion and CMR WIA was acquired in a single scan, lasting approximately 90 minutes. All patients were screened with a safety questionnaire prior to entry into the scanner to ensure they were safe to undergo the scan and did not have contra-indications such as metal fragments in the eyes or non-CMR conditional pacemakers. Patients were required to abstain from caffeine containing substances for at least 24 hours prior to CMR as this would counteract the effects of adenosine.

An electrocardiogram was performed to assess for any conduction delays and patients underwent a history and examination to ensure they were suitable for adenosine perfusion

imaging. Contra-indications included high degree atrioventricular block, severe asthma and use of dipyridamole. Bloods were taken to check renal function prior to administration of gadolinium. Gadolinium was not administered if the estimated glomerular filtration rate was less than 30 ml/min/1.73m$^2$.

An 18 gauge cannula was inserted into the right antecubital fossa for administration of the gadolinium contrast as a rapid bolus followed by flush and a 20 gauge cannula into the left antecubital fossa for administration of adenosine peripherally. Images were acquired using a clinical 3.0 T scanner (Magnetom Skyra, Siemens AG Healthcare Sector, Erlangen, Germany) with an anterior 18 element matrix coil and 8–12 elements of a matrix spine coil (Figure 5.5).


**Figure 5.5**: Siemans Skyra 3T scanner in the Cardiovascular Biomedical Research Unit at the Royal Brompton Hospital.

Image acquisition was retrospectively ECG gated unless otherwise specified. Pilot imaging was first obtained using a balanced steady state free precession (bSSFP) sequence to ensure that the patient was optimally positioned within the scanner. Anatomic imaging was then acquired using free breathing multiple slice half-Fourier spin echo (HASTE) sequences were used in transverse, coronal and sagittal planes of the thorax. A bSSFP sequence was used to obtain breath-hold cine images in three long-axis planes, followed by a contiguous stack of short axis slices from the atrioventricular ring to the apex.

### 5.7.2 CMR perfusion imaging

The end-systolic long-axis cine images were used to plan the short axis perfusion acquisition at the base, mid ventricle and apex. The centre frequency of the magnet was manually adjusted to ensure maximum separation of fat and water. Shimming was performed to ensure maximum magnetic field homogeneity and minimise off-resonance effects. Test images were taken to identify any potential artefacts or wrap and field of view was adjusted where necessary.

For assessment of quantitative perfusion, CMR first pass perfusion was recorded at peak adenosine hyperaemia and at basal resting conditions. For peak adenosine hyperaemia, adenosine was infused at 140 mcg/kg/min into the 20 gauge cannula in the left antecubital fossa, using the same protocol as followed invasively. The patient was given at least 3 minutes of adenosine infusion. Symptoms, change in heart rate and blood pressure were monitored to assess for signs of peak hyperaemia.

After measurement of heart rate and blood pressure at peak stress, gadolinium contrast (Gadovist, Bayer-Schering, Berlin, Germany, 0.05 mmol/kg) was rapidly injected at 3.5 ml/s into a large bore cannula (18 Gauge) situated in the right antecubital fossa, followed by 25 ml saline at 7 ml/s using a power injector (Medrad UK, Ely, Cambridgeshire, UK) to ensure a compact bolus. Patients were instructed to take slow gentle breaths during image acquisition. Myocardial first-pass perfusion imaging was performed using a rate-3 parallel accelerated bSSFP sequence. Three short axis images and an image of the arterial input function were acquired every cardiac cycle for a total of 70 cycles. Initial proton density-weighted images were acquired prior to the arrival of contrast by imaging without a saturation recovery pre-pulse and using a low flip angle for read out. These were used for subsequent surface coil intensity correction.

Following acquisition of peak stress first pass perfusion, the adenosine infusion was stopped and a top up bolus of gadolinium (0.05mmol/kg) was administered. Late enhancement images were acquired with an inversion recovery-prepared segmented turbo fast low-angle shot sequence 10 minutes after injection of gadolinium (see below). After a minimum of 20 minutes after the last bolus of gadolinium, rest perfusion imaging was carried out at the same slice positions and gadolinium bolus preparation. Blood pressure and pulse during rest perfusion were again recorded.

### 5.7.3 Flow velocity mapping of the coronary arteries using CMR

The coronary artery origins were identified using multiple transverse diastolic segmented gradient echo scout acquisitions (TE/TR: 3.3 ms/7 ms, acquired resolution 1 mm x 1 mm x 4

mm, acquisition window 110 ms). From these, oblique and double oblique images were acquired to image the left anterior descending (LAD) and right coronary artery (RCA) in-plane. Through-plane breath-hold interleaved spiral phase velocity maps (TE/TR: 5.2 ms/19 ms) were then acquired in a straight section of each proximal artery, matched as closely as possible to the locations of the invasive measurements (Figure 1). The sequence incorporated 1-1 water excitation and 8 spiral interleaves (11.75 ms duration) were required to fill k-space. Phase map subtraction of datasets with symmetric bi-polar velocity encoding gradients resulted in through-plane velocity maps sensitive to a flow velocity of +/−30 cm/s. These datasets were acquired in alternate cardiac cycles following a single dummy cardiac cycle, resulting in a total breath-hold duration of 17 cardiac cycles. The spatial resolution was 1.4 mm x 1.4 mm (reconstructed to 0.7 mm x 0.7 mm) and the slice thickness was 8 mm.

Locations were directed by the invasive fluroscopic images to ensure the same location as invasive data acquisition where possible. Sensitivity to off-resonance artefact was minimised using localised second-order shimming and frequency adjustment based on the signal from a user-defined region of interest positioned over the heart. For right coronary studies, an additional breath-hold spiral phase velocity mapping acquisition was performed using fat-excitation (Keegan et al. 2004). This was later used to correct for the through-plane velocity of the RCA. Spiral acquisitions were repeated to allow analysis of intra-study reproducibility. For each breath-hold acquisition, a circular cross-sectional area was automatically defined over the vessel on a mid-diastolic frame. Semi-automatic custom MATLAB software was then used to track the artery from frame to frame and to generate a velocity-time curve (6). As the spatial resolution of the data was limited, no attempt was made to measure changes in the vessel cross-sectional area throughout the cardiac cycle. The velocity-time curves were corrected for through-plane motion of the vessel using a region of adjacent myocardium (LAD) or in the surrounding epicardial fat (RCA) (6, 10).

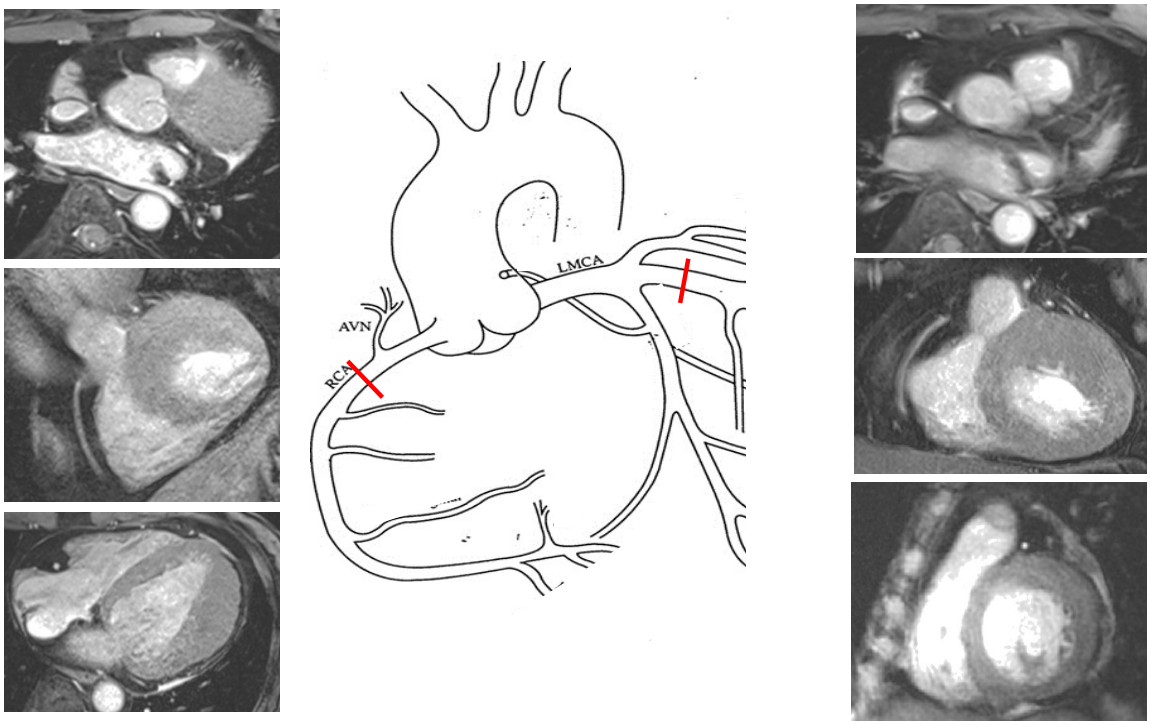


**Figure 5.6** Localisation of the coronary arteries using CMR was performed using scout images of the aortic root to localise the origin and course of the left anterior descending and right coronary artery. These were then cross-cut until a clear cross sectional image of artery was obtained.

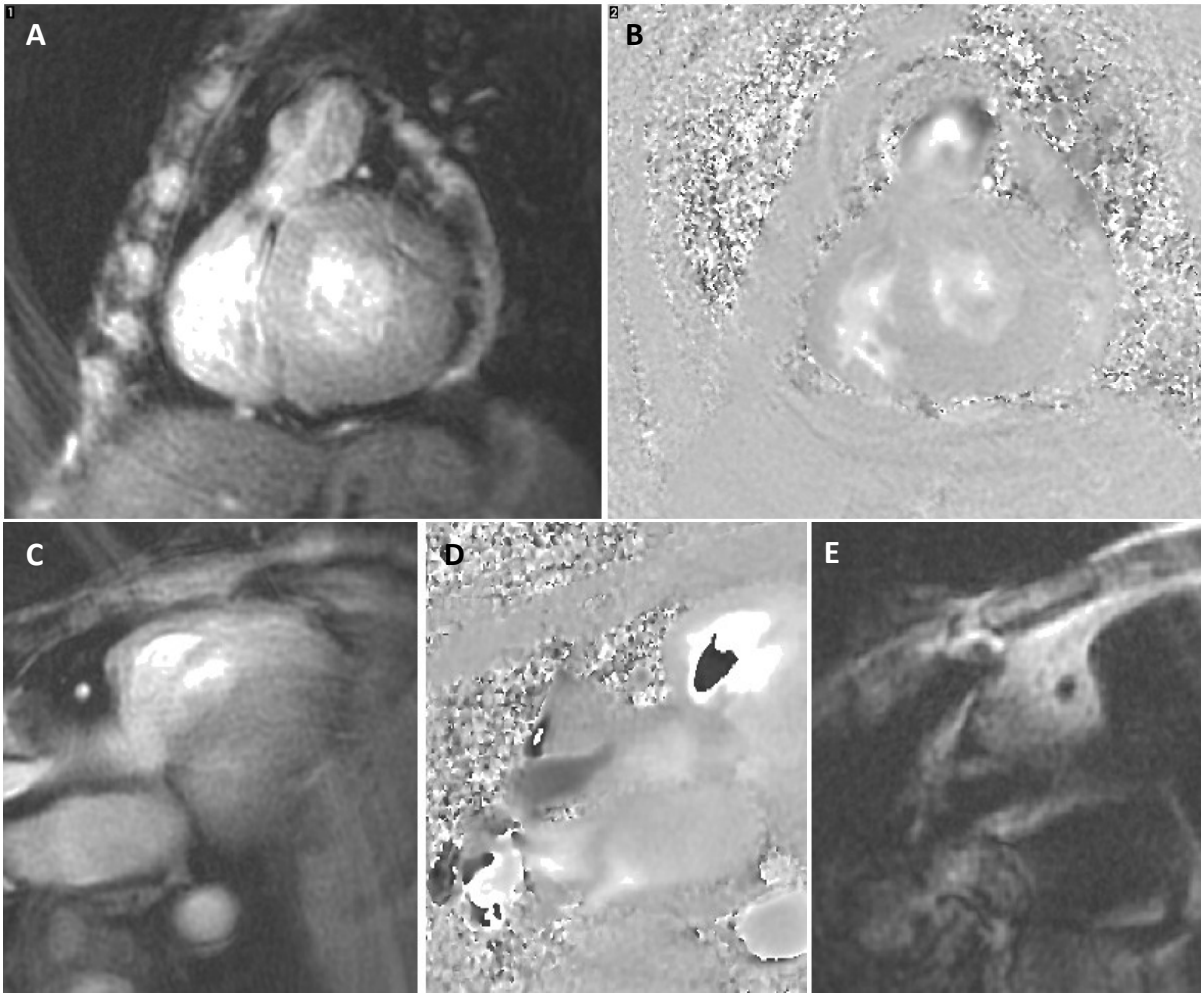


**Figure 5.7**: Cross sectional imaging of LAD (top panels) and RCA using phase encoded (A and C), velocity encoded (B and D) and fat excitation imaging (E).

### 5.7.4: Measurement of aortic distension

Following acquisition of localiser images and vertical and horizontal long axis balanced steady state free precession (bSSFP) cine images of the heart, bSSFP cine images were acquired in the three chamber and left ventricular outflow tract views to show the ascending aorta in-plane. A breath-hold retrospectively gated segmented gradient echo sequence (TE/TR 3.6 ms/6.6 ms) was then used to acquire through-plane cross sectional area changes in the proximal ascending aorta. The spatial resolution was 1.2 x 1.2 mm (reconstructed to 0.6 x 0.6 mm) with a slice thickness of 8 mm. Five k-space lines were acquired per cardiac

cycle resulting in data with a true temporal resolution of 32.8 ms which was then reconstructed over 50 cine frames (reconstructed temporal resolution 19 ms assuming a heart rate of 60 beats per minute)(Figure 1). The acquisition plane was located 35mm above the aortic root as this was typically in a straight section of the aorta with minimal through-plane motion through the cardiac cycle The segmented gradient echo cine acquisition was repeated for assessment of intra-study reproducibility. In each, the aortic cross sectional area was manually contoured and plotted against time from the R wave.

To minimise circadian variation in coronary flow between studies, readings were taken under standardised conditions, with both procedures performed at the same time of day where possible, with a minimum of 30 minutes lying supine at rest prior to data acquisition. Patients refrained from caffeine containing substances and smoking prior to each procedure. Where possible both studies were performed on the same day, however this was not always possible.

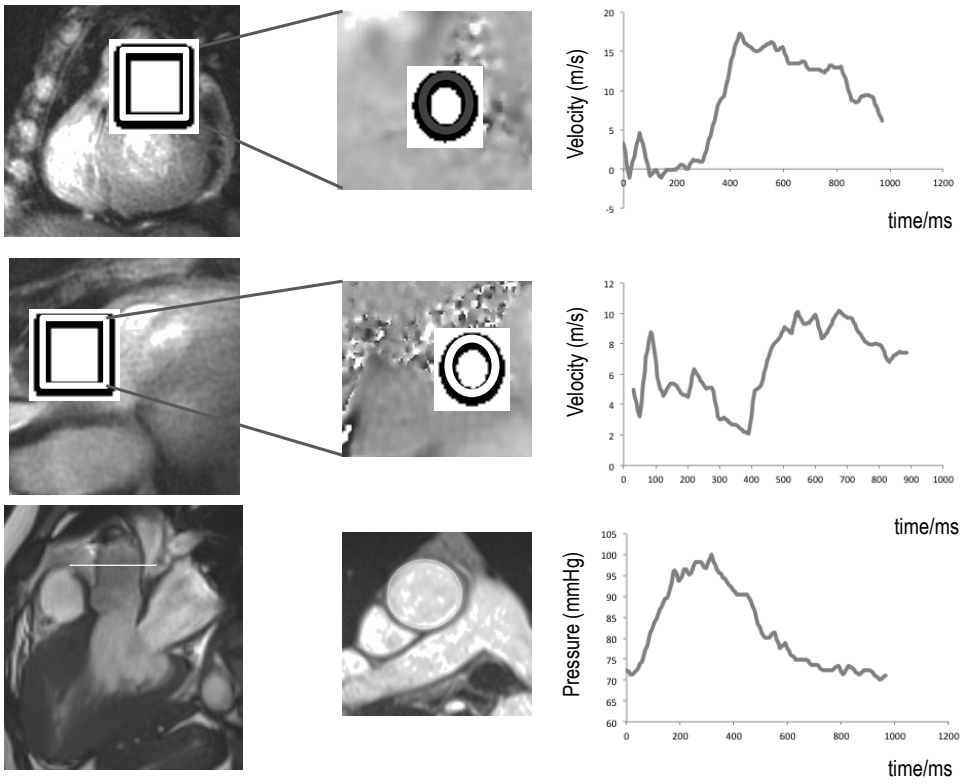


**Figure 5.8**: Early diastolic cross sectional imaging of LAD (top panel) and RCA (middle panel) using breath-hold spiral phase velocity mapping. For derivation of pressure data, a cross sectional plane was identified 35mm above the aortic valve plane (bottom panel), a high temporal resolution gradient echo sequence was used to acquire aortic areas throughout the cardiac cycle and these were used to derive the central aortic pressure during the cardiac cycle.

### 5.7.5 Derivation of central aortic pressure from aortic distension data

The central aortic pressure was derived from the aortic distension and the brachial systolic and diastolic blood pressure measurements as follows (Quail et al. 2014; Meinders & Hoeks 2004):

$$p(t) = P_d \exp\left[\alpha\left(\frac{A(t)}{A_d} - 1\right)\right]$$

where $\alpha$ was initially set as:

$$\alpha = \frac{A_d Ln\left(\frac{P_s}{P_d}\right)}{A_s - A_d}$$

where p(t) is the CMR-derived pressure curve, $P_s$ is the brachial systolic pressure, $P_d$ is the brachial diastolic pressure, $A_s$ and $A_d$ are the systolic and diastolic aortic areas and A(t) is the area curve. The model was calibrated using an iterative method to reduce the scaling factor, α, to minimise the difference between the mean measured brachial pressure and the mean CMR-derived pressure. This exponential model correlates well with the results of carotid artery applanation tonometry (8) which has been validated against invasive central aortic pressure measurements (Kelly & Fitchett 1992).

### 5.7.6 Assessment of CMR reproducibility and comparison with invasive WIA

The principle waves through the cardiac cycle were calculated for each subject using invasive and CMR data as described above and the values derived from the two techniques compared using Bland Altman analysis and Pearson correlation. For both invasive and noninvasive data, intra-study reproducibility was determined using Bland Altman analysis and reported as mean difference (+/- SD of the differences).

### 5.7.7 CMR data analysis: measurement of LV volumes, mass and wall thickness

Left ventricular wall thickness was measured in the short axis stack at end diastole. The area of greatest wall thickness was identified visually and measured using a custom measuring tool on commercially available software (CMR Tools 2010, Cardiovascular imaging solutions, London, UK).

LV volumes, ejection fraction and mass were assessed using a semi automated algorithm provided by CMRtools. The 2 chamber, 4 chamber, RVOT and short axis stack were selected. The endocardial and epicardial borders were manually traced in diastole and systole for the left ventricle. Thresholding software was used to adjust the blood pool image so it was accurately delineated and excluded the papillary muscles and areas of trabeculation. RV volumes were similarly assessed by delineation of the RV endocardial borders in systole and diastole. RV mass was not routinely measured. The mitral valve, tricuspid valve and aortic valve planes were defined in systole and diastole using the long axis and RVOT views.

The CMR Tools algorithm outputs an end diastolic volume (EDV) and end systolic volume (ESV) stroke volume (SV) and ejection fraction (EF) for each ventricle. The EDV and ESV are calculated using summation of the volume of blood pool for each of the contiguous slices of the ventricle in diastole and systole respectively. The position of the mitral, tricuspid and pulmonary valves is taken into account during the cardiac cycle and no assumptions are made regarding the geometry of the ventricle. The stroke volume is calculated as the LV EDV – LV ESV. The ejection fraction is calculated from the SV/LV EDV. The LV mass is calculated in diastole as the volume of ventricle delineated by the epicardial border minus the EDV.

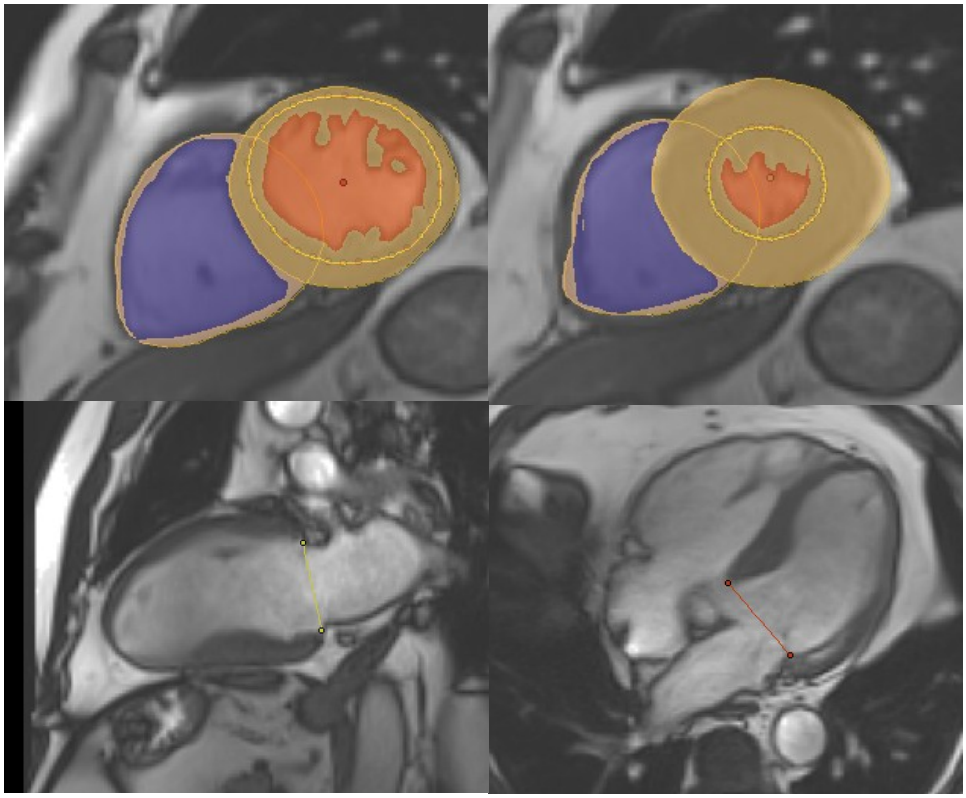

**Figure 5.7.1**: Measurement of LV volumes using CMR tools (screenshot from programme). The semi-automated programme was used to calculate the left ventricular end diastolic and end systolic volumes and measure the left ventricular mass.

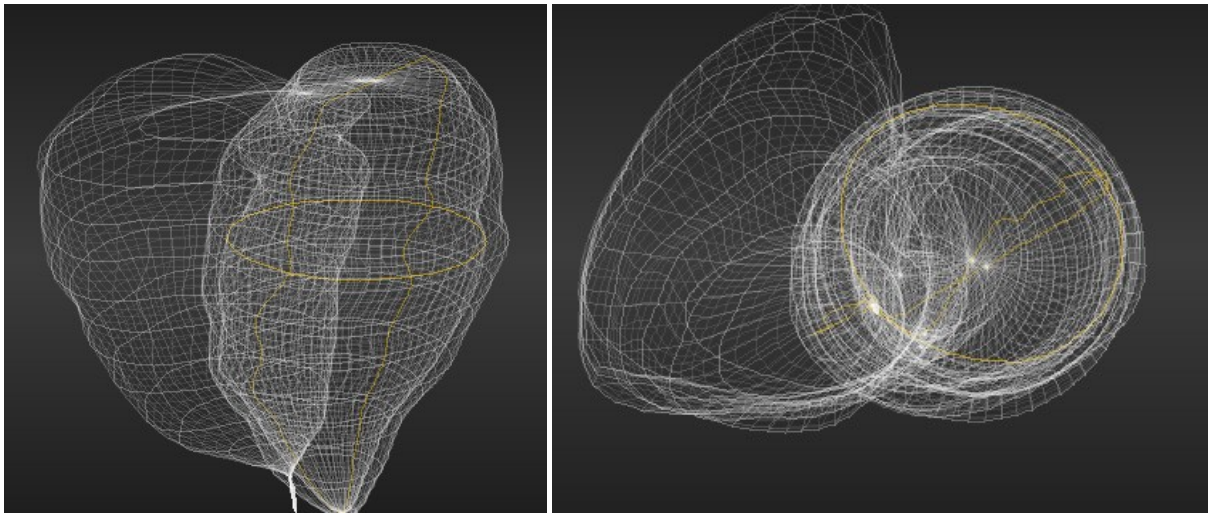

**Figure 5.9**: Using the epicardial and endocardial borders traced at each slice, a model with no geometric assumptions is created for the LV and the RV (screenshot from programme) and used to calculate the LV volumes and mass.

The LV volumes and mass were indexed to body surface area (BSA) using the Du Bois equation (Burton 2008) as follows:

$$Body\ surface\ area = 0.20247 \text{ x } height\ in\ metres^{0.725} \text{x } weight\ in\ kg^{0.425}$$

### 5.7.8 Gadolinium imaging

Following administration of the gadolinium chelate (Gadovist, Bayer Schering, Berlin, Germany) top up, early gadolinium images were acquired during breath-holds to assess for any thrombus or microvascular obstruction. The inversion time (TI) was set at approximately 440ms for early gadolinium imaging. 10 minutes after gadolinium administration, delayed enhancement images were acquired during breath holding using a segmented inversion recovery gradient echo turbo fast low angle shot sequence at end diastole. The inversion time was adjusted to ensure optimum nulling of the signal from the left ventricle, typically starting at a TI of 270ms. Images were acquired in the three long axis planes and the short axis planes as used for cine imaging. The TI was adjusted to ensure continued nulling of the myocardium as the gadolinium washed out with time.

Gadolinium imaging was acquired in two phase encoded directions: right to left and head to foot. This allowed clearer identification of artefact on assessment of gadolinium sequences.

### 5.7.9 Quantification of late gadolinium enhancement

Quantification of the amount of late gadolinium enhancement was performed blinded to clinical data using dedicated software (CMR 42, Circle Cardiovascular Imaging, Calgary, Canada). Late gadolinium enhancement was considered to be present if there was an area of

high signal intensity on a background of correctly nulled myocardium, in the absence of artefact. Artefact was assessed using the two orthogonal phase swap images, as artefact typically changes appearance using a different phase encode direction. Therefore, enhancement was only considered to be present if it was seen on both sets of phase encoded images and in appropriate long and short axis images.

The full width-half maximum method was used to quantify the percentage of the myocardium that is comprised of fibrosis (Spiewak et al. 2010; Flett et al. 2011). Firstly, the endocardial and epicardial borders were defined for each of the short axis gadolinium images. Next the mitral valve position was defined on appropriate long axis imaging. An area of myocardial enhancement was identified and a region of interest (ROI) manually drawn in this area. The custom software then used a multi pass region-growing algorithm which delineated areas of hyperenhancement defined using the hyperenhancement ROI. Any areas of artefact were then manually excluded. The total mass of enhanced tissue was calculated from the total of areas of hyperenhancement identified by this program and divided by to the calculated left ventricular mass to produce a percentage of late gadolinium enhancement (O'Hanlon et al. 2010).

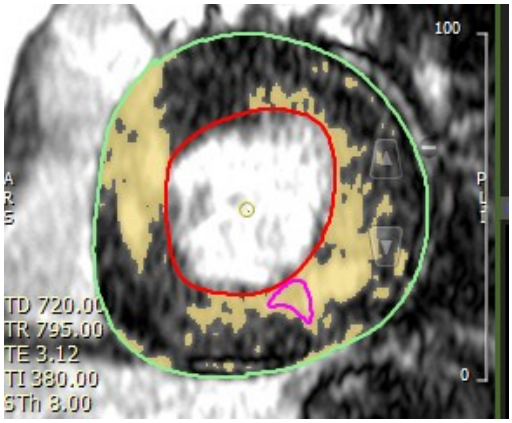

**Figure 5.10**: Quantification of LGE using CMR 42 and the full width-half maximum method. A region of interest within the diseased myocardium is defined and regions with similar signal intensity are automatically identified as LGE.

### 5.8 Data Analysis of CMR Quantitative Perfusion

Absolute myocardial blood flow (MBF) was quantified at rest and at peak stress. First, myocardial perfusion images were corrected for respiratory motion using an automated in-line non-rigid warping registration post processing algorithm. Endocardial and epicardial borders of the LV myocardium were manually traced using Argus CMR software (Syngo, Siemens Healthcare, Erlangen, Germany) to define myocardial regions-of-interest (ROI) in the three short axis levels across the 70 acquired images. ROIs were also be drawn in the blood pool of the arterial input function series to enable quantification of contrast uptake into the blood pool. The myocardium was segmented into 16 segments according to the AHA classification (Cerqueira et al. 2002) with identification of the superior RV insertion point. Care was taken to ensure that ROIs only included the myocardium in the myocardial images and excluded pericardium, blood pool and any artefact. For the AIF, care was taken to ensure the ROI was only within the blood pool.

Although the relationship between signal intensity and concentration of gadolinium contrast is linear at low concentrations, there is increased signal loss at higher concentrations due to increased T2* effects. Therefore a half dose bolus of gadolinium was used to attempt to minimise these effects (Hsu et al. 2012; Mordini et al. 2014). Secondly, a dual-sequence imaging approach was used to obtain myocardial and AIF images in the same sequence. The AIF was obtained using a very short TI and with lower T1 weighting than that of the

myocardium, resulting in improved linearity between the signal intensity and contrast concentration (Gatehouse et al. 2004).

Custom image processing software (Siemens SCR lab, Princeton) was used for analysis and surface coil normalisation. MBF then be quantified pixel-wise using a model-constrained deconvolution as previously validated (Hsu et al. 2012).

This method required certain assumptions. The first is that there was a linear relationship between changes in the signal intensity and changes in the contrast agent concentration. The left ventricular blood pool has the most compact bolus of contrast agent and therefore signal saturation is most likely to be observed here.

Analysis utilises the central volume principle. This states that the gadolinium residue in the myocardial tissue may be considered as the result of the convolution of the measured arterial input and the tissue residue impulse response. The tissue impulse response is the tracer residue curve expected for a hypothetical arterial input equivalent to a very brief impulse. This has some useful properties: the area under the tissue impulse response curve is equal to the effective distribution volume during the first pass of gadolinium. The amplitude of the impulse response is equal to the blood flow into and out of the tissue region of interest (Petersen et al. 2007).

Unfortunately, the tissue impulse response cannot be directly measured. Instead, we use the measured tissue residue curve, *q(t)*, which is comprised of a convolution integral of the arterial input function, *i(t)* and the tissue impulse response, *R(t)*, as follows:

$$q(t) = \int_0^t t(\tau) \cdot R(t-\tau) \cdot d\tau$$

The tissue residue curve is examined over time. The number of time points associated with the arrival of contrast into the myocardium is determined by the temporal resolution of the sequence used for data acquisition. The integral above may be approximated by a sum over time points $t_1$ to $t_n$, the sampling time points. Next, the myocardial impulse response may be represented as a sum of B-splines, which uses a generalisation of the Bézier curve. This improves smoothness of the line (Petersen et al. 2007).

*R(t)* may be found by solution of this equation. However, noise in the data will introduce inaccuracies, which will be amplified by the required differentiation and division. Various solutions have been imposed to limit the effect of noise in the data. Constraint of this deconvolution process will reduce the effect of noise on the solution. Constraint uses an empirical model of perfusion with a rapid rise in signal intensity at time 0 as the contrast arrives in the myocardium, followed by smooth monotonic decay as contrast leaves the myocardium. The assumptions of this technique are that the decline in the signal intensity is primarily dictated by the entry and then washout of gadolinium from the myocardium. The Fermi function is a best approximation of the transfer function (Jerosch-Herold 2004). This function can be expressed as follows:

$$R(t) = Q\ \frac{1}{\left(e^{\frac{t-A}{\quad}}\right) + 1} + I$$

Where Q is the flow rate, t is time and R(t) is the transfer function. A and B are parameters which define the shape of the function. I was added to the model to improve approximation of gadolinium behaviour over time and to correct for extravasation of the contrast into the myocardial interstitum. This can then be solved iteratively using a non linear curve fit to the myocardial signal intensity time curves.

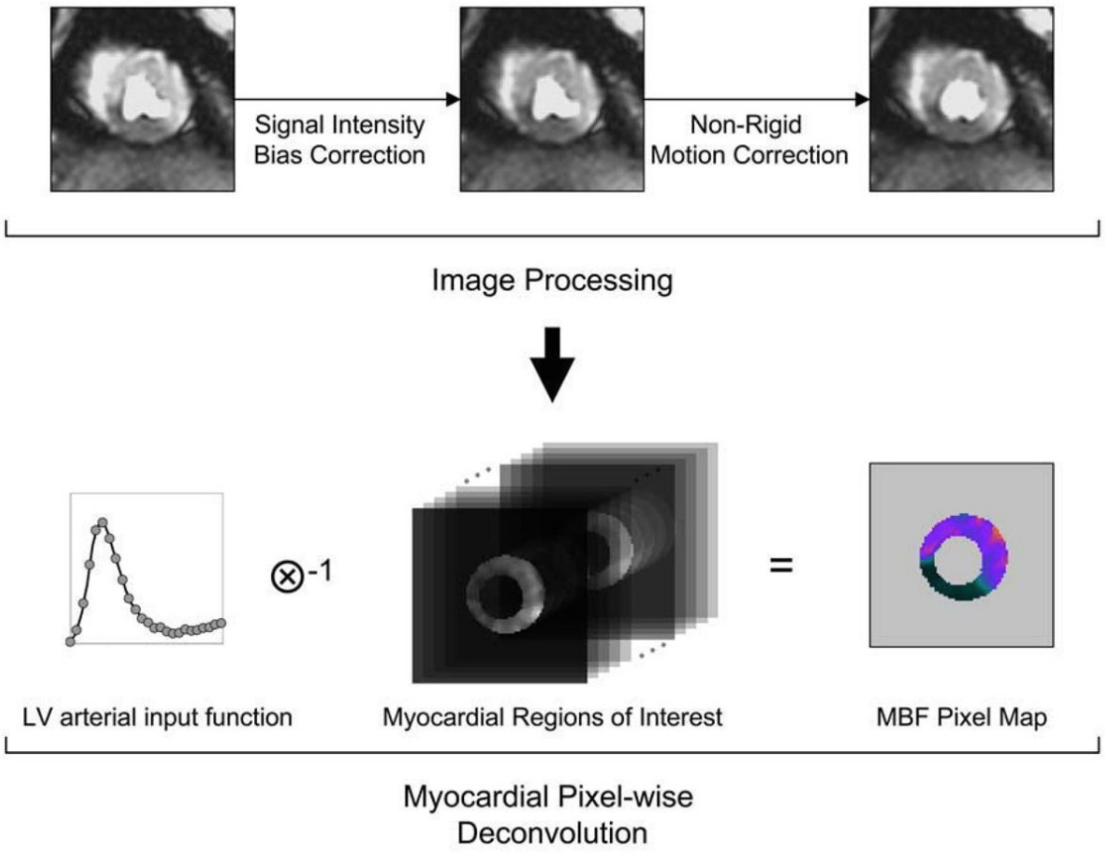


**Figure 5.11** Post processing of first pass CMR perfusion to generate quantitative perfusion values (Hsu et al. 2012)

The transfer function is derived by deconvolution of the AIF from the myocardial response using a modified Fermi constrained algorithm"

The proton density-weighted images acquired at the start of each sequence were used to correct for surface coil intensity. Next rigid and non rigid image registration was performed to correct for translational motion of the myocardium (Hsu et al. 2012). Perfusion was quantified sector wise using a Fermi-constrained deconvolution algorithm. Mean and standard deviation for perfusion per sector at rest and peak adenosine stress was outputted.

### 5.9 Statistical Analysis

All data analysis was performed blinded to patient demographics. Data is presented as mean and standard deviation for normally distributed continuous variables or median and inter-quartile range for non-parametric continuous variables. Data was tested for normality using histograms and a normal test plot.

For comparison of continuous, normally distributed data, a two way Student's t-test was used. The Mann-Whitney U-test was performed if continuous data was not normally distributed. Correlation was assessed using a Pearson's or Spearman's rank correlation as appropriate. Differences between categorical variables were assessed using the Chi-square test or Fishers exact test, dependent on predicted sample size.

A p value of $<0.05$ was considered significant. Power calculations assumed an alpha error probability of 0.05 and 1-beta error probability of 0.8 (80% power). Analysis was performed using SPSS version 19.0 (SPSS for Windows, IBM, New York, USA).

#### 5.9.1 Assessment of reproducibility of data

The reproducibility of WIA was assessed by examination of separate 30 second recordings. The standard deviation of the difference between repeat recordings for each wave was recorded and a Bland Altman plot was used to assess reproducibility.

### 5.9.2 Sample size calculations

To compare wave intensity in patients with HCM and patients with structurally normal hearts, a minimum of 20 patients in each group was required. For normal subjects(Davies et al. 2006), the mean peak intensity of the early backward compression wave was 0.9 ±1.0 $x10^5$ W $m^{-2}s^{-2}$ and the mean peak backward travelling decompression (suction) wave was 5.5 ±4.6 $x10^5$ W $m^{-2}s^{-2}$. Based on our pilot data, we anticipated at least twice times the magnitude of the early backward compression wave in HCM compared to normal subjects and a backward decompression wave at least half the magnitude of that of normal subjects. This required a total of 20 subjects in each group.

Development of CMR-WIA in the coronary arteries is novel and therefore a formal sample size calculation was not possible. We invited all patients participating in the invasive WIA study to return for a research CMR to measure coronary flow and aortic area changes.

# CHAPTER 6

**Mechanisms of Myocardial Ischaemia in Hypertrophic Cardiomyopathy:**

Insights from Wave Intensity Analysis and Magnetic Resonance

## 6.1 Abstract

**Background**: Angina is common in hypertrophic cardiomyopathy (HCM) and associated with abnormal myocardial perfusion. Wave intensity analysis (WIA) of coronary flow may improve mechanistic understanding of chest pain in HCM.

**Methods and Results**: We measured simultaneous pressure and flow in the proximal left anterior descending artery in 33 HCM and 20 control patients at rest and during hyperemia, allowing calculation of wave intensity. Patients also underwent quantitative first- pass perfusion cardiovascular magnetic resonance (CMR) to measure myocardial perfusion reserve (MPR).

Patients with HCM had a lower coronary flow reserve (CFR) than control patients (1.9±0.8 versus 2.7±0.9, p=0.001) and 30% had reversal of coronary flow during systole. Coronary hemodynamics during early systole in HCM were characterised by a much larger fractional backward compression wave (BCW, 38.2±11.1% versus 21.0±6.2% in controls, p<0.001). Patients with severe left ventricular outflow tract (LVOT) obstruction had a bisferiens pressure waveform resulting in an additional proximally originating deceleration wave during systole.

The proportion of waves acting to accelerate coronary flow increased with hyperemia and the magnitude of change was proportional to the MPR (r=0.62, p<0.001).

**Conclusions**: Coronary flow in patients with HCM is deranged. Distally, compression and deformation of intra-myocardial blood vessels during systole result in an abnormally large BCW, while proximally, severe LVOT obstruction is associated with an additional deceleration wave. Perfusion abnormalities in HCM are not simply a consequence of supply/demand mismatch or remodelling of the intra-myocardial blood vessels but represent

a dynamic interaction with myocardial mechanics which may be amenable to newer treatment strategies.

## 6.2 Introduction

Hypertrophic cardiomyopathy (HCM) affects 1 in 500 of the general population (Maron 2002). Left ventricular outflow tract (LVOT) obstruction is present at rest in approximately 30% of these patients, rising to 60-70% with exercise provocation (Maron 2002). Chest pain affects up to half of patients and is thought to result from impaired myocardial perfusion (Elliott et al. 1996). It is difficult to treat (Maron et al. 2009). Severe perfusion abnormalities are independently predictive of death (Cecchi et al. 2003) and development of heart failure (Olivotto et al. 2006). Angina is often debilitating in HCM and there is a major unmet need to improve our understanding of the mechanistic basis for chest pain to improve therapeutic interventions.

Several potential mechanisms have been proposed to explain these perfusion abnormalities, including increased oxygen requirements of the hypertrophied myocardium, impaired ventricular relaxation, , anatomical abnormalities of intramyocardial arterioles and LVOT obstruction (Camici et al. 2012; Maron et al. 2009; Knaapen et al. 2007; Camici et al. 1991). However, the relative contribution of each and the impact of LVOT obstruction compared to myocardial hypertrophy alone remain unclear.

In the healthy heart, the higher impedance of the coronary microcirculation during systole limits coronary flow, with the majority of flow occurring in diastole when the ventricle is relaxed (Spaan et al. 1981). Wave intensity analysis (WIA) describes the waves that cause acceleration or deceleration of coronary blood (Parker 2009) and has allowed elucidation of the dominant mechanisms underlying coronary filling in structurally normal hearts (Davies et al 2006a) and aortic stenosis (Davies et al. 2011). Acceleration of coronary flow results from either compression waves originating from the aortic (proximal) end or expansion waves originating from the microcirculatory (distal) end. Separated wave intensity allows separation of the proximal and distal effects while net wave intensity describes the net result of opposing waves during the cardiac cycle.

In HCM there are increased competing forces both proximally and distally: proximally there are changes in left ventricular contraction and relaxation and possible effects of LVOT obstruction and distally there are changes due to compression and dysfunction of the microcirculation. Coronary flow abnormalities are common in HCM, with flow reversal during systole and higher flow velocities during diastole (Krams et al. 1998; Yang et al. 2004; Kyriakidis et al. 1997).

The aim of this study is to elucidate the mechanism of myocardial ischemia and angina in HCM through the combination of coronary WIA and cardiovascular magnetic resonance (CMR) to measure the impact on myocardial perfusion.

## 6.2 Specific Methods for Chapter

### 6.2.1 Patient selection and recruitment

Patients were recruited from the Royal Brompton and Harefield NHS Foundation Trust, Liverpool Heart and Chest Hospital and Imperial College NHS Foundation Trust. Consecutive patients with HCM and a clinical indication for coronary angiography were invited to participate. Control patients had a structurally normal heart, an indication for coronary catheterization and subsequent angiographically unobstructed coronary arteries. All participants gave written consent. The study was approved by an independent ethics committee.

HCM was defined according to the American Heart Association criteria (Gersh et al. 2011). LVOT obstruction was defined at the time of cardiac catheterization as a resting gradient of 30mmHg or greater. Exclusion criteria were: i) coronary artery disease (defined as >50% narrowing of epicardial coronary arteries >2mm), ii) hypertension not controlled by medical therapy (>140/80mmHg at rest on two successive readings), iii) valvular heart disease (excluding mitral regurgitation due to systolic anterior motion (SAM) of the mitral valve), iv) For controls: diagnosis of microvascular ischemia

Subjects were asked to abstain from smoking and caffeine containing substances for 24 hours prior to examination.

### 6.2.2 Invasive data acquisition

After pressure equalisation with the pressure sensor at the tip of the guiding catheter, the Doppler velocity and pressure wire (Combowire, Volcano Therapeutic) was advanced in the proximal left anterior descending (LAD) coronary artery with optimisation of the Doppler signal. Simultaneous recordings of pressure, flow velocity and electrocardiogram were obtained at rest and peak hyperemia following an intravenous infusion of adenosine (140 μg /kg/minute) for three minutes. Data were similarly obtained in the proximal ascending thoracic aorta. The left ventricular pressure was recorded at rest and during hyperemia.

### 6.2.3 Temporal profile of proximal LAD coronary flow

The cycle length, duration of systole and diastole and time between onset of diastole (defined by the dicrotic notch (Kyriakidis et al. 1997)) to peak coronary flow velocity were calculated for each patient. Coronary volume flow rate was calculated from the product of the coronary flow velocity and the coronary diameter as previously described (Timmer et al. 2011).

### 6.2.4 Calculation of coronary wave intensity

Data were analysed using a customised automated Matlab analysis program (Davies *et al* 2006a). Four to five beats of pressure and flow velocity data were ensemble averaged and a Savitzky- Golay filter (polynomial order 3, frame size 31) was used to calculate the time derivative of the data (Savitsky A 1964). The derivatives of the pressure and flow at each time-point were used to calculate the net wave intensity, with units $Wm^{-2}s^{-2}$. Waves were categorised in terms of direction (forward for waves of proximal origin, backward for waves of distal origin) and associated pressure change (compression – associated with a rise in pressure, expansion – associated with a fall in pressure). The sum of squares method was used to determine the wave speed and allow calculation of the separated wave intensity at rest (Parker 2009). Since this method has been shown to be less accurate under conditions of low coronary resistance (Rolandi et al. 2014), only the net wave intensity was used to compare rest and hyperemia.

### 6.2.5 Resting measurements: separated wave intensity

Cumulative separated wave intensity was defined as the integral of wave intensity over a given peak, with units of $W\ m^{-2}s^{-1}$. For comparison between patients, we also presented the cumulative wave intensity of a particular separated wave as a proportion of the total separated cumulative wave intensity, the 'proportion of separated cumulative wave intensity (%)' (Davies *et al*. 2006a)

For patients with ventricular ectopics, WIA in the proximal LAD was also calculated at rest for a post-ectopic sinus beat and for a single beat of similar cycle length in a period of stable rhythm for comparison.

### 6.2.6 Comparison of rest and hyperemia: net wave intensity

The net wave intensity was calculated at each time-point and also expressed as a proportion of the total net wave intensity, the 'proportion of net cumulative wave intensity (%)'. Similarly, the proportion of accelerating waves (forward compression waves and backward expansion waves) was calculated as the sum of the magnitudes of the net accelerating waves as a proportion of the cumulative net wave intensity.

### 6.2.7 Calculation of coronary flow reserve and coronary resistance

Coronary flow reserve was calculated as the mean coronary flow velocity throughout the cardiac cycle at maximal hyperemia divided by the mean coronary flow velocity at rest. The coronary resistance was calculated as the mean pressure divided by the coronary flow in the LAD.

## 6.3 CMR data acquisition

CMR data were collected on a 3T Siemens Skyra scanner. A balanced steady state free precession (bSSFP) sequence was used to obtain breath-hold cine images in three long-axis planes, followed by a contiguous short axis stack through the ventricle. Myocardial first-pass perfusion imaging was performed using a rate-3 parallel accelerated bSSFP sequence (Ismail et al. 2014). Three short axis images and an image of the arterial input function were acquired every cardiac cycle for 70 cycles. Initial proton density-weighted images prior to the arrival of contrast were used for subsequent surface coil intensity correction.

CMR first pass perfusion was recorded at hyperemia and rest. Adenosine was infused at 140μg /kg/min using the same protocol as the invasive study. At peak hyperemia, a bolus of gadolinium contrast (Gadovist, Bayer-Schering, Berlin, Germany, 0.05mmol/kg) was rapidly injected followed by a 25ml saline flush. Following acquisition of peak stress first pass perfusion, adenosine was stopped and a top up bolus of gadolinium (0.05mmol/kg) was administered. Late gadolinium enhancement (LGE) imaging was performed using an inversion recovery-prepared segmented turbo fast low-angle shot sequence 10 minutes after injection of gadolinium. The inversion recovery time was optimised to null normal myocardium. After 20 minutes, rest perfusion imaging was carried out using the same slice positions and gadolinium bolus.

### 6.3.1 Quantification of CMR volumes, LV wall stress and first pass myocardial perfusion

Ventricular volumes, function, mass, and ejection fraction were assessed using semi-automated software (CMRtools, Cardiovascular Imaging Solutions, London). The mean left ventricular mid-wall active fibre stress was calculated at end-diastole and peak systole as follows (Arts et al. 2003):

*Wall stress=LV pressure(1+3(LV volume)/LV wall volume*

Myocardial blood flow (MBF) was calculated using customised software developed in the Interactive Data Language (Exelis Visual Information Solutions, Boulder, Colorado, USA) to correct surface coil-intensity bias and motion artefacts. MBF was quantified pixel-wise using model-constrained deconvolution as previously validated (Hsu et al. 2012) at rest and hyperemia. LGE was quantified using the full-width, half-maximum method and presented as a percentage of total left ventricular mass, using commercially available software (CMR42, Circle Cardiovascular Imaging, Calgary, Canada).

## 6.4 Statistical analysis

Statistical analysis was performed using Stata version 12 (StatCorp LP). Normally distributed data are presented as mean ± SD, comparison between groups was performed using Student's t-test. Non-normally distributed data are presented as median and inter-quartile range (IQR) and compared using the Mann-Whitney U test. Correlation was assessed using the Pearson correlation coefficient. A p-value$< 0.05$ was considered significant.

## 6.5 Results

Baseline characteristics are shown in Table 6.1. Of the 33 HCM patients, 16 had resting LVOT obstruction (mean gradient 60±36mmHg). All patients were in sinus rhythm at the time of study, with the exception of one patient who developed bigeminy during his CMR perfusion scan.

**Table 6.1:** Patient characteristics for HCM and control subjects enrolled in this study.. Continuous variables are compared using Student's t-test and categorical values using chi-square test.

NYHA–New York Heart Association, LV–left ventricular, EDV–end diastolic volume, ESV–end systolic volume, EF–ejection fraction, LVM–left ventricular mass, i- indexed to body surface area, RVEF–right ventricular ejection fraction, EDP–end diastolic pressure, ACE–angiotensin converting enzyme.

| | **Control** (n=20) | **HCM** (n=33) | **p – value** |
|---|---|---|---|
| Age | 59±15 | 54±14 | 0.89 |
| male, n(%) | 12(60%) | 24(73%) | 0.34 |
| wall thickness,mm | 10±2 | 21±4 | <0.01 |
| LVOT obstruction | 0(0%) | 16(48%) | <0.01 |
| NYHA I/II/III | 13/7/0 | 4/18/11 | <0.01 |
| mean NYHA class | 1.6±0.5 | 2.2±0.6 | 0.03 |
| History of ventricular tachycardia | 0(0%) | 3(9%) | 0.17 |
| Implantable cardioverter defibrillator, n(%) | 0(0%) | 2(6%) | 0.26 |
| Chest pain, n(%) | 16(80%) | 24(73%) | 0.55 |
| Shortness of breath, n(%) | 4(20%) | 26(79%) | <0.01 |
| Syncope, n(%) | 0(0%) | 9(27%) | 0.01 |
| LVEDVi, ml/$m^2$ | 130±42 | 71±21 | 0.01 |
| LVESVi, ml/$m^2$ | 41±24 | 18±9 | <0.01 |
| LVEF, % | 70±8 | 73±14 | 0.07 |
| LVMi, g/$m^2$ | 63±15 | 115±41 | <0.01 |
| RVEF, % | 58±5 | 65±14 | <0.01 |
| LGE (% of total LV mass) | 0% | 22.3±14.1 | <0.01 |
| Rest MBF, ml/kg/min | 1.0±0.3 | 1.1±0.3 | 0.56 |
| Hyperemic MBF, ml/kg/min | 1.8±0.5 | 1.5±0.5 | 0.04 |
| MPR | 1.9±0.5 | 1.4±0.3 | <0.01 |
| Resting heart rate, beats per minute | 68±22 | 64±11 | 0.54 |

| | | | |
|---|---|---|---|
| Resting systolic blood pressure,mmHg | 130±16 | 116±19 | 0.04 |
| Resting diastolic blood pressure,mmHg | 70±10 | 65±15 | 0.26 |
| LV EDP rest, mmHg | 14.2±2.6 | 24.4±8.3 | <0.01 |
| LV EDP hyperemia, mmHg | 13.6±3.1 | 27.7±7.1 | <0.01 |
| | | | |
| **Co Morbidities** | | | |
| Hypertension, n(%) | 12(60%) | 7(21%) | <0.04 |
| Diabetes, n(%) | 2(10%) | 1(3%) | 0.29 |
| Hypercholesterolemia, n(%) | 12(60%) | 4(12%) | <0.01 |
| Current smoker, n(%) | 4(20%) | 4(12%) | 0.44 |
| | | | |
| **Medications** | | | |
| Beta blockers, n(%) | 4(20%) | 26(79%) | <0.01 |
| ACE inhibitors, n(%) | 8(40%) | 3(9%) | <0.07 |
| Calcium channel blockers, n(%) | 0(0%) | 6(18%) | 0.04 |

### 6.5.1 Coronary flow velocities

CFR was lower in HCM compared to controls (1.9±0.8 versus 2.7±0.9, p=0.01). Ten HCM patients with LVOT obstruction and three without LVOT obstruction had flow reversal during systole. No control patients had flow reversal.

### 6.5.2 Assessment of pressure waveforms

Fourteen (88%) patients with LVOT obstruction demonstrated a bisferiens pressure waveform in the proximal LAD (also observed in the proximal aorta), with a transient reduction in pressure during systole (Figure 6.1). This was not seen in control patients or HCM patients without resting LVOT obstruction.

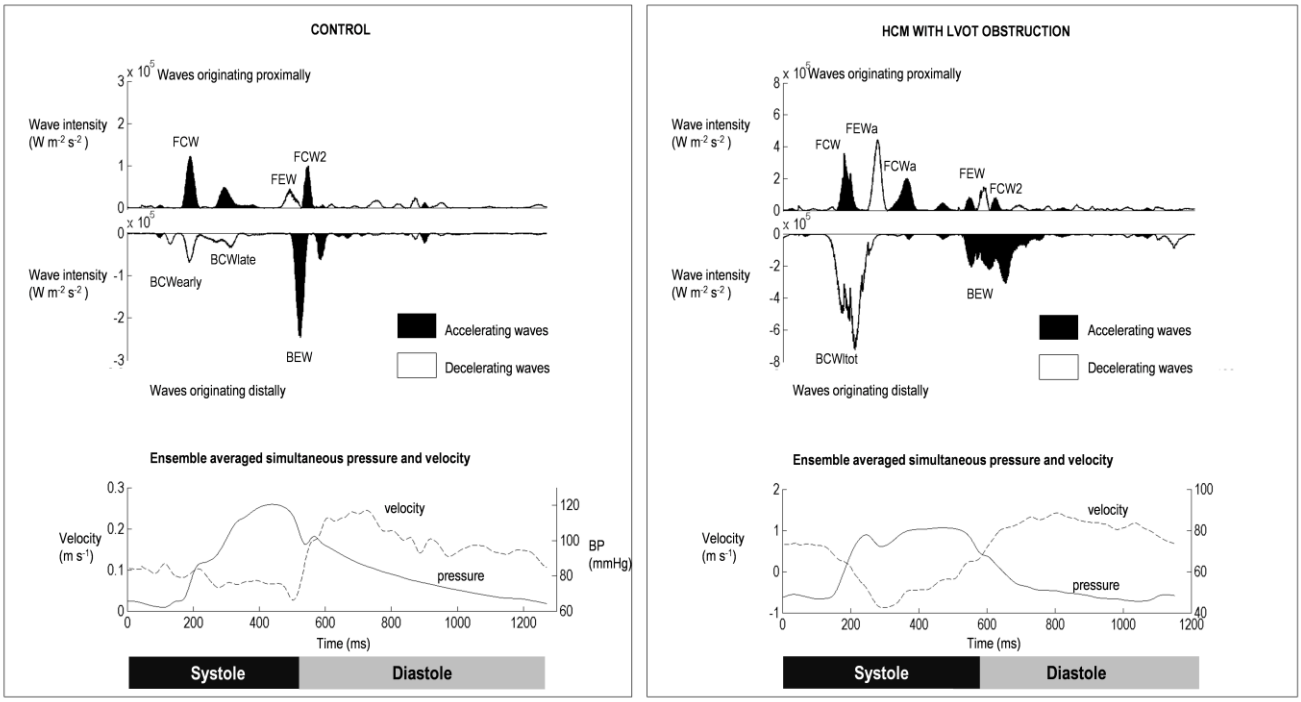


**Figure 6.1:** Example traces for separated wave intensity in a control and an HCM patient with LVOT obstruction at rest. The top panels show the WIA pattern. Proximally originating waves are displayed above the axis and distally originating waves below the axis. The bottom panel shows the ensemble averaged pressure (solid line) and flow velocity (dashed line) during the cardiac cycle. Note the difference in the wave intensity and velocity scales. In controls, the dominant wave is the BEW but in HCM, the BCW is dominant. With severe LVOT obstruction, there is an additional forward deceleration wave ($FEW_a$).

### 6.5.3 Identification of coronary waves

Figure 6.1 shows the results of WIA in a control and a HCM patient with LVOT obstruction. Patients with HCM had a continuous backward compression wave ($BCW_{tot}$) during early systole rather than the separate early and late backward compression waves seen in the controls ($BCW_{early}$ and $BCW_{late,}$ Figure 6.1). 14/16 of patients with LVOT obstruction had an additional forward expansion wave ($FEW_a$) during ventricular systole and 9/16 had an additional forward compression wave ($FCW_a$) following the $FEW_a$ (Figure 6.1). These waves coincided with the transient drop and then rise in proximal LAD pressure seen in the bisferiens pressure waveform, coupled with a decrease in coronary flow velocity (Figure 6.2).

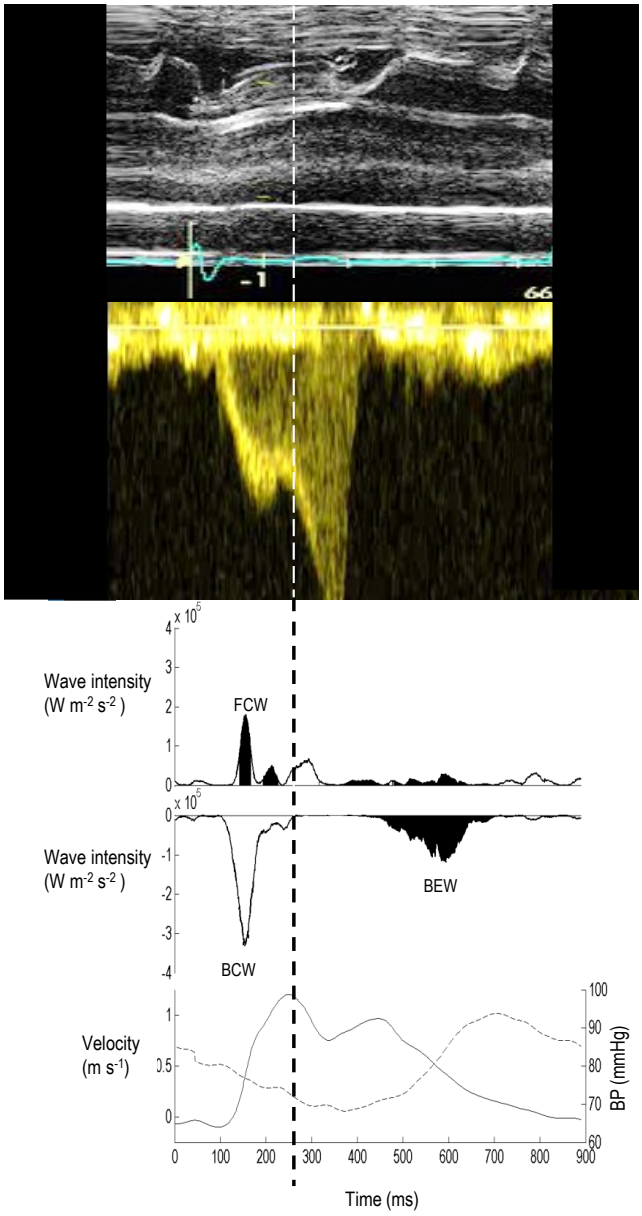


**Figure 6.2**: Obstruction of the LVOT due to SAM of the mitral valve (top panel, M mode through mitral valve) results in a transient reduction in outflow at the point of most severe obstruction (middle panel, continuous wave Doppler) and a decelerating wave ($FEW_a$) which is transmitted into the coronary arteries, causing deceleration of coronary flow and a reduction in coronary pressure (bottom panel). The panels were aligned by the ECG R wave with a minimal time delay to account for distance between measurement sites.

In HCM, a larger proportion of the total separated cumulative wave intensity was comprised of the $BCW_{tot}$ and a smaller proportion by the backward expansion wave (BEW) compared to controls (Table 6.2). There was no significant difference in any of the waves between the LVOT obstruction and no LVOT obstruction HCM groups, with the exception of the additional $FCW_a$ and $FEW_a$ which were present only in the LVOT group.

**Table 6.2:** Separated wave intensity analysis results for HCM and control patients. Values were compared using Student's t – test. A p value of <0.05 was considered significant.

| | Separated cumulative wave intensity /$Wm^{-2}s^{-1}$ x $10^6$ | | | Proportion of separated cumulative wave intensity(%) | | |
|---|---|---|---|---|---|---|
| | **Control** | **HCM** | **p-value** | **Control** | **HCM** | **p-value** |
| Forward compression wave (FCW) | 6.6±4.1 | 7.3±5.1 | 0.61 | 26.8±7.4 | 22.4±10.9 | 0.09 |
| Forward expansion wave (FEW) | 2.8±2.5 | 1.4±1.2 | 0.005 | 9.9±4.6 | 4.2±2.6 | <0.001 |
| Forward expansion wave additional (FEWa) | 0±0 | 2.1±2.6 | <0.001 | 0±0 | 4.1±4.9 | 0.02 |
| Forward compression wave additional (FCWa) | 0±0 | 1.31.9 | 0.002 | 0±0 | 1.5±4.1 | 0.08 |
| 2nd forward compression wave (FCW2) | 2.2±1.8 | 1.3±1.4 | 0.03 | 9.5±4.1 | 2.3±4.6 | <0.001 |
| Backward compression wave (BCWtot) | 4.9±3.0 | 13±8.3 | <0.001 | 21.0±6.2 | 38.2±11.1 | <0.001 |
| Backward expansion wave (BEW) | 8.3±5.1 | 9.8±6.5 | 0.4 | 32.8±6.2 | 27.2±7.9 | 0.006 |

### 6.5.4 Post ectopic beats

Seventeen HCM patients (52%) had ectopic beats at rest during the procedure. Comparing rest and post-ectopic beats, cycle length (974±57ms versus 973±153ms, p=0.9) and coronary flow velocity (0.34±0.15 versus 0.33±0.15m/s, p=0.33) were similar, but mean coronary pressure tended to be lower for the post ectopic beats (106±16 versus 111±18mmHg, p=0.051). The $BCW_{tot}$ was higher (42±9% versus 37±9%, p =0.01), the BEW lower (26±3% versus 30±7%, p=0.01) and $FEW_a$ tended to be higher (8.1±5.1 to 4.1±4.9%, p=0.1) for the post ectopic beat (Figure 6.3). There was no significant difference in the FCW, the FEW or the $2^{nd}$ FCW.

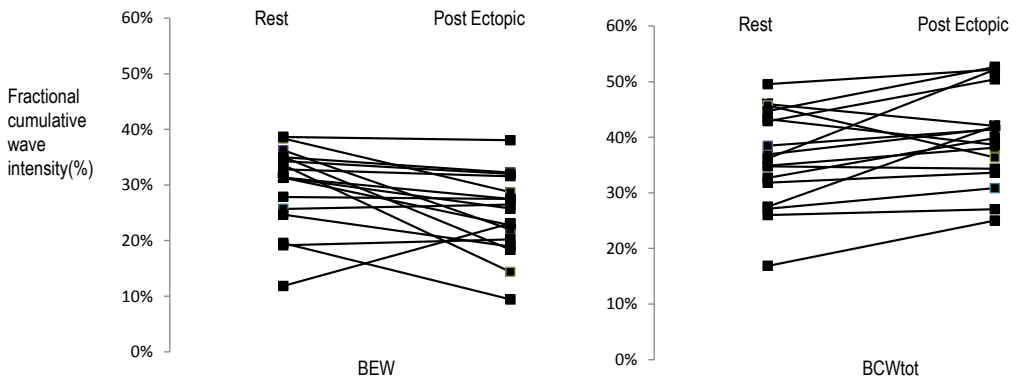


**Figure 6.3:** Comparison of the separated cumulative wave intensity (%) for the BEW and $BCW_{tot}$ at rest and following an ectopic beat in HCM patients.

### 6.5.5 Impact of hyperemia on coronary hemodynamics and myocardial perfusion

During hyperemia, coronary flow velocity increased and coronary resistance fell in all patients. HCM patients had a lower resting coronary resistance (Figure 6.4) than controls. Comparing HCM to controls, resting MBF was similar but hyperemic MBF and MPR were lower (Table 6.1).

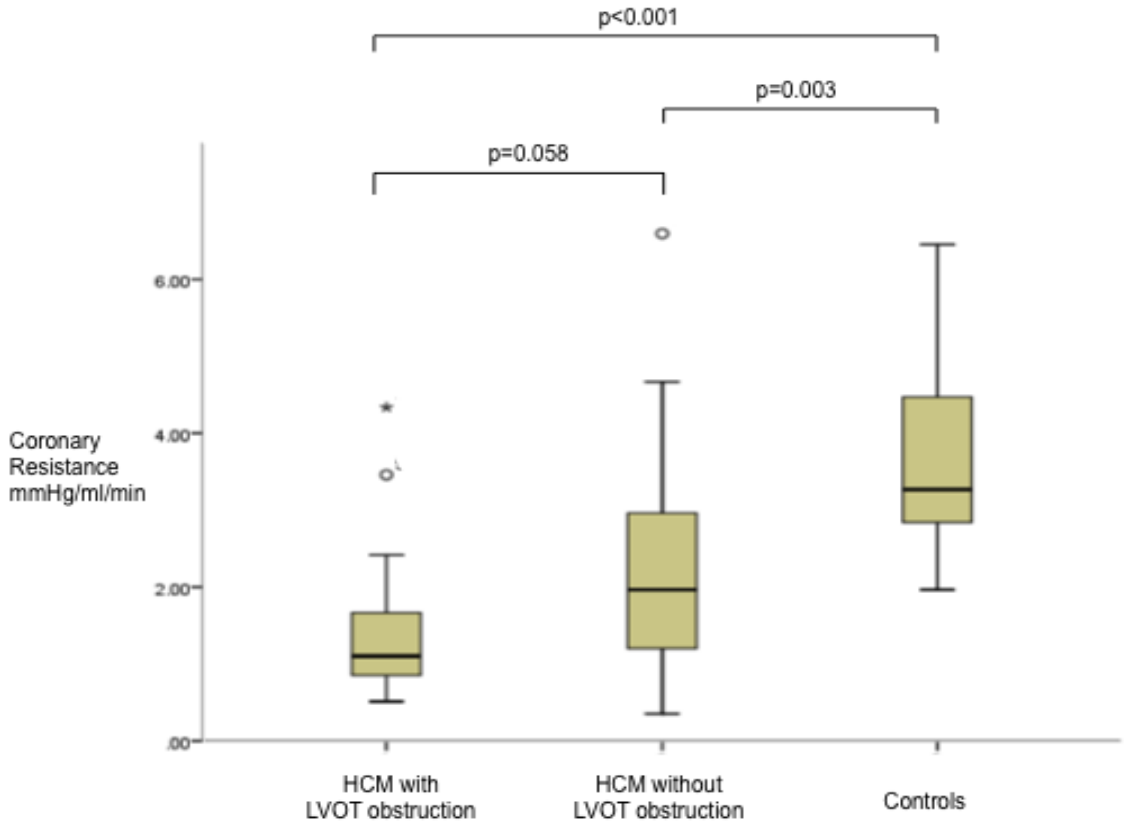


**Figure 6.4**: Comparison of resting coronary resistance in HCM patients with and without LVOT obstruction and control patients. Comparison between groups was performed using ANOVA. A p-value of <0.05 was considered to be significant.

### 6.5.6 Comparison of net wave intensity at rest and during hyperemia (Table 6.4)

At rest there was a higher $BCW_{tot}$ and lower FEW in HCM compared to controls. The FCW was significantly lower but there was no significant difference in the BEW. During hyperemia, there was a significant increase in the size of all waves in both groups but the comparative pattern remained similar. The FCW was smaller and the $BCW_{tot}$ larger in HCM compared to controls. There was no difference in the BEW.

**Table 6.3**: Proportion of net cumulative wave intensity (%) at rest and hyperemia for HCM and control subjects. Values were compared using Student's t – test. A p value of <0.05 was considered significant

* means calculated only for the patients with the additional wave (FCWa, n=14, FEWa, n=9).

| | Rest | | | Hyperemia | | |
|---|---|---|---|---|---|---|
| | **Control** | **HCM** | **p** | **Control** | **HCM** | **p** |
| Forward compression wave (FCW) /% | 30.1±14.9 | 15.7±17.5 | 0.004 | 24.7±15.1 | 11.7±13.1 | 0.002 |
| Forward expansion wave (FEW) /% | 8.8±7.3 | 2.5±3.1 | <0.001 | 6.9±6.9 | 2.7±3.4 | 0.006 |
| Forward compression wave additional (FCWa) /% | 0±0 | 7.4±7.2* | <0.001 | 0±0 | 9.4±9.4* | <0.001 |
| Forward expansion wave additional (FEWa) /% | 0±0 | 3.9±2.7* | <0.001 | 0±0 | 2.2±1.3* | <0.001 |
| 2nd forward compression wave (FCW2) /% | 6.0±6.7 | 3.2±8.1 | 0.21 | 2.1±3.9 | 1.0±2.1 | 0.17 |
| Backward compression wave (BCWtot) /% | 16.6±9.5 | 38.3±19.2 | <0.001 | 27.9±12.6 | 43.2±14.2 | <0.001 |
| Backward expansion wave (BEW) /% | 38.6±13.5 | 37.2±12.3 | 0.7 | 38.4±10.3 | 38.7±11.2 | 0.9 |

**Table 6.4**: Coronary flow and cardiac cycle timings for HCM and control subjects. Values were compared using Student's t – test. A p value of <0.05 was considered significant.

| | Rest | | | Hyperemia | | |
|---|---|---|---|---|---|---|
| | **Controls** | **HCM** | **p-value** | **Controls** | **HCM** | **p-value** |
| Mean coronary flow velocity,m/s | 0.19±0.07 | 0.27±0.11 | 0.001 | 0.49±0.18 | 0.48±0.18 | p=0.78 |
| Cycle length, ms | 948±267 | 937±227 | 0.68 | 873±148 | 864±145 | 0.6 |
| Duration of diastole, ms | 527±157 | 482±82 | 0.21 | 304±115 | 240±120 | 0.02 |
| Time between onset of diastole and peak coronary velocity, ms | 109±32 | 145±72 | 0.007 | 114±42 | 163±76 | 0.009 |
| Diastolic wall stress,kPa | 8.1±1.9 | 8.3±2.3 | 0.78 | 3.2±0.8 | 4.3±1.5 | 0.008 |
| Systolic wall stress,kPa | 105.1±24.7 | 70.7±20.9 | <0.001 | 63.4±15.9 | 41.6±15.0 | <0.001 |

### 6.5.7 LV wall stress

HCM patients had higher LV wall stress in mid-diastole but lower wall stress during systole compared to controls (Table 6.3). For HCM, the systolic wall stress correlated with the BCW (r=0.36, p=0.02) at rest but not during hyperemia (r =-0.29; p=0.12). There was no significant correlation between resting diastolic wall stress and %LGE (r=-0.13, p=0.51).

### 6.5.8 Comparison between wave intensity and CMR measurements

There was no significant correlation between the $\%BCW_{tot}$ at rest and the MBF at rest (r=-0.25, p=0.14) but a significant correlation between the proportion of accelerating waves at

rest and MBF at rest (r=0.35, p=0.02). MPR correlated with the % increase in the BCW during hyperemia (r=-0.34, p=0.03) and with the % increase in the proportion of accelerating waves (r=0.62, p<0.01, Figure 6.5). There was no relationship between MPR and wall thickness (r=0.3, p=0.12) or LV mass (r=-0.17,p=0.39) nor between % LGE and wave intensity measures either at rest or hyperemia.

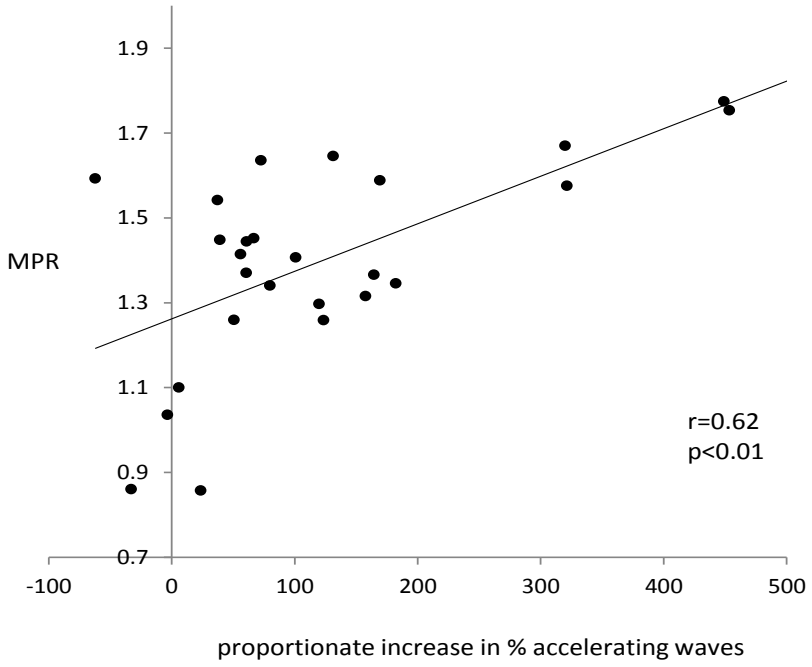


**Figure 6.5**: There was a significant correlation between the myocardial perfusion reserve (MPR) and the proportionate increase in percentage of accelerating waves during hyperemia in patients with HCM. Correlation was assessed using Pearson's correlation coefficient (r).

## 6.6 Discussion

Microvascular ischemia is an important and well-recognised feature of the pathophysiology of HCM. It is associated with chest pain, clinical deterioration, diastolic dysfunction and has prognostic significance (Maron et al. 2009; Cecchi et al. 2003; Olivotto et al. 2006; Camici et al. 1991). A pressing and unmet need in HCM is a better understanding of the mechanisms driving myocardial ischemia (Gersh et al. 2011). HCM is a complex disease and multiple factors contribute to the associated microcirculatory abnormalities: the increased wall thickness results in both a supply/demand mismatch and increased compression of the microcirculation during systole, left ventricular outflow tract obstruction results in high intra-cavity pressures during ventricular systole, and microcirculatory vessels themselves have been shown to be abnormal on histology (Varnava et al. 2000). Most pharmacotherapies in HCM have non-specific actions and consequently there is still a high burden of morbidity (Spoladore et al. 2012). In addition, microvascular dysfunction is often seen in patients with mild or no symptoms and can precede clinical deterioration by a long interval (Cecchi et al. 2003). With the advent of novel agents that may improve microvascular perfusion (Mehta et al. 2011) a better mechanistic understanding of perfusion abnormalities in HCM may lead to a more personalised and targeted approach to treatment.

The present study is the first to use wave intensity to provide detailed analysis of factors affecting coronary flow, particularly LVOT obstruction, and demonstration of its impact on myocardial perfusion. Importantly, we demonstrate the interplay of upstream and downstream determinants of microvascular ischemia with insights into the dominant mechanisms influencing coronary flow. For symptomatic patients, this work supports the need to address the degree of outflow tract obstruction in conjunction with targeted therapy for the microcirculation.

## 6.7 Mechanisms of impaired myocardial perfusion in HCM: insights from WIA

Perfusion abnormalities in HCM have sometimes been assumed to result simply from supply/demand mismatch, however we showed no correlation between the wall thickness or LV mass with the MPR. Rather, we demonstrated that perfusion abnormalities result from dynamic changes in myocardial mechanics throughout the cardiac cycle. We highlight three mechanisms that result in impairment of myocardial perfusion in HCM and which may result in symptoms of chest pain and shortness of breath. All of these mechanisms may occur

separately or simultaneously in a patient. Firstly, extravascular compression and deformation of the intra-myocardial arterioles during ventricular systole results in a large, backward compression wave. This decelerating wave accounts for the retrograde coronary flow in systole seen in some individuals with HCM. Secondly, impaired ventricular relaxation results in a smaller backward expansion wave. This accelerating wave is the main contributor to coronary flow in healthy individuals and its impairment in HCM can have a significant impact on diastolic perfusion. Finally, in some patients with HCM, transient obstruction of flow in the LVOT decreases the proximal driving pressure resulting in a forward deceleration wave that is transmitted into the proximal coronary artery and diminishes forward flow. Coronary flow in HCM is therefore deranged, with opposing forces acting throughout the cardiac cycle. Compensatory vasodilation may preserve resting coronary flow but at the expense of the physiological reserve.

### 6.7.1 Systolic coronary flow reversal in HCM

Compression and deformation of the pre-capillary arteries and arterioles during ventricular systole, results in a very large backward compression wave, sufficient to stop or even reverse flow in the proximal epicardial coronary arteries. Blood is forced back from the intra-myocardial vessels towards the epicardial coronary arteries, while the increased compression of the arterioles results in higher impedances within these vessels. Although the intra-myocardial veins and venules are also compressed, this compression occurs further downstream and therefore the displaced blood is more likely to be pushed further downstream into the venous system.

Although coronary resistance was higher in HCM compared to controls at rest during systole, it was lower during diastole. This resulted in higher coronary flow velocities during diastole. This suggests that despite the adverse remodelling and reduction in vessel density observed in HCM (Varnava et al. 2000), vasodilatation accounts for the reduced coronary resistance during diastole. Although this normalizes myocardial perfusion at rest, it depletes the coronary flow reserve.

Calculated diastolic wall stress was higher in HCM compared to controls, particularly during hyperaemia. Interestingly, systolic wall stress was lower, in keeping with previous work (Hayashida et al. 1991). While fibrosis and myocardial disarray will create localised areas of

high wall stress that were not accounted for, these results and the lack of correlation between wall stress and MPR suggest that wall stress alone is insufficient to explain angina in HCM.

The complexity of coronary hemodynamics and the interaction of proximal and distal effects is well-illustrated by the results for early systole. The contraction of the myocardium compresses the blood in the left ventricle causing a FCW to propagate through the aortic root into the coronary arteries while simultaneously compressing the intra-myocardial blood vessels causing a BCW in the epicardial coronary arteries. In controls the ratio of the net cumulative wave intensity of the FCW to the BCW is approximately 2:1 (Table 6.4) resulting in acceleration of coronary flow during early systole. In HCM, the ratio is reversed, approximately 1:2, which causes deceleration during early systole. The situation is worsened during hyperemia, where the ratio reduces to 1:4 and reversal of blood flow direction is even greater.

### 6.7.2 Impaired relaxation in HCM: effect on the microcirculation

As the ventricle relaxes, compression of the intra-mural vessels is relieved, generating a backward expansion wave (BEW) which accelerates coronary flow to produce higher coronary perfusion during diastole than during systole. In our HCM cohort, the BCW during ventricular contraction was greater than the BEW during ventricular relaxation which is opposite to the pattern seen in controls. Although HCM patients exhibit a reduced coronary resistance at rest compared to controls, coronary flow is still impeded by slower and sometimes incomplete relaxation of the ventricle. Patients with HCM typically have diastolic impairment (Spirito & Maron 1990; Nagueh et al. 2001) with a prolonged time to reach peak diastolic flow compared to controls, a raised EDP and a smaller BEW wave. Diastolic dysfunction results from increased wall thickness, interstitial and replacement fibrosis, and leads to delayed relaxation and increased passive stiffness. It is therefore unsurprising that the BEW did not correlate with the percentage of replacement fibrosis alone.

### 6.7.3 The impact of LVOT obstruction

Patients with severe LVOT obstruction had higher coronary flow velocities than either controls or patients without resting LVOT obstruction. Those with high pressure gradients across the LVOT demonstrated a bisferiens pressure wave in the proximal aorta. This has previously been shown to result from transient obstruction of the LVOT(Doshi et al. 2002).

This bisferiens pressure wave is transmitted into the carotid artery where it can be palpated clinically (Fleming 1957). We have demonstrated that the bisferiens pressure waveform is also transmitted into the proximal coronary artery in the form of a forward expansion wave, $FEW_a$, as the LVOT is transiently obstructed by the mitral valve, followed by a forward compression wave, $FCW_a$, when the obstruction is relieved.

Although a larger BCW or smaller BEW might be expected in patients with LVOT obstruction compared to those without, HCM is clinically extremely heterogenous. Both waves will be affected by the degree of diastolic dysfunction, myocardial fibrosis and ventricular contractility so it is not surprising that division of our patient cohort by presence of LVOT obstruction did not yield significant differences between the two subgroups. The effect of LVOT obstruction on the BCW and BEW may be more easily examined by comparison of sinus and post-ectopic sinus beats in the same patient. Changes in ventricular filling following an ectopic beat results in a greater gradient though the LVOT. This was associated with an increase in the BCW, a reduction in the BEW and increase in the $FEW_a$. Therefore, for the same patient, coronary filling becomes more inefficient with a higher LVOT gradient.

The relative timing of systole and diastole will further disadvantage patients with LVOT obstruction. LVOT obstruction prolongs the duration of LV ejection at the expense of the diastolic phase(Plehn et al. 2004). Despite the favourable reduction in microcirculatory resistance during diastole, there is less time for coronary filling. The situation is exacerbated at higher heart rates, with an even shorter diastolic time despite increased basal metabolic requirements.

### 6.7.4 Changes in wave intensity during hyperemia

Typically, HCM patients show normal perfusion at rest but impaired myocardial perfusion reserve. Myocardial perfusion is complex and mediated by waves generated both proximally and distally throughout the cardiac cycle. Net wave intensity allows a clearer measure of the dominant wave at each point in time during the cardiac cycle. The changes in each wave with hyperemia may explain the variable profile of symptoms in patients with similar levels of hypertrophy or resting blood flow (Figure 6.6).

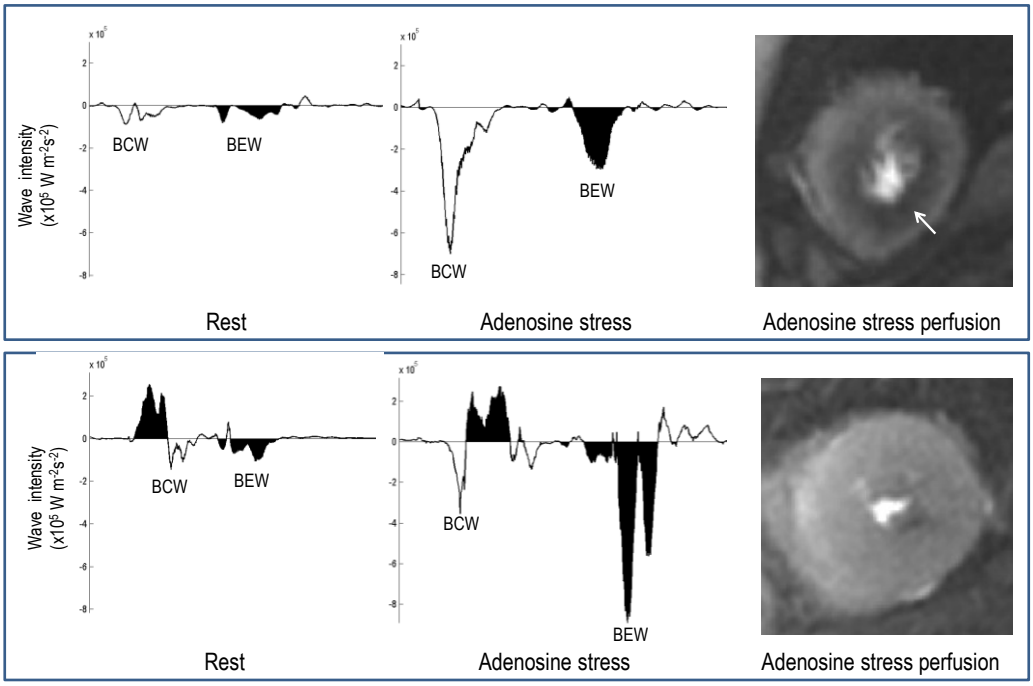


**Figure 6.6**: The relative changes in each wave dictate myocardial perfusion downstream. The two patients above have similar wall thicknesses (22-24mm), no resting LVOT obstruction and normal epicardial coronary arteries. Patient 1 (top) had severe, typical angina whereas patient 2 (bottom) was asymptomatic. The left panel shows net wave intensity at rest, the middle panel net wave intensity during hyperemia (at the same scale) and the right panel a CMR short axis first pass myocardial perfusion image during hyperemia. The top patient has an increase in the BEW but a proportionately greater increase in the BCW during hyperemia which is associated with a large inducible circumferential myocardial perfusion defect during hyperemia (arrowed). The bottom patient has a small increase in the BCW and a large increase in the BEW, resulting in normal myocardial perfusion during hyperemia.

### 6.8 Impact on potential treatment strategies in HCM

Chest pain in HCM is often atypical and may occur at rest (Pasternac et al. 1982). Wave intensity analysis may explain the improvement in myocardial perfusion seen following treatment with beta blockers and calcium channel blockers (Sugihara et al. 1998). Both increase the diastolic duration and reduce myocardial contractility. The longer diastolic time with lower coronary resistance will improve coronary filling, while the reduction in contractility will lead to a reduction in the BCW. These are particularly important during

exercise, where basal metabolic requirements are increased and diastolic duration reduced. These drugs may also reduce or eliminate LVOT obstruction (Vaglio et al. 2008). Perhexiline improved energetics and ventricular relaxation, improving symptoms and exercise capacity (Abozguia et al. 2010).

However, these drugs have limitations and may not improve the extravascular component of coronary resistance to the extent to which they enhance diastolic relaxation. Consequently, treatments for chest pain are often ineffective, particularly where heart rate, blood pressure or side-effects limit up-titration.

Recently, ranolazine, an inhibitor of the late sodium channel, has been proposed as a treatment for HCM. In vitro, ranolazine has been shown to lower diastolic calcium concentration, improving diastolic function (Coppini et al. 2013). This may further improve coronary filling and trials are in process.

Septal reduction therapies are offered to symptomatic patients with LVOT obstruction. These may improve myocardial perfusion (Timmer et al. 2011) and coronary flow reserve (Jaber et al. 2009). Improvements have been assumed to result from reduction in intra-cavity pressures causing a reduction in microvascular compression. We have demonstrated a further mechanism for perfusion abnormalities: a proximally occurring deceleration wave resulting from LVOT obstruction. There are therefore multiple mechanisms by which septal reduction therapy could improve symptoms. Some patients have minimal improvement in symptoms following removal of LVOT obstruction with successful septal reduction therapy, this may be due to a persistent large BCW. In this case, combination therapy with other agents to reduce extravascular compression and prolong diastolic filling time may be of benefit. Addressing upstream and downstream components will be key in management of symptoms in the broader population.

Treatment strategies that reduce decelerating waves, either of proximal or distal origin, will improve the efficiency of coronary filling and should therefore improve myocardial perfusion. Early treatment of perfusion abnormalities in HCM may also potentially prevent subsequent development of heart failure. As perfusion abnormalities are common in HCM, treatments that prolong diastolic filling time may be beneficial in all patients, not just those that experience symptoms. Our work suggests a combination rather than single agent approach may be of benefit in HCM.

## 6.9 Study Limitations

Patients recruited for the study had a clinical indication for invasive coronary angiography, as required by our ethical approval. Therefore the control population typically had risk factors for coronary artery disease, including hypertension and diabetes, both of which are associated with microvascular disease. Notably, controls with cardiac syndrome X were excluded. Had a completely healthy control population been recruited there may have been even greater differences in myocardial perfusion and coronary hemodynamics compared to the HCM population. The mean age of HCM patients was 54 years (range 22-74). Accordingly, our findings cannot be generalised to the pediatric or adolescent population. However, coronary hemodynamics and WIA appeared similar in the 6 patients aged <40 compared to the rest of the sample.

A constant mean wave speed was used in the calculation of the separated wave intensities. While there may be changes in the wave speed throughout the cardiac cycle, these small variations have not been shown to have a significant effect on the separated wave intensity (Davies 2006b) and the net wave intensity, which does not depend on estimation of wave speed, gave similar results.

## 6.10 Conclusion

Wave intensity analysis in HCM demonstrated that coronary flow abnormalities occur due to opposing proximal and distal effects resulting from compression and deformation of the intra-mural blood vessels, ventricular ejection and impaired ventricular relaxation. LVOT obstruction may generate an additional deceleration wave. These abnormalities result in impaired myocardial perfusion in HCM. A clear understanding of the mechanisms underlying perfusion abnormalities may inform a more targeted treatment strategy.

# CHAPTER 7

## Development and validation of high temporal resolution retrospectively-gated spiral phase velocity mapping of the coronary arteries using CMR

A version of this chapter has been published as follows:

Raphael CE, Keegan J, Parker KH, Simpson R, Strain S, de Silva R, Di Mario C, Collinson J, Stables RH, Wage R, Sugathapala M, Prasad SK, Firmin D. Validation of high temporal resolution spiral phase velocity mapping of temporal patterns of left and right coronary artery blood flow against Doppler guidewire. *JCMR* 2015:17:85-91

### 7.1 Abstract

**Background**: Coronary blood flow velocity measurements throughout the cardiac cycle are required for calculation of wave intensity and may also be used to assess coronary flow reserve. The gold standard for measurement is invasive Doppler flow wire assessment, however this is associated with potential risks of bleeding and vessel perforation. CMR measurement would allow non-invasive assessment and may therefore allow study of a wider cohort of patients without clinical risk or use of ionizing radiation.

**Methods**: A retrospectively-gated breath-hold spiral phase velocity mapping sequence with high temporal resolution was developed at 3 Tesla. Serial patients who had undergone Doppler flow wire measurement at the time of angiography were invited for a CMR. Velocity maps were acquired in the proximal right coronary artery and proximal left anterior descending artery. MR velocity-time curves were processed semi-automatically and compared with corresponding Doppler data for temporal agreement in flow-velocity curves, mean velocity throughout the cardiac cycle, peak systolic velocity (PSV) and peak diastolic velocity (PDV).

**Results**: Eighteen subjects (9 proximal right and 15 proximal left arteries) completed CMR examination. When corrected for differences in heart rate between the two studies, MR mean velocity

through the cardiac cycle, PSV and PDV were approximately 40% of the peak Doppler values with a moderate – good linear relationship between the two techniques ($R^2$: 0.4, 0.5 and 0.8 respectively). MR values of PDV/PSV showed a strong linear relationship with Doppler values (slope: 1.05 and 0.98 and $R^2$ 0.9 and 0.7 for right and left arteries respectively). Plots of MR velocities at any time point in the cardiac cycle against Doppler velocities in individual vessels showed a linear relationship with high $R^2$ values (mean +/- SD: 0.8 +/- 0.1).

**Conclusions**: High temporal resolution breath-hold spiral phase velocity mapping of the coronary arteries may be acquired using MR. MR underestimates absolute values of coronary flow velocity when compared to Doppler flow-wire but allows accurate assessment of the temporal patterns of blood flow, suitable for wave intensity analysis.

### 7.2 Background

Wave intensity analysis (WIA) allows phasic flow to be divided into a series of wavefronts that underlie the changes in pressure and flow seen within the coronary arteries (Davies et al. 2006; Davies et al. 2011; Parker 2009). These waves can arise proximally or distally and each can either accelerate or decelerate the flow of blood. WIA characterises coronary artery flow by dividing it into its major contributing waveforms and allows the relative contribution of each to be assessed (Sen et al. 2013). The first in man studies cast new light on how the complex interaction of the ventricle, coronary artery and myocardial microcirculation produce the characteristic left and right coronary flow profiles and greatly improved our understanding of ventricular physiology (Davies et al. 2006). Coronary WIA demonstrated 6 predominant waves occurring during the cardiac cycle. The majority of coronary filling occurs in early diastole as a result of a backward-travelling expansion wave (BEW) generated by myocardial microcirculatory decompression as the ventricle relaxes. This wave is significantly reduced in patients with left ventricular hypertrophy and aortic stenosis (Davies et al. 2006).

Doppler flow wire measurements during invasive coronary angiography are the gold standard for flow velocity measurements (Doucette et al. 1992). A small wire with a Doppler sensor on the tip is positioned directly in the artery of interest under fluroscopic guidance. While the procedure is typically safe, there is a small but significant risk of serious complications including coronary artery perforation and bleeding and patients are exposed to ionizing radiation. The technique has therefore been limited to research measurements and repeat studies to follow disease progression or monitor the effects of treatments have not been performed.

A non-invasive method of WIA would enable the study and characterization of the coronary haemodynamics both in health and in a wider cohort of patients. Cardiovascular magnetic resonance (CMR) is a safe and non-invasive technique that allows assessment of cardiac anatomy and physiology. CMR assessment of blood flow is now a routinely used clinical tool in the heart and large vessels (Keegan, Gatehouse, Mohiaddin, et al. 2004; Keegan, Gatehouse, Yang, et al. 2004) and has recently been used to measure flow for WIA in the aorta (Biglino et al. 2012). Application to the coronary arteries is complicated by their small size, cardiac and respiratory motion, vessel tortuosity and lower flow velocities compared to large arteries requiring highly sensitive velocity encoding gradients.

Non-Cartesian techniques for assessing coronary flow velocity at 1.5 Tesla were developed at the Brompton and allow more efficient data acquisition compared to conventional Cartesian techniques. These enabled imaging during a single breath-hold with reasonable spatial and temporal resolution (Keegan, Gatehouse, Yang, et al. 2004; Keegan, Gatehouse, Mohiaddin, et al. 2004). Coronary flow velocities were sampled every 30 ms and temporal flow velocity profiles were similar to expected in healthy volunteers. An early study using 4 or 5 cine frames per cardiac cycle showed that MR measures of absolute coronary flow showed good agreement with Doppler values but the temporal resolution was insufficient to assess the temporal flow velocity pattern (Hundley et al. 1996). MR measures of peak flow velocity are known to be significantly lower than those measured by Doppler but previous work using a navigator gated sequence showed a close linear relationship between the techniques, allowing accurate non invasive measurement of coronary flow reserve (Nagel et al. 1999).

We validated CMR measures of coronary flow velocity using a sequence with a high temporal resolution and retrospective gating to allow acquisition throughout the cardiac cycle.

## 7.3 Methods

### 7.3.1 Patient selection

Serial patients undergoing invasive Combowire study for the previous study were invited for an additional research CMR. The study was approved by an independent ethics committee and all patients gave written informed consent.

### 7.3.2 Acquisition of invasive coronary wave intensity data

Following diagnostic coronary angiography, an intra-arterial pressure and Doppler velocity wire (Combowire, Volcano Therapeutic) was positioned in the proximal left anterior descending artery

(LAD) and the proximal right coronary artery (RCA). After pressure equalisation with the pressure sensor at the tip of the guiding catheter, the Doppler velocity and pressure wire (Combowire, Volcano Therapeutic) was advanced into the artery with optimisation of the Doppler signal. A fluoroscopic recording was made to document the location of measurements and to act as a reference for the subsequent CMR study. Flow velocity and electrocardiogram were acquired at rest for a period of 60 seconds in each artery.

### 7.3.3 Acquisition of Cardiovascular magnetic resonance data

An interleaved spiral phase velocity sequence, was custom developed by Dr Jenny Keegan on a 3 Tesla Magnetom Skyra MR scanner (Siemens AG Healthcare Sector, Germany). A 1-1 water excitation eliminated off-resonance blurring of fat. Full k-space coverage was achieved in 8 spiral interleaves of 11.8 ms duration. Phase map subtraction of datasets with symmetric bi-polar velocity encoding gradients resulted in through-plane velocity maps, with a phase shift of ±180° representing a flow velocity of ±30cm/s i.e. flow would alias if it exceeded 30cm/s. For patients with high flow velocities, this limit was increased to ±40cm/s. Following a single dummy cycle, these velocity encoded datasets were acquired in alternating cardiac cycles in an end-expiratory breath-hold of 17 cardiac cycles duration, TE 5.2 ms, TR 19 ms, slice thickness 8mm, spatial resolution 1.4 x 1.4 mm (reconstructed to 0.7 x 0.7 mm through zero-filling) and repeat time 19ms. The number of coil elements used was limited to 6 from the anteriorly-positioned cardiac coil and 6 from the posterior spine coil in order to reduce reconstruction time and to minimise wrap. Retrospective ECG gating allowed full coverage of the entire cardiac cycle in 50 cine frames.

The coronary artery origins were identified using transverse segmented gradient echo scout acquisitions. From these, oblique and double oblique images were acquired to image the artery in-plane. A region of interest in a straight section of the proximal artery was selected and through-plane acquisition spiral coronary artery phase velocity maps were then acquired at this location (Figure 7.1). Where possible, locations were directed by the invasive fluroscopic images to ensure the same location as invasive data acquisition. Sensitivity to off-resonance artefact was minimised using localised second-order shimming and frequency adjustment based on the signal from a user-defined region of interest positioned over the heart. For right coronary studies, an additional breath-hold spiral phase velocity mapping acquisition was performed using fat-excitation (Keegan, Gatehouse, Yang, et al. 2004). This was later used to correct for the through-plane velocity of the RCA. Spiral acquisitions were repeated to allow analysis of inter breath-hold reproducibility.

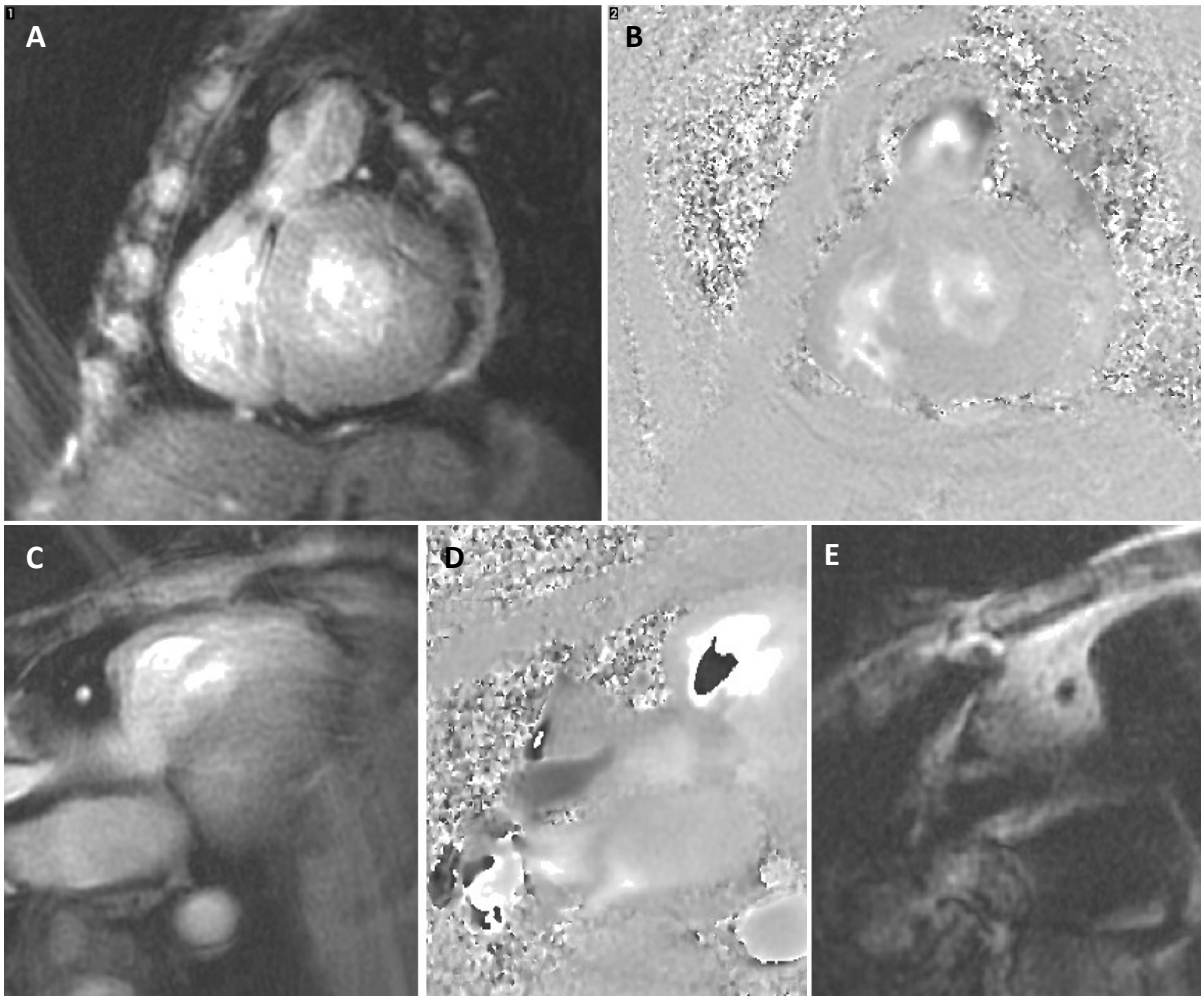


**Figure 7.1**: Cross sectional imaging of LAD (top panels) and RCA using phase encoded (A and C), velocity encoded (B and D) and fat excitation imaging (E)

To minimise circadian variation in coronary flow between studies, readings were taken under standardised conditions, with both procedures performed at the same time of day, with a minimum of 30 minutes lying supine at rest prior to data acquisition. Patients refrained from caffeine containing substances and smoking prior to each procedure.

### 7.4.1 Analysis of invasive flow velocity data

Ensemble-averaged Doppler velocity temporal profiles were produced, averaging data over 4-6 cardiac cycles and using a Savitzy-Golay filter (Savitzky & Golay 1964). If there was flow reversal (in some of the HCM patients) and the bi-directional peak flow detection algorithm failed to work reliably, the unidirectional peak flow detection algorithm was used instead. The Doppler traces typically showed a degree of mirror artefact whereby the trace is reflected about the horizontal zero velocity line (Figure 7.2). In subjects with reverse systolic flow, the unidirectional peak flow detection picked up the mirrored (positive) velocity rather than the negative velocity. If it was clear from the

relative intensities of the real and mirrored signals and the signal on bidirectional mode that the flow was indeed negative, then that peak flow velocity was reversed to record a negative value. If it was not clear from the traces whether the flow was positive or negative - usually when the absolute velocity was very low or, less often, when the mirror intensity was low - then that section of the trace (typically 50 – 100 ms) was eliminated for the purposes of comparison with MR.

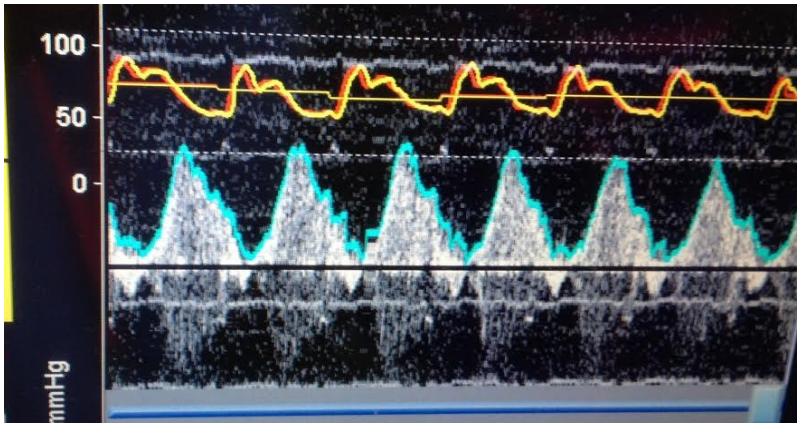


**Figure 7.2:** Velocity signal output from Volcano console showing a subject with coronary flow velocity reversal during systole that was not well detected by the automatic detection algorithm

### 7.4.2 Analysis of MR flow velocity data

The MR flow velocity data output was of the mean flow velocity in the vessel rather than the peak velocity, which is the output from the Doppler flow wire. We elected to use the mean because the small size of the coronary arteries meant that the peak velocity would measure a single pixel and therefore would be extremely noisy. Velocity-time curves for the mean velocity were generated for each breath-hold by two independent observers using semi-automatic custom MATLAB software developed by Dr Keegan and Stephen Strain at the Royal Brompton Hospital (Keegan et al. 2015). The user marks the centre of the vessel on the cross-sectional segmented gradient echo scout image and following multi-level thresholding, a circular ROI is automatically defined around the coronary artery using a modified Hough transform based algorithm(Atherton & Kerbyson 1999). This initial ROI is copied to the first frame of the spiral magnitude dataset which is put through a spatial band pass filter to identify objects of similar size. A search for local maxima within a specified range of the initial ROI center locates circular objects of the specified size and the one closest to the initial position is selected as the location of the artery in that time-frame. This new ROI location is copied to the corresponding velocity map and to the next frame in the spiral magnitude dataset where the process is repeated, thereby allowing automatically tracking of the artery from frame to frame of the acquisition. Data is then manually reviewed by the user to ensure the artery location has been accurately tracked by the automated software. This has been shown to have excellent agreement with

manually derived measures of coronary flow velocity with a much faster image processing time (Keegan et al. 2015).

The resulting velocity-time curve produced is a composite of the through-plane velocity of coronary blood flow and the through-plane velocity of the vessel itself. For the LAD, the velocity of a tracked region of nearby myocardium was used as a marker of the through-plane velocity, while for the RCA, the adjacent myocardium was typically too thin to use for correction and the velocity of a tracked region of interest in the surrounding epicardial fat was used instead (Keegan, Gatehouse, Yang, et al. 2004). This method has previously been shown to agree well with correction using adjacent myocardium (Keegan, Gatehouse, Yang, et al. 2004).

The following parameters were extracted from the invasive and non invasive velocity-time curves: peak systolic velocity (PSV), peak diastolic velocity (PDV), time to peak systolic velocity (TPSV), time to peak diastolic velocity (TPDV), flow and mean velocity through the cardiac cycle (MV). For each pair of Doppler and MR velocity time-curves, peak systolic velocity (PSV), peak diastolic velocity (PDV), and mean velocity through the cardiac cycle (MV) were determined. Each parameter was then compared using simple linear regression. Coronary blood flow velocity will increase with heart rate(McGinn et al. 1990; Di Mario et al. 1995) and therefore analyses were repeated after adjustment for heart rate differences between the MR and Doppler data.

To assess temporal flow patterns, the MR velocities throughout the cardiac cycle were plotted against the corresponding Doppler velocities or each vessel. Where necessary, the MR trace was slightly shifted relative to the invasive trace to correct for small changes in the ECG triggering between the MR and Doppler studies.

**7.5 Statistical analysis**

All analyses were performed using IBM SPSS Statistics 19 Package. Normally distributed data were presented as mean± standard deviation and categorical data as number (percentage of total).

PSV, PDV and mean velocity through the cardiac cycle were compared between MR and invasive measurements using simple linear regression. To assess temporal flow patterns, the MR velocities throughout the cardiac cycle were plotted against the corresponding Doppler velocities or each vessel. The relationship between the two techniques was assessed with simple linear regression.

For assessment of reproducibility, the inter-observer variability and the inter breath-hold reproducibility of the semi-automatic analysis were determined in a subset of 15 vessels (10 LAD and 5 RCA) using standard deviation of the paired differences, Pearson correlation coefficient and Bland Altman analysis (Bland & Altman 1986).

### 7.6 Results

Eighteen patients were recruited in total and clinical characteristics are summarized in Table 7.1. Fourteen patients had HCM, one had cardiac syndrome X and three were subsequently found to have angiographically normal coronary arteries with atypical symptoms of chest pain. No patients had flow limiting coronary artery disease and 10 (56%) had smooth, angiographically normal coronary arteries. All patients were in sinus rhythm at the time of study.

**Table 7.1**: Characteristics of study population for CMR coronary flow velocity validation study

| | |
|---|---|
| Age | 56±13 |
| Gender (% male) | 12 (67%) |
| **Comorbidities** | |
| Hypertension | 7 (39%) |
| Diabetes | 1 (6%) |
| Hypercholesterolaemia | 7 (38%) |
| Smoker | 1 (6%) |
| Family history coronary artery disease | 2 (11%) |
| **Medications** | |
| Beta blockers | 10 (56%) |
| ACE inhibitors | 2 (11%) |
| Calcium channel blockers | 1 (6%) |
| Aspirin | 5 (28%) |
| Statin | 6 (33%) |

Since the RCA was extremely mobile in the hypercontractile HCM ventricle, acquisition of RCA Doppler data was complicated by Combowire motion artefact in 9 of the cases. Consequently, good quality Doppler data were available in 18 LAD arteries and in 9 RCAs. Good quality MR data were acquired in 24 (89%) of these vessels (15 LAD arteries and 9 RCA). The three other patients were excluded due to arrhythmia (one patient) and high LVOT gradients causing artefact that precluded measurement of coronary flow velocity (2 patients).

There was no significant difference in heart rate between the non-invasive and invasive studies (67.5 ±13.1 vs 64.6±12.4 beats per minute, $p = 0.13$). The systolic and diastolic blood pressures were

significantly higher during the invasive Doppler study (137±21 versus 115±18 mmHg and 81±13 versus 67±10 mmHg, both $p < .001$). Table 7.2 shows the inter-observer reproducibility of the semi-automatic analyses. Figure 7.2 shows the inter breath-hold reproducibility of the temporal flow patterns. In each case, the temporal flow patterns using MR were very similar to Doppler. Bland Altman plots for inter breath-hold reproducibility are shown in Figure 7.3.

**Table 7.2**: Inter observer reproducibility of coronary flow velocity measures using the semi-automatic velocity processing. MV = mean velocity, PSV = peak systolic velocity, TPSV = time to peak systolic velocity, DPV = diastolic peak velocity and TDPV = time to diastolic peak velocity.

| | **mean ± SD** | **mean (± SD) of paired differences** |
|---|---|---|
| mean velocity (mm/s) | 81.0±23.9 | -3.7±7.3 |
| coronary flow (ml/min) | 61.4±26.3 | -2.7±5.7 |
| PSV (mm/s) | 74.5±33.1 | -1.4±16.0 |
| TPSV (ms) | 114.1±55.6 | -1.9±13.3 |
| PDV (mm/s) | 173.1±69.9 | -3.3±16.2 |
| TPDV (ms) | 521.3±106.7 | -9.4±28.5 |

**Table 7.3:** Inter breath-hold comparison of coronary blood flow parameters (mean ± SD of the difference and coefficient of determination ($R^2$). Analysis by the same observer. MV = mean velocity, PSV = peak systolic velocity, TPSV = time to peak systolic velocity, DPV = diastolic peak velocity and TDPV = time to diastolic peak velocity.

| | **mean ± SD of the difference** | **$R^2$** |
|---|---|---|
| mean velocity (mm/s) | -2.4+/-6.9 | 0.92 |
| coronary flow (ml/min) | -1.9+/-4.8 | 0.97 |
| PSV (mm/s) | 1.7+/-15.8 | 0.97 |
| TPSV (ms) | -4.4+/-22.1 | 0.87 |
| PDV (mm/s) | -3.5+/-11.6 | 0.98 |
| TPDV (ms) | -0.1+/-49.3 | 0.86 |

**Figure 7.3:** Inter breath-hold Bland Altman plots of mean velocity (MV), flow, peak systolic velocity (PSV), peak diastolic velocity (PDV) and time to peak systolic velocity (TPSV) and time to peak diastolic velocity (TPDV).

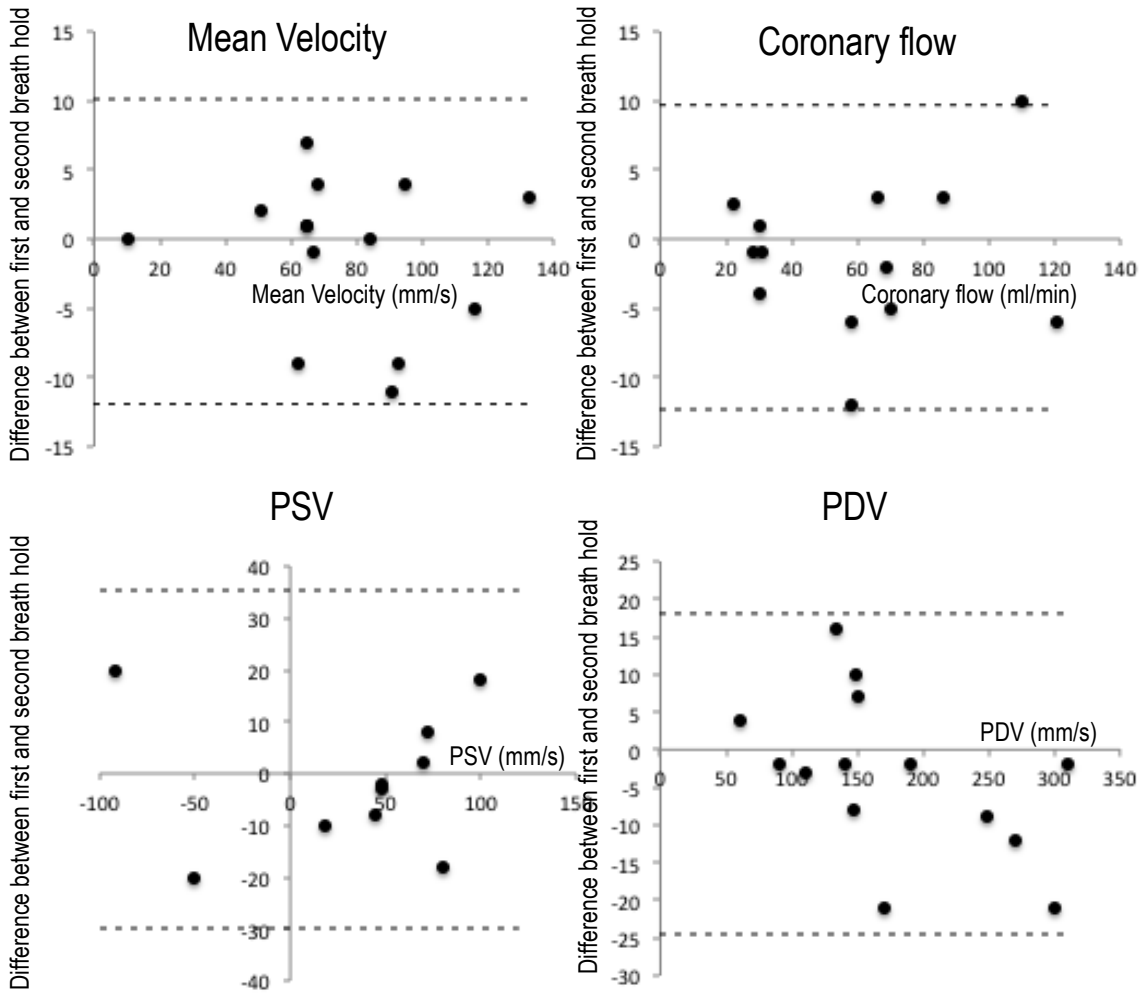

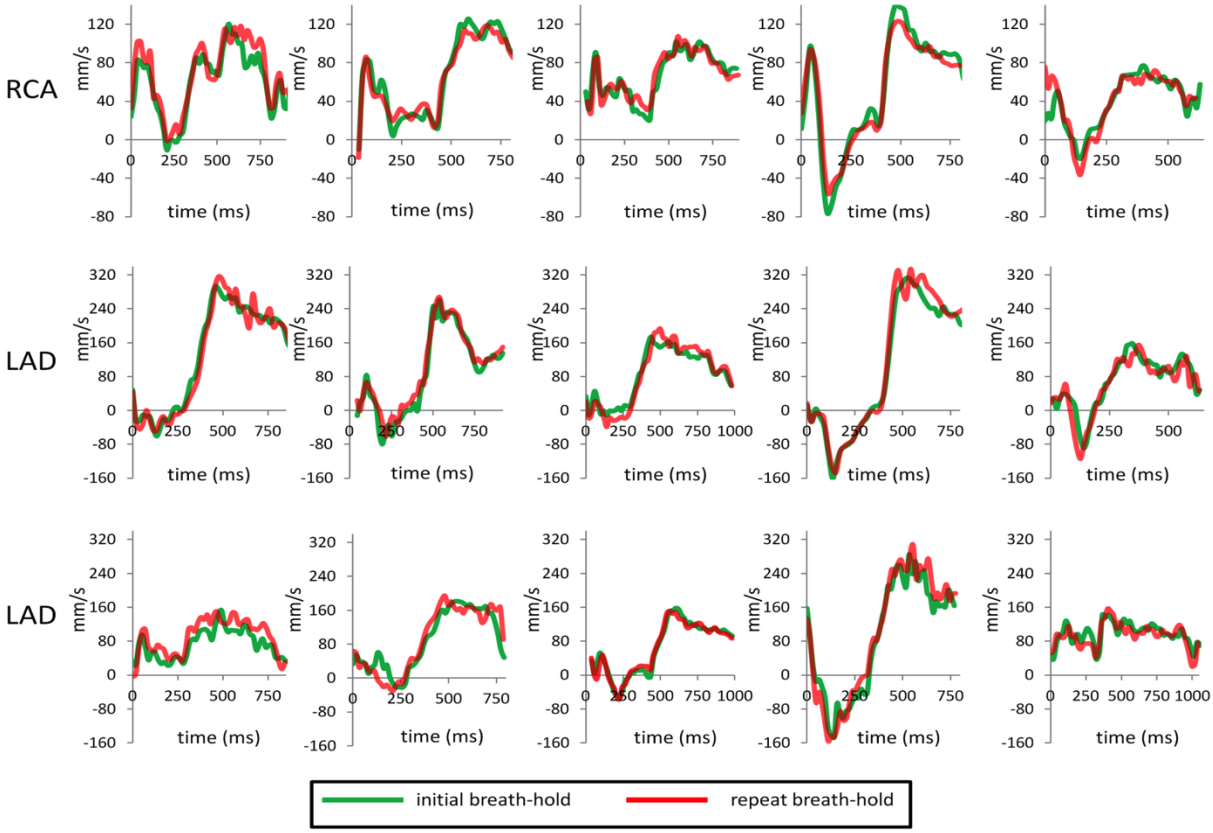


**Figure 7.4:** MR velocity-time curves assessed with the semi-automatic technique for repeated breath-holds in 5 right coronary arteries (top) and 10 left anterior descending arteries (middle and bottom).

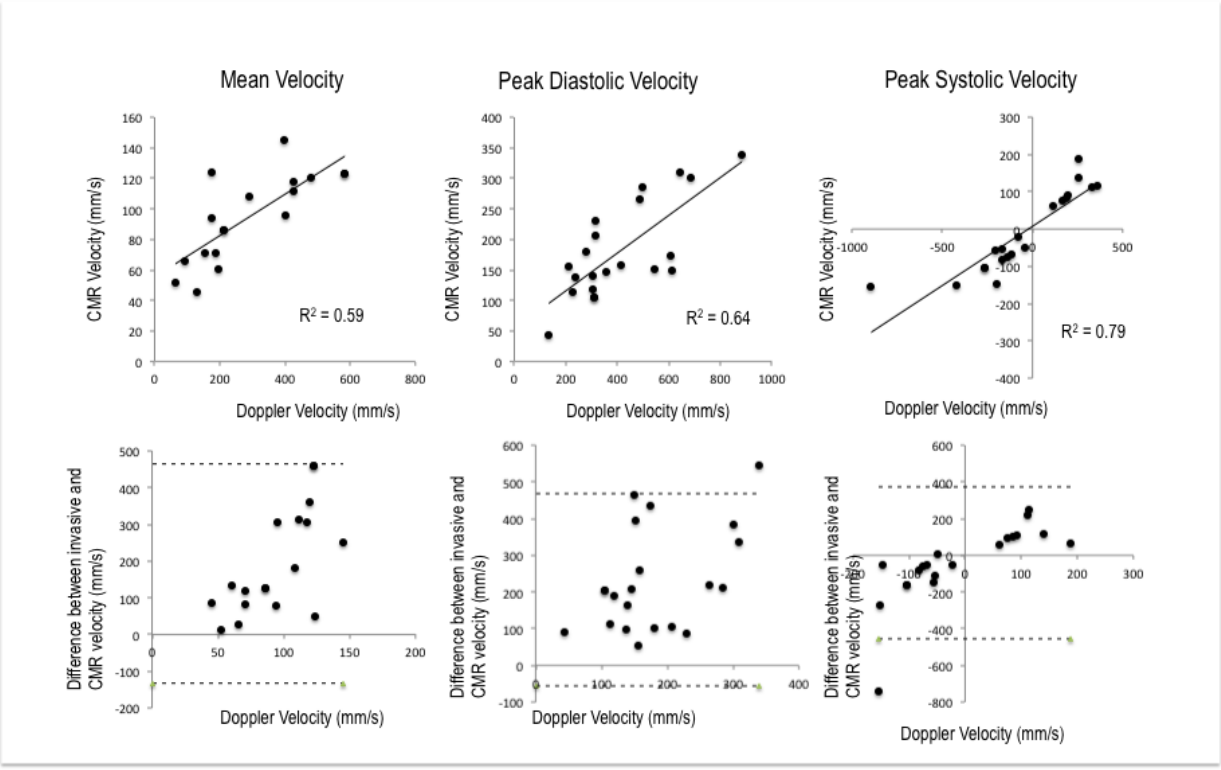


**Figure 7.5**: MR measurement of mean velocity (a), peak diastolic velocity (b) and peak systolic velocity (c) against Doppler values in 24 vessels, scaled to adjust for differences in heart rate between the two acquisitions. The top panels show comparison between Doppler and CMR values while the bottom panels are Bland-Altman plots. As expected, the velocities measured with Doppler were higher than those measured using CMR but with a moderate-strong correlation between the two.

**Figure 7.6** MR versus Doppler values of PDV/PSV for the RCA and LAD vessels (top panels) and Bland Altman Plots for agreement (bottom panels). Coefficient of determination was calculated using Pearson's correlation co-efficient. The relationships are linear with slopes close to unity (RCA: slope 1.05, LAD: slope 0.98) and high coefficients of determination.

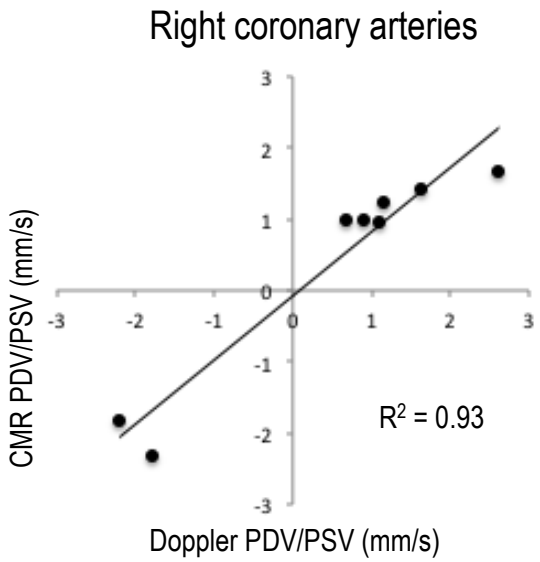
Right coronary arteries
CMR PDV/PSV (mm/s)
Doppler PDV/PSV (mm/s)
R2 = 0.93

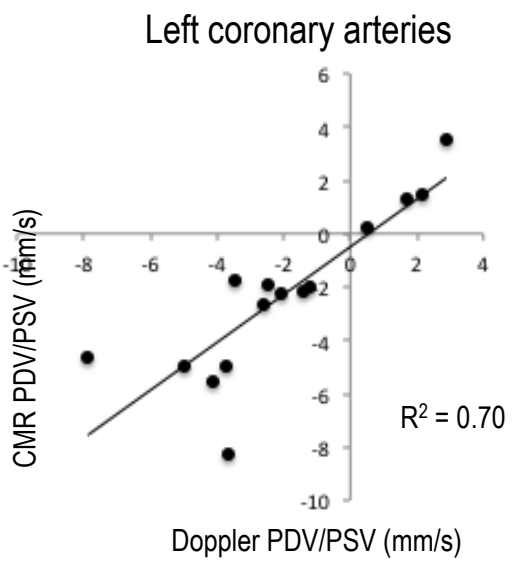
Left coronary arteries
CMR PDV/PSV (mm/s)
Doppler PDV/PSV (mm/s)
R2 = 0.70

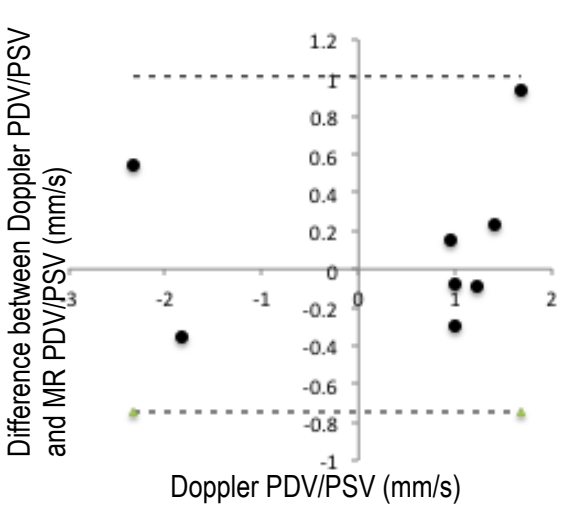
Difference between Doppler PDV/PSV and MR PDV/PSV (mm/s)
Doppler PDV/PSV (mm/s)

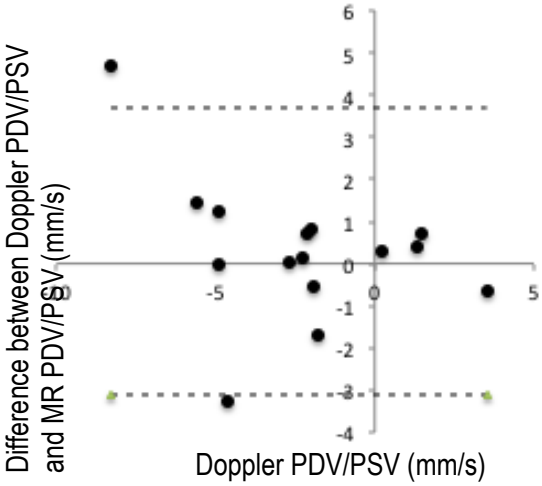
Difference between Doppler PDV/PSV and MR PDV/PSV (mm/s)
Doppler PDV/PSV (mm/s)

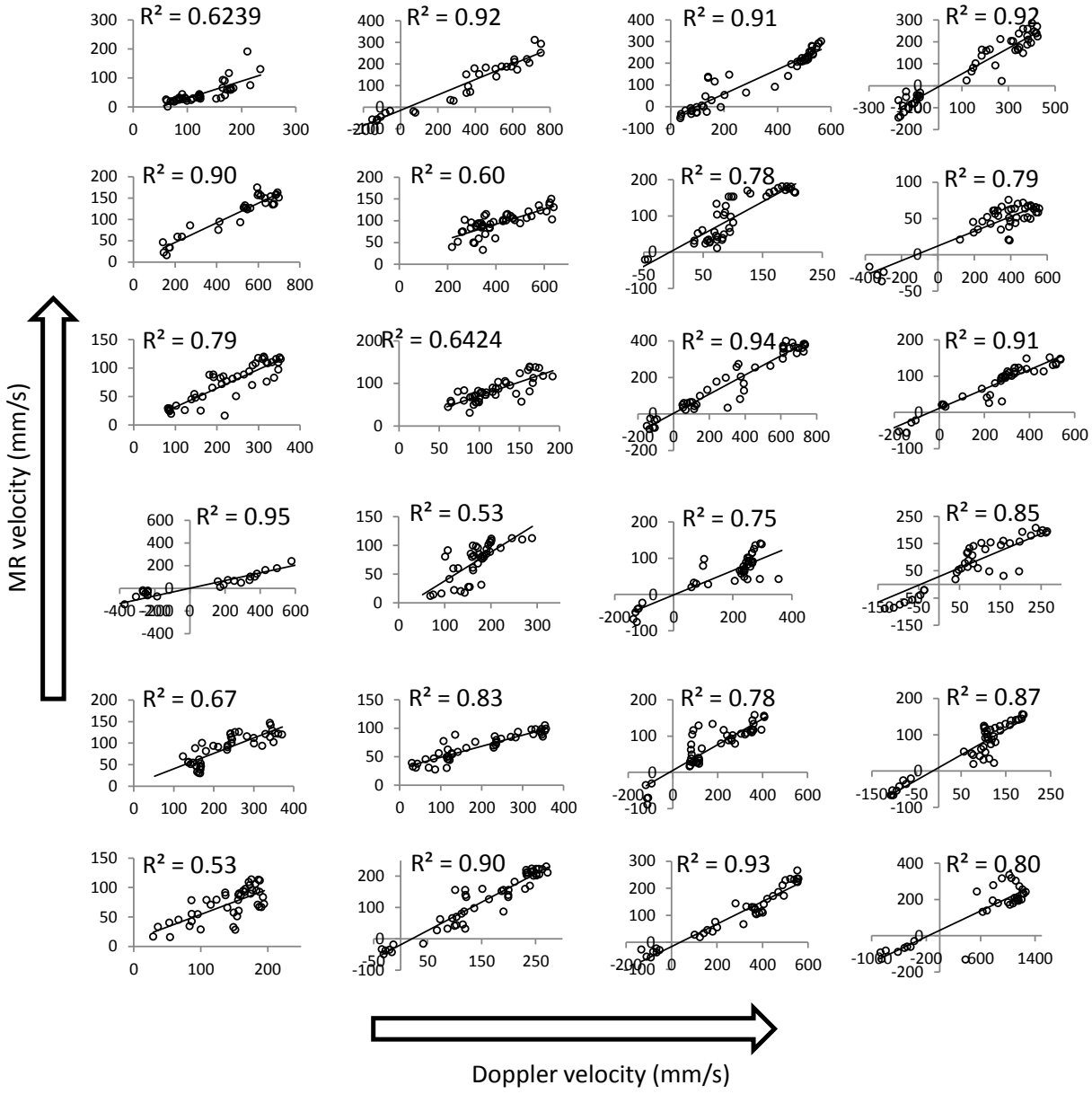


**Figure 7.7** MR measured velocities at all time points in the cardiac cycle plotted against corresponding Doppler velocities for all 24 vessels. Linear regressions are superimposed on each plot. The slopes of the regression plots vary from vessel to vessel (mean 0.66 ± 0.21, range 0.36 – 0.98) which results in the scatter in MV, PSV and PDV seen in Figure 7.6. Higher regression slopes are seen in patients in whom the heart rate during the MR study was higher than that during the invasive study. Although the slope varies, the relationships between the MR and Doppler velocities for each patient are linear with high coefficients of determination (R = 0.9± 0.12).

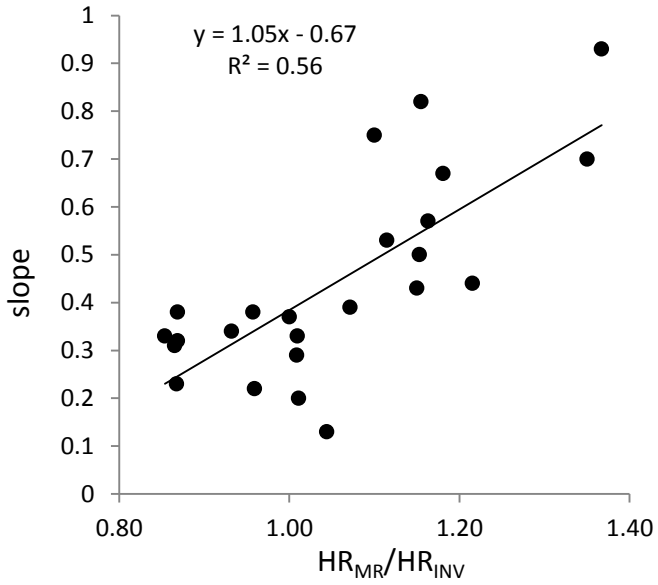


**Figure 7.8:** Slope of MR velocity versus Doppler velocity regression lines of Figure 7.7 against the ratio of the heart rate during the MR study ($HR_{MR}$) to that in the invasive study ($HR_{INV}$).

### 7.7 Discussion

We validated a retrospectively-gated MR spiral phase velocity mapping sequence which allowed the acquisition of reproducible temporal patterns of coronary artery blood flow throughout the cardiac cycle in the left and right coronary arteries with a high temporal resolution, suitable for WIA. The inter breath-hold reproducibility of the technique was excellent for MV, flow, PSV, TPSV and DPV and the temporal profile showed a close agreement with that of invasive data.

The agreement between MR and Doppler assessed PDV/PSV was excellent with a slope close to unity, suggesting that change in velocity was accurately measured non invasively. Regression plots of the MR measured velocities against the Doppler measured velocities throughout the cardiac cycle showed good correlation.

There have been a few previous reports using spiral phase velocity mapping in the coronary arteries (Keegan, Gatehouse, Yang, et al. 2004; Marcus et al. 1982), including a recent study at 3T (Brandts et al. 2010). However, our study was the first to validate the data against invasively measured flow velocity. Retrospective ECG gating allowed measurement of coronary flow velocity through the entire cardiac cycle, required for wave intensity analysis in the coronary arteries.

### 7.7.1 Absolute differences in coronary velocity between invasive and MR studies

The MR measured velocities at any time point in the cardiac cycle were typically ~40% of the corresponding Doppler velocities. The MR values represent the mean velocity within a ROI encompassing the coronary artery whereas with Doppler, the recorded velocities are the peak values within the sample volume. Previous work similarly showed that MR measured PDV using a segmented gradient echo technique was 37% of the corresponding Doppler value (Nagel et al. 1999). Comparing Doppler values to the peak pixel velocities within the MR ROIs, rather than the mean values would be technically possible but the relatively low spatial resolution of the MR acquisition (1.4 x 1.4 mm, reconstructed to 0.7 x 0.7 mm) would mean that the peak value recorded would be taken from one pixel and the result would depend on the exact location of that pixel relative to the peak of the spatial flow profile. The MR data would therefore continue to underestimate the Doppler values and at the same time, would be considerably noisier since it would be derived from a single pixel rather than the cross-sectional average. Accordingly, since WIA uses the derivates of coronary velocity with respect to time rather than the absolute values of coronary flow velocity, we decided to use the mean value to reduce noise and spurious peaks due to artefact.

The systolic and diastolic blood pressures at the time of the invasive study were significantly higher than those at the time of the MR study due to increased physiological and psychological stress on the patient during invasive study. In addition, while overall there was no significant difference between the heart rates in the two studies, some individual patients had a large difference in heart rate between the two studies. The difference in physiological state between the two studies is likely to result in poorer agreement between MR and invasive values. Although we aimed to perform both studies on the same day, this was not always practical and did not correct for the differing stress response to two very different examinations. We therefore elected to correct the coronary flow velocities for differences in heart rate between the MR and invasive studies.

Previous work has shown that the change in blood flow velocity with increasing heart rate is approximately linear (Di Mario et al. 1995; McGinn et al. 1990) and a simple scaling of the MR measured velocities to the same heart rate as the corresponding Doppler velocities was used to account for this. Although this correction was unlikely to entirely adjust for the effect of an increased heart rate, since there will be a greater effect on diastole than on systole, it seemed more physiologically appropriate than comparison of points acquired at markedly different heart rates.

## 7.8 Study Limitations

For the MR velocity-time curve analysis, the coronary artery ROI was automatically defined on the diastolic segmented gradient echo scout image, rather than on the spiral magnitude data, as this has

higher spatial resolution (1 mm x 1 mm rather than 1.4 mm x 1.4 mm) and is less susceptible to off-resonance blurring. The analysis method developed assumes that the cross-section of the coronary artery is circular and does not change through the cardiac cycle, although a coronary artery diameter change of approximately 10% is expected during the cardiac cycle (Ge et al. 1994). The spatial resolution of our acquisition technique was not sufficient to measure such small changes and we therefore used a fixed region of interest size throughout the cardiac cycle.

While the Doppler guidewire is commonly regarded as the gold-standard for coronary artery blood flow velocity assessment, in our study population, it was more difficult to obtain good quality studies in the proximal RCA (9 vessels) than in the LAD artery (18 vessels), despite highly experienced operators. This was potentially due to the higher mobility of the RCA, particularly with a hypercontractile LV in HCM. Consequently, we studied a greater number of LAD arteries compared to RCA arteries. To attempt to perform the MR and Doppler studies in the same location of the vessel, we recorded used a proximal location in the vessel and recorded position fluroscopically at the time of angiography. However, SNR constraints required that the MR slice thickness was relatively large (8 mm) and the flexibility of slice positioning was consequently more limited than invasive Doppler measurement position.

### 7.9 Conclusions

Spiral flow velocity mapping using CMR allows non-invasive measurement of coronary flow velocities in the coronary arteries. While absolute measures of velocity obtained using CMR were lower than those using the Doppler Flowire, the data was reproducible and showed good agreement with invasive data for temporal profile. The data appear suitable for coronary flow velocity acquisitions for CMR wave intensity analysis.

# CHAPTER 8

## Feasibility of Cardiovascular Magnetic Resonance Derived Coronary Wave Intensity Analysis

### 8.1 Abstract


**Background**

Wave intensity analysis (WIA) of the coronary arteries allows description of the predominant mechanisms influencing coronary flow at each point in the cardiac cycle. The data are traditionally derived from pressure and velocity changes measured invasively in the coronary artery. Cardiovascular magnetic resonance (CMR) allows measurement of coronary velocities using flow velocity mapping and derivation of central aortic pressure from aortic distension. We assessed the feasibility of WIA of the coronary arteries using CMR and validated it against invasive data.

**Methods**

Serial patients who had undergone invasive WIA were invited for a research CMR study. Velocity maps were acquired in the proximal left anterior descending and proximal right coronary artery using a retrospectively-gated breath-hold spiral phase velocity mapping sequence with high temporal resolution (19 ms). A breath-hold segmented gradient echo sequence was used to acquire through-plane cross sectional area changes in the proximal ascending aorta. Brachial blood pressure was recorded for calibration. Acquisitions of both were repeated for assessment of intra-study reproducibility. CMR-derived aortic pressures and CMR-measured velocities were used to derive wave intensity. The separated cumulative wave intensities derived from CMR were compared to invasive data in 8 left and 4 right coronary arteries. Intra-study reproducibilities of invasive and non-invasive WIA were assessed using Bland Altman analysis.

**Results**

The combination of the CMR-derived pressure and velocity data produced the expected pattern of forward and backward compression and expansion waves. The intra-study reproducibility of the CMR derived % separated cumulative wave intensities (mean ±standard deviation of differences) was $-1.7x10^{-11}$±6.8. Intra-study reproducibility for the corresponding invasive data was 3.8±4.4. The non-invasive and invasive studies showed reasonable agreement ($r^2$=0.57) with a mean difference of $1.9x10^{-10}$± 10.8.

**Conclusion**

This proof of concept study demonstrated that CMR may be used to reproducibility perform coronary WIA non-invasively, with reasonable agreement with invasive WIA. The technique allows WIA to be performed in a wider range of patients and pathologies than those who may be studied invasively.

## 8.2 Background

Wave intensity analysis (WIA) allows phasic flow to be divided into a series of wavefronts that underlie the changes in pressure and flow seen within a vessel. In the coronary arteries, waves can arise proximally (due to ventricular ejection) or distally (from the microcirculation) and each can either accelerate or decelerate the flow of blood. In the healthy heart there are 6 predominating waves that influence coronary flow, with the majority of coronary flow occurring in diastole due to a backward-travelling expansion wave due to decompression of the coronary microcirculation. Studies in conditions with increased microvascular compression such as left ventricular hypertrophy (Davies et al 2006a) and aortic stenosis (Davies et al. 2011) demonstrated attenuation of this wave, providing a mechanism for chest pain in these patients.

While invasive measurement has traditionally been used to acquire data for wave intensity analysis, this has several limitations, including the potential for complications resulting from coronary angiography and requirement for ionising radiation. This has largely limited wave intensity to a research procedure following clinically indicated cardiac catheterisation. Therefore patient selection is skewed by clinical requirement for cardiac catheterisation, truly asymptomatic patients are unlikely to be studied and serial assessment of wave intensity over time is challenging. A non-invasive method of WIA is therefore desirable.

Non-invasive wave intensity requires high temporal resolution measurement of velocity and pressure data. For the coronary arteries, velocity data has been successfully measured using ultrasound (echocardiography) (Voci, Pizzuto, and Romeo 2004; Kenny, Wisbey, and Shapiro 1994) while distension of the carotid arteries has been used as a surrogate measure for pressure changes (Niki et al. 2002; Li and Guo 2013), Visualisation of the coronary arteries using echocardiography can be challenging and is usually limited to the mid-distal LAD. Measurement is complicated by off-axis imaging planes (Voci, Pizzuto, and Romeo 2004). Cardiovascular magnetic resonance (CMR) offers several potential advantages in flow velocity measurement. High temporal resolution (19 ms) interleaved spiral phase velocity using CMR has recently been shown to allow accurate and reproducible assessment of the temporal patterns of coronary artery blood flow (6). Using this technique, through-plane velocity data with high sensitivity to flow are acquired in a breath-hold, with retrospective ECG gating allowing full coverage of the cardiac cycle in typically 50 frames. Although, as expected, measured velocities are under-estimated relative to invasive Doppler guide wire due to

partial volume averaging, temporal flow patterns in both the left and right coronary arteries have been shown to agree well with those seen invasively.

CMR measurement of aortic distension has been shown to provide a good estimate of central aortic pressure (Quail et al. 2014) and may provide a suitable pressure surrogate. WIA has recently been successfully performed using CMR in the ascending and descending aorta (Biglino, Steeden, et al. 2012), however it has never been attempted in the highly-mobile, small-caliber, tortuous coronary arteries, nor validated against invasively acquired data. Accordingly, we assessed the feasibility of coronary WIA using CMR and validated it against invasive measures in the same patients.

## 8.3 Methods

Serial patients who had undergone invasive WIA were invited for a research CMR study. Patients were recruited from the Royal Brompton and Harefield NHS Foundation Trust and Liverpool Heart and Chest Hospital. All patients gave written consent for additional research measurements. The study was approved by an independent ethics committee.

### 8.3.1 Invasive data acquisition

Following coronary angiography, if no significant epicardial coronary artery disease was identified, a Doppler velocity and pressure wire (Combowire, Volcano Therapeutic) was positioned in the proximal left anterior descending (LAD) artery. Wire position and signal were optimised and simultaneous recordings of pressure, flow velocity and electrocardiogram were acquired at 1000Hz, for a period of 60 seconds. To assess reproducibility, a further recording was taken in the same vessel location. Data were similarly obtained in the proximal ascending thoracic aorta and proximal right coronary artery (RCA).

### 8.3.2 Acquisition of CMR data

CMR images were acquired using a 3 Tesla Magnetom Skyra MR scanner (Siemens AG Healthcare Sector, Germany). Following acquisition of localiser images and vertical and horizontal long axis balanced steady state free precession (bSSFP) cine images of the heart, bSSFP cine images were acquired in the three chamber and left ventricular outflow tract views to show the ascending aorta in-plane. A breath-hold retrospectively gated segmented gradient echo sequence (TE/TR 3.6 ms/6.6 ms) was then used to acquire through-plane cross sectional area changes in the proximal ascending aorta. The spatial resolution was 1.2 x 1.2 mm (reconstructed to 0.6 x 0.6 mm) with a slice thickness of 8 mm. Five k-space lines were acquired per cardiac cycle resulting in data with a true temporal resolution of 32.8 ms which was then reconstructed over 50 cine frames (reconstructed temporal resolution 19 ms assuming a heart rate of 60 beats per minute)(Figure 8.1). The acquisition plane was located 35mm above the aortic root as this was typically in a straight section of the aorta with minimal

through-plane motion through the cardiac cycle The segmented gradient echo cine acquisition was repeated for assessment of intra-study reproducibility. In each, the aortic cross sectional area was manually contoured and plotted against time from the R wave.

The coronary artery origins were identified using multiple transverse diastolic segmented gradient echo scout acquisitions (TE/TR: 3.3 ms/7 ms, acquired resolution 1 mm x 1 mm x 4 mm, acquisition window 110 ms). From these, oblique and double oblique images were acquired to image the left anterior descending (LAD) and right coronary artery (RCA) in-plane. Through-plane breath-hold interleaved spiral phase velocity maps (TE/TR: 5.2 ms/19 ms) were then acquired in a straight section of each proximal artery, matched as closely as possible to the locations of the invasive measurements (Figure 8.1). The sequence incorporated 1-1 water excitation and 8 spiral interleaves (11.75 ms duration) were required to fill k-space. Phase map subtraction of datasets with symmetric bi-polar velocity encoding gradients resulted in through-plane velocity maps sensitive to a flow velocity of +/−30 cm/s. These datasets were acquired in alternate cardiac cycles following a single dummy cardiac cycle, resulting in a total breath-hold duration of 17 cardiac cycles. The spatial resolution was 1.4 mm x 1.4 mm (reconstructed to 0.7 mm x 0.7 mm) and the slice thickness was 8 mm.

Locations were directed by the invasive fluroscopic images to ensure the same location as invasive data acquisition where possible. Sensitivity to off-resonance artefact was minimised using localised second-order shimming and frequency adjustment based on the signal from a user-defined region of interest positioned over the heart. For right coronary studies, an additional breath-hold spiral phase velocity mapping acquisition was performed using fat-excitation (Keegan et al. 2004). This was later used to correct for the through-plane velocity of the RCA. Spiral acquisitions were repeated to allow analysis of intra-study reproducibility. For each breath-hold acquisition, a circular cross-sectional area was automatically defined over the vessel on a mid-diastolic frame. Semi-automatic custom MATLAB software was then used to track the artery from frame to frame and to generate a velocity-time curve (6). As the spatial resolution of the data was limited, no attempt was made to measure changes in the vessel cross-sectional area throughout the cardiac cycle. The velocity-time curves were corrected for through-plane motion of the vessel using a region of adjacent myocardium (LAD) or in the surrounding epicardial fat (RCA) (6, 10).

To minimise circadian variation in coronary flow between studies, readings were taken under standardised conditions, with both procedures performed at the same time of day where possible, with a minimum of 30 minutes lying supine at rest prior to data acquisition. Patients refrained from

caffeine containing substances and smoking prior to each procedure. Where possible both studies were performed on the same day, however this was not always possible.

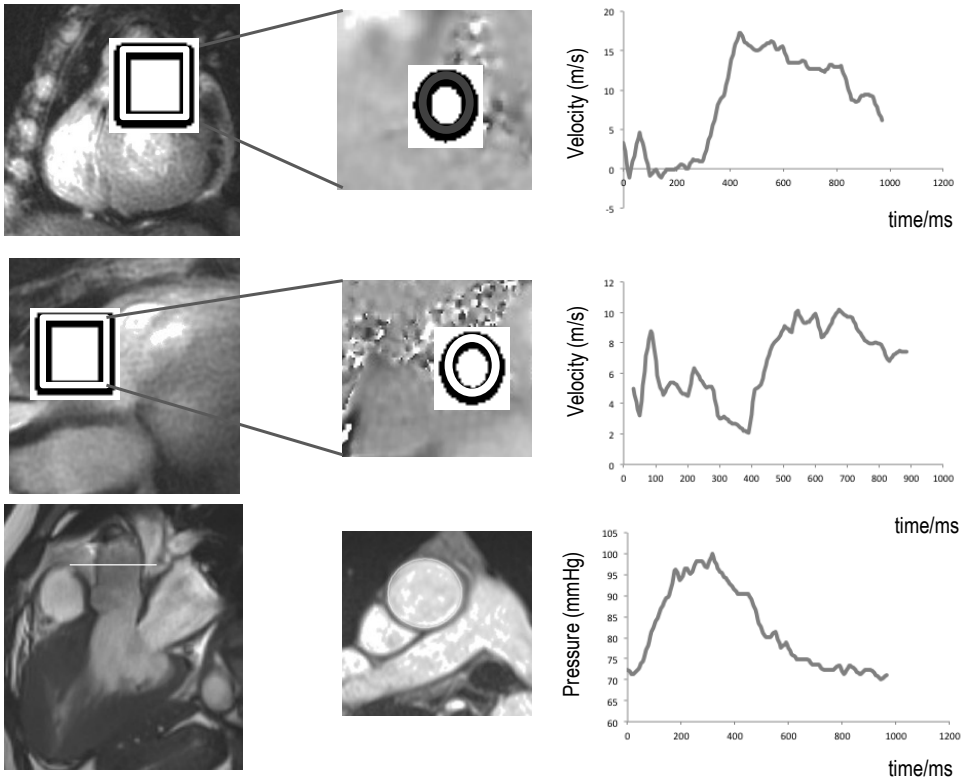


**Figure 8.1**: Early diastolic cross sectional imaging of LAD (top panel) and RCA (middle panel) using breath-hold spiral phase velocity mapping. For derivation of pressure data, a cross sectional plane was identified 35mm above the aortic valve plane (bottom panel), a high temporal resolution gradient echo sequence was used to acquire aortic areas throughout the cardiac cycle and these were used to derive the central aortic pressure during the cardiac cycle.

### 8.4 Derivation of central aortic pressure from aortic distension data

The central aortic pressure was derived from the aortic distension and the brachial systolic and diastolic blood pressure measurements as follows (Quail et al. 2014; Meinders and Hoeks 2004):

$$p(t) = P_d \exp\left[\alpha\left(\frac{A(t)}{A_d} - 1\right)\right]$$

where $\alpha$ was initially set as:

$$\alpha = \frac{A_d Ln\left(\frac{P_s}{P_d}\right)}{A_s - A_d}$$

where p(t) is the CMR-derived pressure curve, $P_s$ is the brachial systolic pressure, $P_d$ is the brachial diastolic pressure, $A_s$ and $A_d$ are the systolic and diastolic aortic areas and A(t) is the area curve. The model was calibrated using an iterative method to reduce the scaling factor, α, to minimise the difference between the mean measured brachial pressure and the mean CMR-derived pressure. This exponential model correlates well with the results of carotid artery applanation tonometry which has been validated against invasive central aortic pressure measurements (Kelly and Fitchett 1992).

### 8.5 Exclusion of subjects

Since the magnitude of maximal aortic distension varies between subjects, we excluded subjects with minimal aortic distension (defined as less than 10% increase in area at the point of maximal distension). 10% was chosen as the minimal distension since our pixel area was 1.2x1.2mm2, the average size of an aorta at minimal cross sectional lumen area was approximately 460mm$^2$ (Voges et al. 2012), and therefore this excluded apparent aortic increase within the error bars related to partial volume effects.

### 8.6.1 Wave intensity analysis of invasive data

WIA describes the myocardial mechanics that influence coronary blood flow and divides these into proximally and distally originating factors in the time domain, during the cardiac cycle. Acceleration of coronary flow results from either compression waves originating from the aortic (proximal) end or expansion waves originating from the microcirculatory (distal) end. Deceleration of coronary flow may result from expansion waves originating proximally or compression waves originating from the microcirculation (Parker 2009). Analysis requires simultaneous assessment of the first derivatives of central aortic pressure and of coronary blood flow velocity, together with an estimate of the wave speed.

The water hammer equations allow description of wavefronts according to the changes in pressure and velocity. They are derived from conservation of mass and momentum. The water hammer equations are used to derive the forward and backward originating waves as follows:

Forward wavefronts:

$$dP_+ = \rho c\, dU_+$$

Backward wavefronts:

$$dP_- = \rho c\, dU_-$$

Where ρ is the blood density (taken as 1050kg/m3, c is the wave speed, *dU* is the incremental change in coronary flow velocity and + and – indicate forward and backward waves.

The wave speed is calculated using the following formula:

$$c = \frac{1}{\rho}\sqrt{\frac{\sum dP^2}{\sum dU^2}}$$

Data were analysed using a customised automated Matlab analysis program as previously described (Davies 2006a) . For the invasive data, four to five beats of pressure and flow velocity data were ensemble averaged to minimise the effect of noise without loss of data quality. A Savitzky- Golay filter was used to smooth the data without loss of true peaks and troughs (Savitsky A 1964). The derivates of the pressure and flow at each time-point were used to calculate the net wave intensity and the sum of squares method to determine the wave speed and allow calculation of the separated wave intensity.

Separated cumulative wave intensity was defined as the integral of wave intensity over a given peak, with units of $Wm^{-2}s^{-1}$. For comparison between patients, we also presented the wave intensity of a particular separated wave as a proportion of the total separated cumulative wave intensity, the 'proportion of separated cumulative wave intensity (%)'.

### 8.6.2 Wave intensity analysis of CMR data

The mean aortic velocity and aortic-distension derived central aortic pressure were calculated as described above and data were lined up gated to the R wave and interpolated to 5ms time points. Although this interpolation was of a higher temporal resolution than the individual sequences used for data collection, wave intensity values are dependent on the sampling frequency and therefore interpolation was necessary to imitate the standard sampling frequency employed invasively (Davies 2006a). Data were passed through a Savitsky-Golay filter and the sum of squares method was used to derive the wave speed using the same cutstomised Matlab program used for invasive analysis.

## 8.7 Statistical analysis

All analyses were performed using IBM SPSS Statistics 19 Package. Normally distributed data were presented as mean± standard deviation and categorical data as number (percentage of total. The principle waves through the cardiac cycle were calculated for each subject using invasive and CMR data as described above and the values derived from the two techniques compared using Bland Altman analysis and Pearson correlation. For both invasive and noninvasive data, intra-study

reproducibility was determined using Bland Altman analysis and reported as mean difference (+/- SD of the differences).

### 8.8 Results

Eight subjects with study of 14 arteries completed CMR and Doppler flow wire studies as specified. Baseline characteristics for included and excluded patients are summarized in Table 8.1. Indication for cardiac catheterisation was hypertrophic cardiomyopathy (6 patients) or atypical chest pain (2 patients). All patients were in sinus rhythm at the time of study. Although every effort was made to standardise measurement conditions, the psychological stress of an invasive procedure resulted in a higher blood pressure during invasive compared to CMR measurements (SBP 130±22mmHg versus 115±22mmHg, $p<0.01$) and a numerically higher heart rate (71±11 versus 66±9 beats per minute, $p=0.19$).

**Table 8.1:** Characteristics of all subjects included in CMR-WIA feasibility study.

| | |
|---|---|
| Age | 49.8±13.3 |
| Gender (% male) | 6( 75%) |
| **Comorbidities** | |
| Hypertension | 2 (25%) |
| Diabetes | 0 (0%) |
| Hypercholesterolaemia | 2 (25%) |
| Smoker | 1 (13%) |
| **Medications** | |
| Beta blockers | 5 (63%) |
| ACE inhibitors | 0 (0%) |
| Calcium channel blockers | 0 (0%) |
| Aspirin | 2 (25%) |
| Statin | 2 (25%) |

### 8.8.1 Agreement with invasive wave intensity analysis

Traditionally, wave intensity of the coronary arteries produces a plot of 6 waves, however as most of our subjects had HCM, the early and late backward compression wave (BCW) were fused and we therefore measured these as a single wave, the backward compression wave total (BCWtot). Summary values for invasive and CMR derived separated wave intensity values are presented in Table 8.2. Plots of invasive against CMR derived wave intensity analysis showed reasonable agreement between the two measures. . Figure 8.2 shows Bland Altman and linear regression plots for CMR versus invasive WIA. The non-invasive and invasive studies showed reasonable agreement ($r^2$=0.57, p<0.001) with a mean difference (±SD) of 0.0± 10.8. Two of the greatest outlying points are from one patient (LAD) who also had poor invasive reproducibility.

Traditionally, wave intensity of the coronary arteries shows 6 dominant waves: the forward compression wave (FCW), forward expansion wave (FEW), second forward compression wave (FCW2), early backward compression wave (early BCW), late backward compression wave (late BCW) and backward expansion wave (BEW). Forward travelling waves arise from the proximal circulation while backwards travelling waves arise from the distal circulation. The FCW, FCW2 and BEW accelerate coronary blood flow while the early BCW, late BCW and FEW decelerate it. However as most of our subjects had HCM, the early and late backward compression waves were fused and were therefore measured these as a single wave, the backward compression wave total (BCWtot).

CMR derived WIA shows the expected distribution and relative intensity of waves. While the wave distribution profiles are similar (Figure 8.2), differences in the trigger times between the techniques resulted in consistently earlier timing of CMR waves compared to invasive data.

Table 8.2 shows summary data (mean ± standard deviation) for invasive and CMR wave intensities. As expected, the absolute wave energies were higher using invasive compared to CMR measures, however when expressed as a proportion of the total wave intensity, the two were comparable (Table 8.2). The intra-study reproducibilities of % separated cumulated wave intensities by both invasive

and CMR techniques is shown in the Bland Altman plots of Figure 8.3. The intra-study reproducibility of the CMR derived % separated cumulative wave intensities (mean ±standard deviation of differences) was 0.0±6.8. Intra-study reproducibility for the corresponding invasive data was 3.8±4.4. The values for each individual wave are shown in Table 8.3.

**Table 8.2:** Invasive and CMR derived values for separated wave intensity analysis. Values are compared using Student's t-test. A p-value of <0.05 was considered significant. While the absolute values were higher for invasively derived data compared to CMR, the proportion of each wave was similar for both techniques.

| | Separated cumulative wave intensity /$Wm^{-2}s^{-1}$ x $10^6$ | | | Proportion of separated cumulative wave intensity | | |
|---|---|---|---|---|---|---|
| | **Invasive** | **CMR** | **p-value** | **Invasive** | **CMR** | **p-value** |
| Forward compression wave (FCW) | 6.6±4.3 | 4.1±2.3 | 0.02 | 30.0±15.4 | 24.4±8.3 | 0.32 |
| Forward expansion wave (FEW) | 1.7±3.2 | 1.2±1.2 | 0.98 | 5.6±5.4 | 6.7±4.9 | 0.64 |
| 2nd forward compression wave (FCW2) | 2.4±3.3 | 2.5±0.6 | 0.22 | 5.2±3.0 | 4.2±2.5 | 0.48 |
| Backward compression wave (BCWtot) | 8.7x±6.0 | 6.6±3.4 | <0.01 | 33.4±11.0 | 41.5±11.1 | 0.16 |
| Backward expansion wave (BEW) | 7.4±5.7 | 4.1±2.7 | <0.01 | 25.7±8.6 | 25.0±6.3 | 0.63 |

**Table 8.3:** Mean and standard deviation of the difference for invasive and CMR data. Values were compared using Student's t test and a p-value of <0.05 was considered significant.

| | Invasive vs CMR data | Invasive vs Invasive data | CMR vs CMR data |
|---|---|---|---|
| Forward compression wave | 7.4±14.7 | -1.6±6.2 | 0.2±5.9 |
| Forward expansion wave | -1.1±7.1 | 0.4±2.2 | 0.2±4.8 |
| Forward compression wave 2 | 1.1±4.0 | -1.1±3.0 | 3.4±4.4 |
| Backward compression wave total | -8.0±10.8 | 2.1±4.7 | -1.1±7.3 |
| Backward expansion wave | 0.6±10.5 | 0.1±5.1 | -2.8±9.2 |

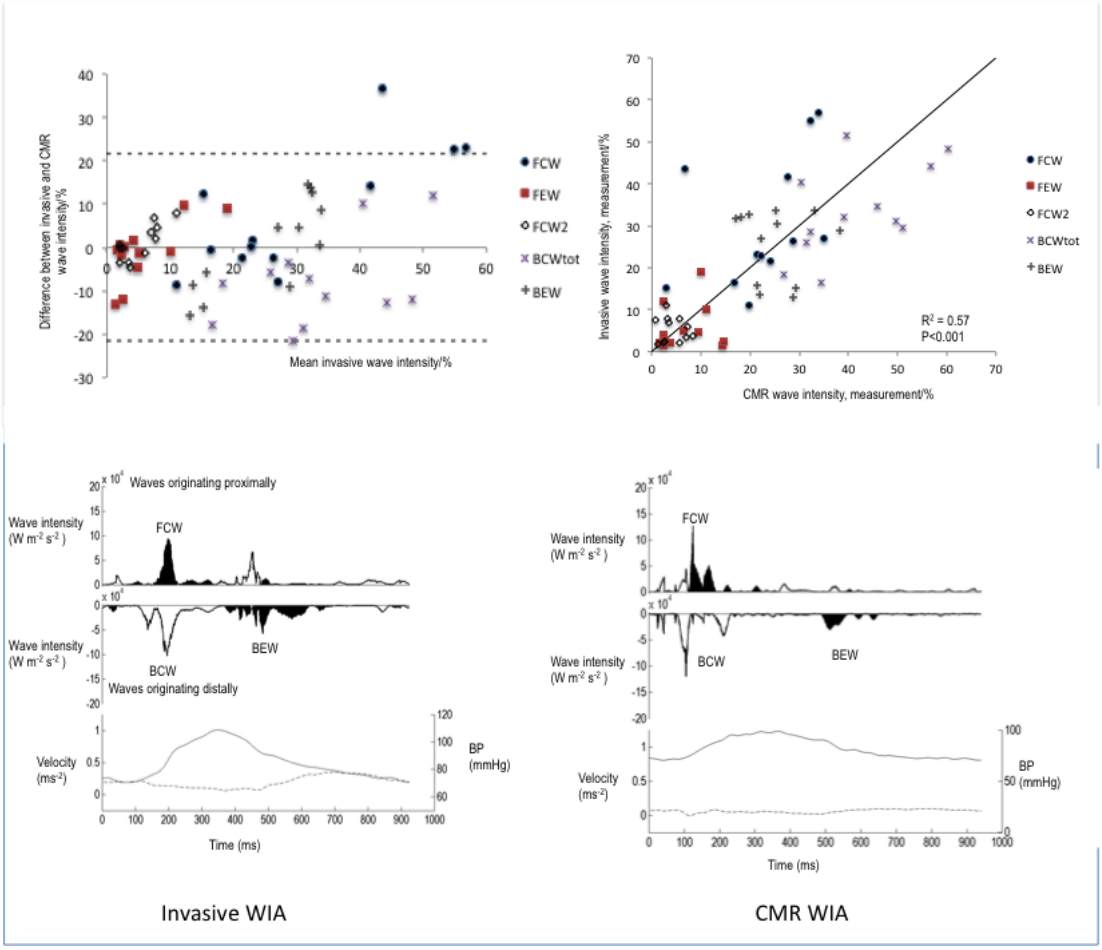


**Figure 8.2**: Comparison of invasive and CMR-derived wave intensity analysis. All 5 waves are displayed on a single plot, assessed for agreement with invasive data as the gold standard using Bland Altman analysis (top left panel) and using the Pearson correlation coefficient (top right panel). The bottom panels display a visual comparison of WIA using invasive (left) and CMR derived (right) data in the same patient, with the corresponding pressure and flow velocity data shown below. While the absolute values for each wave were greater for CMR compared to invasive measures, the pattern of wave intensity and relative size of each wave was similar between the two traces

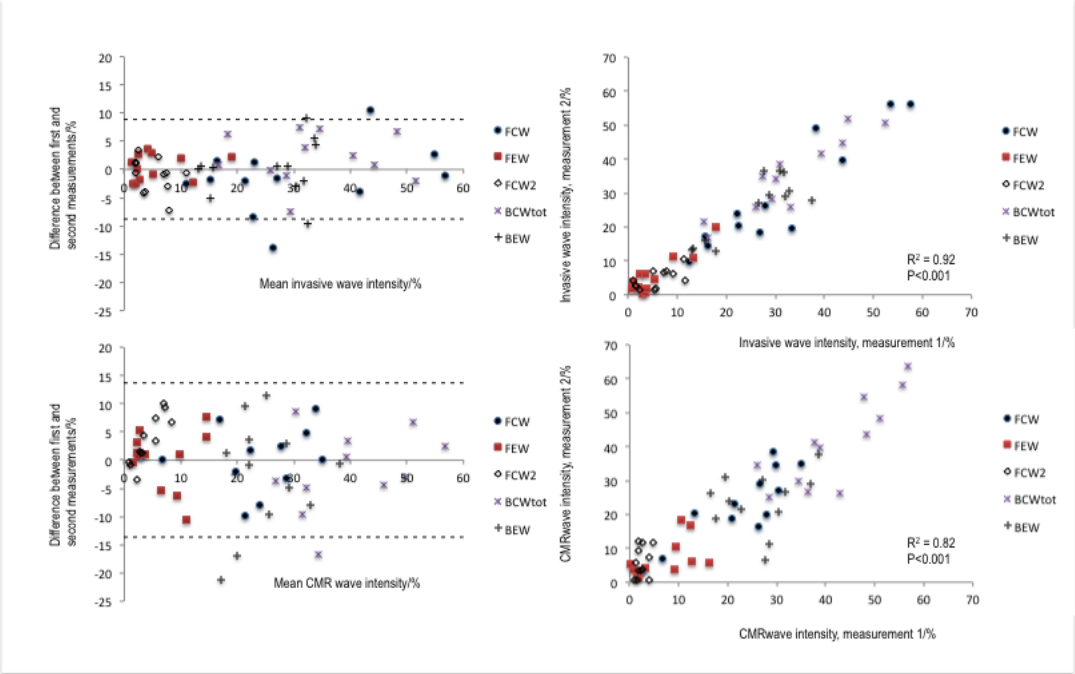


**Figure 8.3**: Reproducibility of invasive (top panels) versus CMR-derived (bottom panels) wave intensity values using Bland Altman plots (left) and Pearson correlation coefficient (right).

## 8.9 Conclusion

In this study, we demonstrated that CMR derived velocity and pressure data have the potential to be used for wave intensity analysis of the proximal coronary arteries. We performed CMR and invasive wave intensity analysis in 14 unobstructed coronary arteries and compared the absolute and proportionate values of each wave using the two measurement techniques. CMR analysis produced similar patterns of wave intensity to invasive data, with acceptable reproducibility.

### 8.9.1 The need for non-invasive coronary wave intensity analysis

Wave intensity was first performed in the coronary arteries in man in 2006 (Davies 2006a). The results provided a definitive answer to why coronary flow peaks in diastole. The complex interaction between the epicardial coronary arteries, ventricular contraction and relaxation and blood within the microcirculatory component was elegantly described throughout the cardiac cycle through identification of six predominant waves that governed changes in coronary flow(Sen et al. 2013). In the healthy heart, a large backward expansion wave was responsible for the increased coronary flow in early diastole, as compression on the microcirculation is relieved (Davies, Whinnett, Francis, Manisty, et al. 2006). In disease states such as aortic stenosis, the microcirculation is expanded due to left ventricular hypertrophy and plays a larger role in mediation of coronary flow (Davies et al. 2011). In left ventricular hypertrophy, the backward expansion wave is attenuated due to poor ventricular relaxation, and the backward compression wave is increased due to compression and deformation of the expanded microcirculation. Wave intensity has been used to explain the effect of mechanical treatments such as intra-aortic balloon pumps (De Silva et al. 2014) and aortic valve replacement (Davies et al. 2011) on coronary filling patterns.

While the technique has provided valuable advances in understanding of the mechanisms responsible for abnormalities in coronary filling, expansion into a wider range of pathology has been limited by the requirement for invasive study. Currently, coronary wave intensity data has all been derived from invasive measure, requiring coronary intubation and placement of a coronary wire into the artery for measurement of phasic pressure and flow changes. This has limited recruitment of patients for research which means that healthy controls have not been studied, nor the majority of coronary pathology.

Coronary flow abnormalities have been shown in a large population of cardiovascular disease (Skalidis et al. 2004; Aburawi et al. 2014; Zografos, Kokladi, and Katritsis 2010; Celik et al. 2004). Study with wave intensity is likely to allow better understanding of the mechanism of chest pain and perfusion abnormalities in these disease states. Study in larger patient cohorts and with longitudinal repeat measurement may also allow assessment of medication effects and even prognosis. A non invasive technique for coronary wave intensity analysis is therefore desirable.

### 8.9.2 CMR compared to echocardiography for non-invasive coronary data acquisition

Until recently, non invasive wave intensity analysis had only been performed using ultrasound of the carotid arteries (Niki et al. 2002; Zambanini et al. 2005; Zhang et al. 2010). Echocardiography may allow coronary wave intensity but is limited by the need for favourable acoustic windows and the recorded coronary flow velocity will be highly dependent on the angle of the ultrasound beam in relation to the coronary artery (Rigo 2005). A significant advantage of CMR is the ability for cross sectional imaging in any plane, ensuring that coronary flow is measured perpendicular to the vessel (Gatehouse et al. 2005). CMR will also allow measurement at any proximal location in the coronary tree and is not limited by vessel location relative to the ultrasound probe. Recent advances in CMR using a retrospectively gated flow velocity sequence allowed acquisition over the entire cardiac profile with a high temporal resolution sufficient for wave intensity analysis.

Biglino performed wave intensity analysis using CMR in the ascending and descending aorta in healthy controls, patients with coronary heart disease (Biglino, Steeden, et al. 2012) and congenital heart disease (Biglino et al. 2014). They demonstrated that wave intensity in the aorta was feasible using phase contrast CMR, with temporal wave intensity profiles that were in keeping with previously demonstrated invasive profiles, however they did not validate the technique against invasive data. In both their study and ours, spiral k-space trajectories allowed sufficient temporal resolution for velocity data, producing a suitable velocity profile for wave intensity analysis.

### 8.9.3 Use of aortic distension as a surrogate measure for pressure

Vessel distension has been successfully employed as a surrogate for pressure changes within the vessel of interest in the ultrasound derived carotid (Niki et al. 2002; Zambanini et al. 2005) and CMR derived aortic (Biglino, Steeden, et al. 2012; Biglino et al. 2014) WIA papers. We elected to use changes in proximal aortic distension to derive changes in central aortic pressure over the cardiac cycle as this had previously been validated using CMR (Quail et al. 2014). Compared to vessel diameter changes, which was the technique employed for ultrasound-derived wave intensity, measurement of cross sectional area changes offered several advantages. Firstly, measurement error in calculation of vessel distension was likely smaller compared to calculation from aortic diameter, since areas changes derived from vessel diameter changes required squaring of the measurements, increasing the potential for error. Secondly, contouring of vessel area meant there was no assumption of vessel circularity throughout the cardiac cycle.

Aortic distension is known to vary between individuals. Older patients and those with longstanding hypertension typically have a reduction in aortic distension and increased stiffness of the aorta (Laurent et al. 2006; Mackey et al. 2002; Vlachopoulos, Aznaouridis, and Stefanadis 2010). Patients with hypertrophic cardiomyopathy have also been shown to have reduced aortic distension (Biglino, Schievano, et al. 2012). In this feasibility study, we only included patients with an aortic distension of 10% or greater. Use of alternative non-invasive central aortic pressure surrogates such as a supra-systolic brachial cuff (Park et al. 2014) may allow study of patients with minimal aortic distension and may improve non invasive wave intensity analysis techniques.

Biglino (Biglino, Steeden, et al. 2012) used the gradient of the velocity-log (area) curve in early systole to derive the wave speed for CMR derived WIA of the aorta, however this was not suitable for coronary wave intensity since our velocity and area data were not measured in the same location and the distension of the aorta is much greater than that of the coronary arteries. We therefore elected to derive the central aortic pressure from area measurements as previously validated (Quail et al. 2014) and use the sum of squares method using the CMR derived velocity and pressure changes to derive the wave speed (Davies, Whinnett, Francis, Willson, et al. 2006).

### 8.9.4 Can CMR derived data replace invasive wave intensity analysis?

This study was the first to successfully use CMR data to derive wave intensity of the proximal coronary arteries and showed acceptable agreement with invasive data and similar reproducibility to that of the invasive technique. Compared to invasively derived WIA, CMR data showed greater variability in the forward compression wave, which is a key wave in assessment of coronary physiology and lower values for absolute wave intensity. This may be reduced by averaging the results of several breath-hold acquisitions. However, the trade off would be increased acquisition and analysis time and potential for mis-registration between breath-holds.

Currently, compared to CMR, invasive data acquisition is simpler and allows acquisition of multiple cardiac cycles, although significantly limits the population likely to be studied. CMR WIA may allow longitudinal follow up of the same patient, to assess response to treatment and may allow derivation of normal ranges for individual waves in the entirely healthy population. Further work to evaluate alternative pressure-surrogate measures and establish whether averaging across multiple velocity and pressure cycles derived from CMR results in improved reproducibility may further improve the technique.

### 8.9.5 Study Limitations

In the CMR study, pressure and flow velocity data were not acquired simultaneously and the pressure data were derived from the proximal ascending aorta rather than the coronary artery. However, all data was gated to the R wave which enabled alignment of the velocity and derived pressure traces. Timing of each wave was consistently earlier with CMR than invasive WIA due to differing methods of gating, but the pattern of waves were similar.

Due to the selection of our subjects, who largely had hypertrophic cardiomyopathy, reversal of coronary flow during systole was common. This produced limitations in the measurement of invasive data, as the internal algorithm of the Combowire struggled to identify small reversals in coronary flow and often instead traced the positive reflected “mirror” of the coronary flow trace. With CMR data, there was no mirroring and the technique clearly differentiated forward and reverse flow.

We only included patients with an aortic distension of greater than 10%. This removed a large proportion of our subjects. This was largely due to limitation in choice of subject as they had a clinical requirement for coronary angiography in order to be included in the study. Alternative pressure surrogates such as supra-brachial cuff measurements with transformation to a central aortic pressure may be more suitable for a wider cohort of patients (Park et al. 2014).

Where possible, CMR and invasive measures were obtained on the same day, however this was not always possible due to patient preference and work flow logistics. Measurements were taken for both CMR and invasive wave intensity analysis with patients supine and resting for at least half an hour before data acquisition, however the physical and physiological added stresses of the invasive procedure meant that resting blood pressure and heart rate were higher at the time of invasive measurement compared to CMR measurement.

### 8.9.6 Conclusion

CMR derived pressure and flow data may be used to perform coronary wave intensity analysis. The technique was not suitable in older and hypertensive patients in whom increased aortic stiffness leads to lower aortic distension. However, In selected patients, there was reasonable agreement with invasive data and good reproducibility.

# CONCLUSIONS

In this thesis, I have assessed coronary flow abnormalities in hypertrophic cardiomyopathy. Patients with HCM typically have abnormal resting phasic coronary flow with systolic reversal of flow and higher diastolic flow velocities. The coronary flow reserve is reduced compared to controls. Using wave intensity analysis, I evaluated the underlying mechanisms behind these abnormalities, exploring the impact of increased microcirculatory compression on coronary flow, with an increased backward compression wave during systole and the effect of impaired ventricular relaxation, with an attenuated backward expansion wave.

**Thesis Aim 1:**

To use coronary wave intensity analysis to better understand the mechanisms of chest pain and perfusion defects in hypertrophic cardiomyopathy

***Rationale***: Although chest pain is very common in HCM, it is not well understood and treatment is difficult. Improved understanding of the underlying mechanisms of chest pain in this complex disease will allow more targeted treatment

***Hypothesis 1***: WIA allows explanation of the observed perfusion abnormalities in hypertrophic cardiomyopathy, with a smaller backward travelling suction wave (due to impaired relaxation) and a larger backward travelling compression wave (due to increased microcirculatory compression) compared to normal subjects.

I used WIA to demonstrate an increased backward compression wave during systole and relatively reduced backward expansion wave due to impaired ventricular relaxation in HCM patients compared to control subjects. I was therefore able to confirm my first hypothesis.

Interestingly, I also found that left ventricular outflow tract obstruction was responsible for additional proximally originating waves which further decelerate coronary flow. A proximally occurring expansion wave resulted in the bisferiens pulse which is clinically palpated in ptients with severe outflow tract obstruction.

Using CMR, I demonstrated the downstream effect of coronary flow and wave intensity abnormalities, demonstrating that the proportion of wave intensity that results in coronary flow acceleration correlates with absolute myocardial perfusion as measured using first pass myocardial perfusion imaging. This was the first study that directly assessed the impact of wave intensity abnormalities to a downstream result and was particularly interesting in the case of HCM, where abnormal perfusion is known to be associated with a much greater incidence of both death and heart failure.

**Thesis Aim 2:**

To develop coronary wave intensity analysis using cardiovascular magnetic resonance

***Rationale***: Coronary WIA allows detailed mechanistic understanding of myocardial mechanics that underlie disease processes. However, invasive data acquisition is associated with a small but significant risk of complications and a non-invasive alternative would be desireable and allow study of a wider population of patients.

***Hypothesis 2***: Wave intensity analysis can be performed non-invasively using cardiovascular magnetic resonance in patients with hypertrophic cardiomyopathy.

Finally, I assessed whether CMR was a suitable tool for non-invasive wave intensity. This first required development and testing of a retrospectively-gated spiral phase contrast flow velocity sequence, allowing acquisition of coronary flow velocity data throughout the cardiac cycle. Combined with measurement of aortic distension, this provided sufficient information for CMR-derived wave intensity analysis, allowing assessment of a much wider cohort of patients than merely those with a clinical indication for coronary angiography.

I found that in selected patients, wave intensity analysis could be performed using CMR, with results that showed reasonable agreement to invasively acquired data. Although patient numbers were small, the findings were encouraging. If validated in a larger cohort, CMR-WIA will allow study of a wider cohort of HCM patients, including the younger population and extension into other disease states that may not be appropriate for invasive study.

**Study Limitations**

The work contained in this thesis is subject to certain limitations. Firstly, patients recruited had a clinical indication for invasive coronary angiography, as required by our ethical approval. The mean age of HCM patients was 54 years (range 22-74). Accordingly, our findings cannot be generalised to the pediatric or adolescent population. Data acquisition was performed during clinical angiography and so operators were not blinded to the patient diagnosis. Similarly, analysis was performed using semi automated programs, but the operator was not blinded to subject diagnosis.

In the CMR-WIA study, pressure and flow velocity data were not acquired simultaneously and the pressure data were derived from the proximal ascending aorta rather than the coronary artery. Due to the selection of our subjects, who largely had HCM, reversal of coronary flow during systole was common. This produced limitations in the measurement of invasive data, as the internal algorithm of the Combowire struggled to identify small reversals in coronary flow and often instead traced the positive reflected "mirror" of the coronary flow trace. With CMR data, there was no mirroring and the technique clearly differentiated forward and reverse flow.

Where possible, CMR and invasive measures were obtained on the same day, however this was not always possible due to patient preference and work flow logistics. Measurements were taken for both CMR and invasive wave intensity analysis with patients supine and resting for at least half an hour before data acquisition, however the physical and physiological added stresses of the invasive procedure meant that resting blood pressure and heart rate were higher at the time of invasive measurement compared to CMR measurement.

**Future Directions**

The work contained in this thesis has improved understanding of the mechanisms underlying chest pain and abnormal coronary flow in HCM. It has clearly delineated three main mechanisms underlying perfusion abnormalities in this population. While this is an interesting finding, it requires further work to result in direct benefit for patients. Having defined the major mechanisms, the next step is to test current medications and surgical therapies for efficacy at treating these abnormalities. Currently medications may not be well suited for HCM as they have largely been developed for angina due to coronary artery disease. Novel therapies may be more suited and further work would ideally look at subjects before and after treatment to assess the affect on both coronary flow and wave intensity patterns.

For CMR-WIA, we have performed a small, proof of concept study that has shown promising results. Further work would extend and test this technique in a larger cohort of healthy volunteers and other disease states. Ideally this should validate the technique against the invasive gold standard. If such work demonstrates acceptable reproducibility and agreement with invasive data, this would allow extension of this technique into a much larger population of patients and pathologies. This would also aid the ability to measure WIA before and after treatment with novel and established therapies in HCM as it would no longer require invasive testing.

# BIBLIOGRAPHY


Abozguia, K., Elliott, P., McKenna, W., Phan, T.T., Nallur-Shivu, G., Ahmed, I., Maher, A.R., Kaur, K., Taylor, J., Henning, A., Ashrafian, H., Watkins, H. & Frenneaux, M. (2010) Metabolic modulator perhexiline corrects energy deficiency and improves exercise capacity in symptomatic hypertrophic cardiomyopathy. *Circulation* 122, 1562–9.

Aburawi, E.H., Munkhammar, P., Carlsson, M., El-Sadig, M. & Pesonen, E. (2014) Coronary flow dynamics in children after repair of Tetralogy of Fallot. *International journal of cardiology* 172, 122–6.

Ahn, H.-S., Kim, H.-K., Park, E.-A., Lee, W., Kim, Y.-J., Cho, G.-Y., Park, J.-H. & Sohn, D.-W. (2013) Coronary Flow Reserve Impairment in Apical vs Asymmetrical Septal Hypertrophic Cardiomyopathy. *Clinical cardiology* 36, 207–16.

Akasaka, T., Yoshida, K., Hozumi, T., Takagi, T., Kaji, S., Kawamoto, T., Morioka, S. & Yoshikawa, J. (1997) Retinopathy identifies marked restriction of coronary flow reserve in patients with diabetes mellitus. *Journal of the American College of Cardiology* 30, 935–41.

Argulian, E. & Chaudhry, F. a (2012) Stress testing in patients with hypertrophic cardiomyopathy. *Progress in cardiovascular diseases* 54, 477–82.

Arts, T., Bovendeerd, P., Delhaas, T. & Prinzen, F. (2003) Modeling the relation between cardiac pump function and myofiber mechanics. *Journal of biomechanics* 36, 731–6.

Ball, W., Ivanov, J., Rakowski, H., Wigle, E.D., Linghorne, M., Ralph-Edwards, A., Williams, W.G., Schwartz, L., Guttman, A. & Woo, A. (2011) Long-term survival in patients with resting obstructive hypertrophic cardiomyopathy comparison of conservative versus invasive treatment. *Journal of the American College of Cardiology* 58, 2313–21.

Basso, C., Thiene, G., Corrado, D., Buja, G., Melacini, P. & Nava, a (2000) Hypertrophic cardiomyopathy and sudden death in the young: pathologic evidence of myocardial ischemia. *Human pathology* 31, 988–98.

Baumgart, D., Haude, M., Goerge, G., Ge, J., Vetter, S., Dagres, N., Heusch, G. & Erbel, R. (1998) Improved assessment of coronary stenosis severity using the relative flow velocity reserve. *Circulation* 98, 40–6.

Bonow, R.O., Rosing, D.R., Bacharach, S.L., Green, M. V, Kent, K.M., Lipson, L.C., Maron, B.J., Leon, M.B. & Epstein, S.E. (1981) Effects of verapamil on left ventricular systolic function and diastolic filling in patients with hypertrophic cardiomyopathy. *Circulation* 64, 787–96.

Borg, T.K. & Caulfield, J.B. (1981) The collagen matrix of the heart. *Federation proceedings* 40, 2037–41.

Bos, J.M., Maron, B.J., Ackerman, M.J., Haas, T.S., Sorajja, P., Nishimura, R.A., Gersh, B.J. & Ommen, S.R. (2010) Role of family history of sudden death in risk stratification and prevention of sudden death with implantable defibrillators in hypertrophic cardiomyopathy. *The American journal of cardiology* 106, 1481–6.

Bravo, P.E., Zimmerman, S.L., Luo, H.-C., Pozios, I., Rajaram, M., Pinheiro, A., Steenbergen, C., Kamel, I.R., Wahl, R.L., Bluemke, D. a, Bengel, F.M., Abraham, M.R. & Abraham, T.P. (2013) Relationship of delayed enhancement by magnetic resonance to myocardial perfusion by positron emission tomography in hypertrophic cardiomyopathy. *Circulation. Cardiovascular imaging* 6, 210–7.

Brock, R. (1957) Functional obstruction of the left ventricle; acquired aortic subvalvar stenosis. *Guy's Hospital reports* 106, 221–38.

Burton, R.F. (2008) Estimating body surface area from mass and height: theory and the formula of Du Bois and Du Bois. *Annals of human biology* 35, 170–84.

Camici, P., Chiriatti, G., Lorenzoni, R., Bellina, R., Gistri, R., Italiani, G., Parodi, O., Salvadori, P., Nista, N. & Papi, L. (1991)a) coronary vasodilation is impaired in HCM more so in patients with chest pain. *JACC* 17, 879–86.

Camici, P., Chiriatti, G., Lorenzoni, R., Bellina, R.C., Gistri, R., Italiani, G., Parodi, O., Salvadori, P.A., Nista, N. & Papi, L. (1991)b) Coronary vasodilation is impaired in both hypertrophied and nonhypertrophied myocardium of patients with hypertrophic cardiomyopathy: a study with nitrogen-13 ammonia and positron emission tomography. *Journal of the American College of Cardiology* 17, 879–86.

Camici, P., Ferrannini, E. & Opie, L.H. (1989) Myocardial metabolism in ischemic heart disease: basic principles and application to imaging by positron emission tomography. *Progress in cardiovascular diseases* 32, 217–38.

Camici, P.G., Olivotto, I. & Rimoldi, O.E. (2012) The coronary circulation and blood flow in left ventricular hypertrophy. *Journal of molecular and cellular cardiology* 52, 857–64.

Cannon, R.O., Dilsizian, V., O'Gara, P.T., Udelson, J.E., Schenke, W.H., Quyyumi, A., Fananapazir, L. & Bonow, R.O. (1991) Myocardial metabolic, hemodynamic, and electrocardiographic significance of reversible thallium-201 abnormalities in hypertrophic cardiomyopathy. *Circulation* 83, 1660–7.

Canty, J.M. (1988) Coronary pressure-function and steady-state pressure-flow relations during autoregulation in the unanesthetized dog. *Circulation research* 63, 821–36.

Cape, E.G., Jones, M., Yamada, I., VanAuker, M.D. & Valdes-Cruz, L.M. (1996) Turbulent/viscous interactions control Doppler/catheter pressure discrepancies in aortic stenosis. The role of the Reynolds number. *Circulation* 94, 2975–81.

Cecchi, F., Olivotto, I., Gistri, R., Lorenzoni, R., Chiriatti, G. & Camici, P.G. (2003) Coronary microvascular dysfunction and prognosis in hypertrophic cardiomyopathy. *The New England journal of medicine* 349, 1027–35.

Celik, S., Dagdeviren, B., Yildirim, A., Gorgulu, S., Uslu, N., Eren, M., Gurol, T., Ozen, E. & Tezel, T. (2004) Determinants of coronary flow abnormalities in obstructive type hypertrophic cardiomyopathy: noninvasive assessment by transthoracic Doppler echocardiography. *Journal of the American Society of Echocardiography : official publication of the American Society of Echocardiography* 17, 744–9.

Cerqueira, M.D., Weissman, N.J., Dilsizian, V., Jacobs, A.K., Kaul, S., Laskey, W.K., Pennell, D.J., Rumberger, J.A., Ryan, T. & Verani, M.S. (2002) Standardized myocardial segmentation and nomenclature for tomographic imaging of the heart. A statement for healthcare professionals from the Cardiac Imaging Committee of the Council on Clinical Cardiology of the American Heart Association. *Circulation* 105, 539–42.

Chan, R.H., Maron, B.J., Olivotto, I., Pencina, M.J., Assenza, G.E., Haas, T., Lesser, J.R., Gruner, C., Crean, A.M., Rakowski, H., Udelson, J.E., Rowin, E., Lombardi, M., Cecchi, F., Tomberli, B., Spirito, P., Formisano, F., Biagini, E., Rapezzi, C., De Cecco, C.N., Autore, C., Cook, E.F., Hong, S.N., Gibson, C.M., Manning, W.J., Appelbaum, E. & Maron, M.S. (2014) Prognostic value of quantitative contrast-enhanced cardiovascular magnetic resonance for the evaluation of sudden death risk in patients with hypertrophic cardiomyopathy. *Circulation* 130, 484–95.

Chilian, W.M., Layne, S.M., Klausner, E.C., Eastham, C.L. & Marcus, M.L. (1989) Redistribution of coronary microvascular resistance produced by dipyridamole. *The American journal of physiology* 256, H383–90.

Choudhury, L., Elliott, P., Rimoldi, O., Ryan, M., Lammertsma, A.A., Boyd, H., McKenna, W.J. & Camici, P.G. (1999) Transmural myocardial blood flow distribution in hypertrophic cardiomyopathy and effect of treatment. *Basic research in cardiology* 94, 49–59.

Cleland, J.G.F., Daubert, J.-C., Erdmann, E., Freemantle, N., Gras, D., Kappenberger, L. & Tavazzi, L. (2005) The effect of cardiac resynchronization on morbidity and mortality in heart failure. *The New England journal of medicine* 352, 1539–49.

Coppini, R., Ferrantini, C., Yao, L., Fan, P., Del Lungo, M., Stillitano, F., Sartiani, L., Tosi, B., Suffredini, S., Tesi, C., Yacoub, M., Olivotto, I., Belardinelli, L., Poggesi, C., Cerbai, E. & Mugelli, A. (2013) Late sodium current inhibition reverses electromechanical dysfunction in human hypertrophic cardiomyopathy. *Circulation* 127, 575–84.

Cummings, K.W., Bhalla, S., Javidan-Nejad, C., Bierhals, A.J., Gutierrez, F.R. & Woodard, P.K. ( A pattern-based approach to assessment of delayed enhancement in nonischemic cardiomyopathy at MR imaging. *Radiographics : a review publication of the Radiological Society of North America, Inc* 29, 89–103.

Daly, C. & Kwong, R.Y. (2013) Cardiac MRI for myocardial ischemia. *Methodist DeBakey cardiovascular journal* 9, 123–31.

Davies, J.E., Sen, S., Broyd, C., Hadjiloizou, N., Francis, D.P., Foale, R., Parker, K.H., Hughes, A.D., Chukwuemeka, A., Casula, R., Malik, I.S., Mikhail, G.W. & Mayet, J. (2011) Arterial pulse wave dynamics after percutaneous aortic valve replacement: fall in coronary diastolic suction with increasing heart rate as a basis for angina symptoms in aortic stenosis. *Circulation* 124, 1565–72.

Davies, J.E., Whinnett, Z.I., Francis, D.P., Manisty, C.H., Aguado-Sierra, J., Willson, K., Foale, R., Malik, I.S., Hughes, A.D., Parker, K.H. & Mayet, J. (2006)a) Evidence of a dominant backward-propagating “suction” wave responsible for diastolic coronary filling in humans, attenuated in left ventricular hypertrophy. *Circulation* 113, 1768–78.

Davies, J.E., Whinnett, Z.I., Francis, D.P., Willson, K., Foale, R.A., Malik, I.S., Hughes, A.D., Parker, K.H. & Mayet, J. (2006)b) Use of simultaneous pressure and velocity measurements to estimate arterial wave speed at a single site in humans. *American journal of physiology. Heart and circulatory physiology* 290, H878–85.

Debl, K., Djavidani, B., Buchner, S., Lipke, C., Nitz, W., Feuerbach, S., Riegger, G. & Luchner, A. (2006) Delayed hyperenhancement in magnetic resonance imaging of left ventricular hypertrophy caused by aortic stenosis and hypertrophic cardiomyopathy: visualisation of focal fibrosis. *Heart (British Cardiac Society)* 92, 1447–51.

Dimitrow, P.P., Galderisi, M. & Rigo, F. (2005) The non-invasive documentation of coronary microcirculation impairment: role of transthoracic echocardiography. *Cardiovascular ultrasound* 3, 18.

Dole, W.P. (1987) Autoregulation of the coronary circulation. *Progress in cardiovascular diseases* 29, 293–323.

Doshi, S.N., Kim, M.C., Sharma, S.K. & Fuster, V. (2002) Images in cardiovascular medicine. Right and left ventricular outflow tract obstruction in hypertrophic cardiomyopathy. *Circulation* 106, e3–4.

Doucette, J.W., Corl, P.D., Payne, H.M., Flynn, A.E., Goto, M., Nassi, M. & Segal, J. (1992) Validation of a Doppler guide wire for intravascular measurement of coronary artery flow velocity. *Circulation* 85, 1899–911.

Eberli, F.R., Ritter, M., Schwitter, J., Bortone, A., Schneider, J., Hess, O.M. & Krayenbuehl, H.P. (1991) Coronary reserve in patients with aortic valve disease before and after successful aortic valve replacement. *European heart journal* 12, 127–38.

Elliott, P.M., Anastasakis, A., Borger, M.A., Borggrefe, M., Cecchi, F., Charron, P., Hagege, A.A., Lafont, A., Limongelli, G., Mahrholdt, H., McKenna, W.J., Mogensen, J., Nihoyannopoulos, P., Nistri, S., Pieper, P.G., Pieske, B., Rapezzi, C., Rutten, F.H., Tillmanns, C., Watkins, H., O'Mahony, C., Zamorano, J.L., Achenbach, S., Baumgartner, H., Bax, J.J., Bueno, H., Dean, V., Deaton, C., Erol, C., Fagard, R., Ferrari, R., Hasdai, D., Hoes, A.W., Kirchhof, P., Knuuti, J., Kolh, P., Lancellotti, P., Linhart, A., Piepoli, M.F., Ponikowski, P., Sirnes, P.A., Tamargo, J.L., Tendera, M., Torbicki, A., Wijns, W., Windecker, S., Alfonso, F., Basso, C., Cardim, N.M., Gimeno, J.R., Heymans, S., Holm, P.J., Keren, A., Lionis, C.,

Muneretto, C., Priori, S., Salvador, M.J. & Wolpert, C. (2014) 2014 ESC Guidelines on diagnosis and management of hypertrophic cardiomyopathy: The Task Force for the Diagnosis and Management of Hypertrophic Cardiomyopathy of the European Society of Cardiology (ESC). *European Heart Journal* 35, 2733–79.

Elliott, P.M., Gimeno, J.R., Tomé, M.T., Shah, J., Ward, D., Thaman, R., Mogensen, J. & McKenna, W.J. (2006) Left ventricular outflow tract obstruction and sudden death risk in patients with hypertrophic cardiomyopathy. *European heart journal* 27, 1933–41.

Elliott, P.M., Kaski, J.C., Prasad, K., Seo, H., Slade, a K., Goldman, J.H. & McKenna, W.J. (1996)a) Chest pain during daily life in patients with hypertrophic cardiomyopathy: an ambulatory electrocardiographic study. *European heart journal* 17, 1056–64.

Elliott, P.M., Rosano, G.M., Gill, J.S., Poole-Wilson, P.A., Kaski, J.C. & McKenna, W.J. (1996)b) Changes in coronary sinus pH during dipyridamole stress in patients with hypertrophic cardiomyopathy. *Heart (British Cardiac Society)* 75, 179–83.

Fleming, P.R. (1957) The mechanism of the pulsus bisferiens. *British heart journal* 19, 519–24.

Flett, A.S., Hasleton, J., Cook, C., Hausenloy, D., Quarta, G., Ariti, C., Muthurangu, V. & Moon, J.C. (2011) Evaluation of techniques for the quantification of myocardial scar of differing etiology using cardiac magnetic resonance. *JACC. Cardiovascular imaging* 4, 150–6.

Gatehouse, P.D., Elkington, A.G., Ablitt, N.A., Yang, G.-Z., Pennell, D.J. & Firmin, D.N. (2004) Accurate assessment of the arterial input function during high-dose myocardial perfusion cardiovascular magnetic resonance. *Journal of magnetic resonance imaging : JMRI* 20, 39–45.

Gersh, B.J., Maron, B.J., Bonow, R.O., Dearani, J. a, Fifer, M. a, Link, M.S., Naidu, S.S., Nishimura, R. a, Ommen, S.R., Rakowski, H., Seidman, C.E., Towbin, J. a, Udelson, J.E. & Yancy, C.W. (2011)a) 2011 ACCF/AHA guideline for the diagnosis and treatment of hypertrophic cardiomyopathy: a report of the American College of Cardiology Foundation/American Heart Association Task Force on Practice Guidelines. *The Journal of thoracic and cardiovascular surgery* 142, e153–203.

Gersh, B.J., Maron, B.J., Bonow, R.O., Dearani, J.A., Fifer, M.A., Link, M.S., Naidu, S.S., Nishimura, R.A., Ommen, S.R., Rakowski, H., Seidman, C.E., Towbin, J.A., Udelson, J.E. & Yancy, C.W. (2011)b) 2011 ACCF/AHA guideline for the diagnosis and treatment of hypertrophic cardiomyopathy: executive summary: a report of the American College of Cardiology Foundation/American Heart Association Task Force on Practice Guidelines. *Circulation* 124, 2761–96.

Geske, J.B., Sorajja, P., Nishimura, R. a & Ommen, S.R. (2007) Evaluation of left ventricular filling pressures by Doppler echocardiography in patients with hypertrophic cardiomyopathy: correlation with direct left atrial pressure measurement at cardiac catheterization. *Circulation* 116, 2702–8.

Gistri, R., Cecchi, F., Choudhury, L., Montereggi, A., Sorace, O., Salvadori, P.A. & Camici, P.G. (1994) Effect of verapamil on absolute myocardial blood flow in hypertrophic cardiomyopathy. *The American journal of cardiology* 74, 363–8.

Guttmann, O.P., Rahman, M.S., O'Mahony, C., Anastasakis, A. & Elliott, P.M. (2014) Atrial fibrillation and thromboembolism in patients with hypertrophic cardiomyopathy: systematic review. *Heart (British Cardiac Society)* 100, 465–72.

Hadjiloizou, N., Davies, J.E., Malik, I.S., Aguado-Sierra, J., Willson, K., Foale, R. a, Parker, K.H., Hughes, A.D., Francis, D.P. & Mayet, J. (2008) Differences in cardiac microcirculatory wave patterns between the proximal left mainstem and proximal right coronary artery. *American journal of physiology. Heart and circulatory physiology* 295, H1198–H1205.

Hayashida, W., Kumada, T., Kohno, F., Noda, M., Ishikawa, N., Kojima, J., Himura, Y. & Kawai, C. (1991) Left ventricular regional relaxation and its nonuniformity in hypertrophic nonobstructive cardiomyopathy. *Circulation* 84, 1496–504.

Herrmann, J., Kaski, J.C. & Lerman, A. (2012) Coronary microvascular dysfunction in the clinical setting: from mystery to reality. *European heart journal* 33, 2771–2782.

Ho, C.Y. (2011) New Paradigms in Hypertrophic Cardiomyopathy: Insights from Genetics. *Progress in pediatric cardiology* 31, 93–98.

Hsu, L.-Y., Groves, D.W., Aletras, A.H., Kellman, P. & Arai, A.E. (2012) A quantitative pixel-wise measurement of myocardial blood flow by contrast-enhanced first-pass CMR perfusion imaging: microsphere validation in dogs and feasibility study in humans. *JACC. Cardiovascular imaging* 5, 154–66.

Hughes, A.D., Parker, K.H. & Davies, J.E. (2008) Waves in arteries: A review of wave intensity analysis in the systemic and coronary circulations. *Artery Research* 2, 51–59.

Hughes, S.E. (2004) The pathology of hypertrophic cardiomyopathy. *Histopathology* 44, 412–27.

Ismail, T.F., Hsu, L.-Y., Greve, A.M., Gonçalves, C., Jabbour, A., Gulati, A., Hewins, B., Mistry, N., Wage, R., Roughton, M., Ferreira, P.F., Gatehouse, P., Firmin, D., O'Hanlon, R., Pennell, D.J., Prasad, S.K. & Arai, A.E. (2014) Coronary microvascular ischemia in hypertrophic cardiomyopathy - a pixel-wise quantitative cardiovascular magnetic resonance perfusion study. *Journal of cardiovascular magnetic resonance : official journal of the Society for Cardiovascular Magnetic Resonance* 16, 49.

Iwanaga, S., Ewing, S.G., Husseini, W.K. & Hoffman, J.I. (1995) Changes in contractility and afterload have only slight effects on subendocardial systolic flow impediment. *The American journal of physiology* 269, H1202–12.

Jaber, W., Yang, E.H., Nishimura, R., Sorajja, P., Rihal, C.S., Elesber, A., Eeckhout, E. & Lerman, A. (2009) Immediate improvement in coronary flow reserve after alcohol septal ablation in patients with hypertrophic obstructive

cardiomyopathy. *Heart (British Cardiac Society)* 95, 564–9.

Jackson, G., Richardson, P.J., Atkinson, L., Armstrong, P. & Oram, S. (1978) Angina with normal coronary arteriograms. Value of coronary sinus lactate estimation in diagnosis and treatment. *British heart journal* 40, 976–8.

Jenni, R., Kaufmann, P.A., Jiang, Z., Attenhofer, C., Linka, A. & Mandinov, L. (2000) In vitro validation of volumetric blood flow measurement using Doppler flow wire. *Ultrasound in medicine & biology* 26, 1301–10.

Jerosch-Herold, M. (2004) Perfusion reserve in asymptomatic individuals. *The international journal of cardiovascular imaging* 20, 579–86.

Jörg-Ciopor, M., Namdar, M., Turina, J., Jenni, R., Schwitter, J., Turina, M., Hess, O.M. & Kaufmann, P. a (2004) Regional myocardial ischemia in hypertrophic cardiomyopathy: impact of myectomy. *The Journal of thoracic and cardiovascular surgery* 128, 163–9.

Kawarai, H., Kajimoto, K., Minami, Y., Hagiwara, N. & Kasanuki, H. (2011) Risk of sudden death in end-stage hypertrophic cardiomyopathy. *Journal of cardiac failure* 17, 459–64.

Keegan, J., Gatehouse, P.D., Yang, G.-Z. & Firmin, D.N. (2004) Spiral phase velocity mapping of left and right coronary artery blood flow: correction for through-plane motion using selective fat-only excitation. *Journal of magnetic resonance imaging : JMRI* 20, 953–60.

Kelly, R. & Fitchett, D. (1992) Noninvasive determination of aortic input impedance and external left ventricular power output: a validation and repeatability study of a new technique. *Journal of the American College of Cardiology* 20, 952–63.

Kenny, A., Wisbey, C.R. & Shapiro, L.M. (1994) Profiles of coronary blood flow velocity in patients with aortic stenosis and the effect of valve replacement: a transthoracic echocardiographic study. *British heart journal* 71, 57–62.

Khir, A.W. & Parker, K.H. (2002) Measurements of wave speed and reflected waves in elastic tubes and bifurcations. *Journal of biomechanics* 35, 775–83.

Knaapen, P., Germans, T., Camici, P.G., Rimoldi, O.E., Folkert, J., Berg, J.M., Dijkmans, P.A., Boellaard, R., Van, W.G., Götte, M.J.W., Twisk, J.W.R., Rossum, A.C. Van, Adriaan, A., Visser, F.C., Cate, F.J., Dockum, W.G. Van, Go, M.J.W., Lammertsma, A. & Visser, F.C. (2007) Determinants of coronary microvascular dysfunction in symptomatic hypertrophic cardiomyopathy. *Am J Physiol Heart Circ Physiol* 294, H986–H993.

Kofflard, M.J.M., Ten Cate, F.J., van der Lee, C. & van Domburg, R.T. (2003) Hypertrophic cardiomyopathy in a large community-based population: clinical outcome and identification of risk factors for sudden cardiac death and clinical deterioration. *Journal of the American College of Cardiology* 41, 987–93.

Kolyva, C., Spaan, J.A.E., Piek, J.J. & Siebes, M. (2008) Windkesselness of coronary arteries hampers assessment of human coronary wave speed by single-point technique. *American journal of physiology. Heart and circulatory physiology* 295, H482–90.

Krams, R., Ten Cate, F.J., Carlier, S.G., Van Der Steen, a F.W. & Serruys, P.W. (2004) Diastolic coronary vascular reserve: a new index to detect changes in the coronary microcirculation in hypertrophic cardiomyopathy. *Journal of the American College of Cardiology* 43, 670–7.

Krams, R., Kofflard, M.J.M., Duncker, D.J., Von Birgelen, C., Carlier, S., Kliffen, M., Cate, F.J.T. & Serruys, P.W. (1998)a) Decreased Coronary Flow Reserve in Hypertrophic Cardiomyopathy Is Related to Remodeling of the Coronary Microcirculation. *Circulation* 97, 230–233.

Krams, R., Kofflard, M.J.M., Duncker, D.J., Von Birgelen, C., Carlier, S., Kliffen, M., Cate, F.J.T. & Serruys, P.W. (1998)b) Decreased Coronary Flow Reserve in Hypertrophic Cardiomyopathy Is Related to Remodeling of the Coronary Microcirculation. *Circulation* 97, 230–233.

Krams, R., Sipkema, P. & Westerhof, N. (1989) Varying elastance concept may explain coronary systolic flow impediment. *The American journal of physiology* 257, H1471–9.

Kwong, R.Y. & Korlakunta, H. (2008) Diagnostic and prognostic value of cardiac magnetic resonance imaging in assessing myocardial viability. *Topics in magnetic resonance imaging : TMRI* 19, 15–24.

Kyriacou, A., Whinnett, Z.I., Sen, S., Pabari, P. a, Wright, I., Cornelussen, R., Lefroy, D., Davies, D.W., Peters, N.S., Kanagaratnam, P., Mayet, J., Hughes, A.D., Francis, D.P. & Davies, J.E. (2012) Improvement in coronary blood flow velocity with acute biventricular pacing is predominantly due to an increase in a diastolic backward-travelling decompression (suction) wave. *Circulation* 126, 1334–44.

Kyriakidis, M.K., Dernellis, J.M., Androulakis, A.E., Kelepeshis, G.A., Barbetseas, J., Anastasakis, A.N., Trikas, A.G., Tentolouris, C.A., Gialafos, J.E. & Toutouzas, P.K. (1997) Changes in phasic coronary blood flow velocity profile and relative coronary flow reserve in patients with hypertrophic obstructive cardiomyopathy. *Circulation* 96, 834–41.

Lakdawala, N.K., Thune, J.J., Maron, B.J., Cirino, A.L., Havndrup, O., Bundgaard, H., Christiansen, M., Carlsen, C.M., Dorval, J.-F., Kwong, R.Y., Colan, S.D., Køber, L. V & Ho, C.Y. (2011) Electrocardiographic features of sarcomere mutation carriers with and without clinically overt hypertrophic cardiomyopathy. *The American journal of cardiology* 108, 1606–13.

Laurent, S., Cockcroft, J., Van Bortel, L., Boutouyrie, P., Giannattasio, C., Hayoz, D., Pannier, B., Vlachopoulos, C., Wilkinson, I. & Struijker-Boudier, H. (2006) Expert consensus document on arterial stiffness: methodological issues and clinical applications. *European heart journal* 27, 2588–605.

Li, Y. & Guo, L. (2013) Clinical value of carotid wave intensity analysis for differentiating nonobstructive hypertrophic cardiomyopathy from left ventricular hypertrophy secondary to systemic hypertension. *Journal of clinical ultrasound : JCU* 41, 151–7.

Lin, G., Nishimura, R.A., Gersh, B.J., Phil, D., Ommen, S.R., Ackerman, M.J. & Brady, P.A. (2009) Device complications and inappropriate implantable cardioverter defibrillator shocks in patients with hypertrophic cardiomyopathy. *Heart (British Cardiac Society)* 95, 709–14.

Lorenzoni, R., Gistri, R., Cecchi, F., Olivotto, I., Chiriatti, G., Elliott, P., McKenna, W.J. & Camici, P.G. (1998) Coronary vasodilator reserve is impaired in patients with hypertrophic cardiomyopathy and left ventricular dysfunction. *American heart journal* 136, 972–81.

Mackey, R.H., Sutton-Tyrrell, K., Vaitkevicius, P. V, Sakkinen, P.A., Lyles, M.F., Spurgeon, H.A., Lakatta, E.G. & Kuller, L.H. (2002) Correlates of aortic stiffness in elderly individuals: a subgroup of the Cardiovascular Health Study. *American journal of hypertension* 15, 16–23.

Mahrholdt, H., Wagner, A., Judd, R.M., Sechtem, U. & Kim, R.J. (2005) Delayed enhancement cardiovascular magnetic resonance assessment of non-ischaemic cardiomyopathies. *European heart journal* 26, 1461–74.

Maki, S., Ikeda, H., Muro, A., Yoshida, N., Shibata, A., Koga, Y. & Imaizumi, T. (1998) Predictors of sudden cardiac death in hypertrophic cardiomyopathy. *The American journal of cardiology* 82, 774–8.

Maron, B.J. (2002) Hypertrophic cardiomyopathy: a systematic review. *JAMA* 287, 1308–20.

Maron, B.J. (2009) Distinguishing hypertrophic cardiomyopathy from athlete's heart physiological remodelling: clinical significance, diagnostic strategies and implications for preparticipation screening. *British journal of sports medicine* 43, 649–56.

Maron, B.J. (2010) Contemporary insights and strategies for risk stratification and prevention of sudden death in hypertrophic cardiomyopathy. *Circulation* 121, 445–56.

Maron, B.J., Gardin, J.M., Flack, J.M., Gidding, S.S., Kurosaki, T.T. & Bild, D.E. (1995) Prevalence of hypertrophic cardiomyopathy in a general population of young adults. Echocardiographic analysis of 4111 subjects in the CARDIA Study. Coronary Artery Risk Development in (Young) Adults. *Circulation* 92, 785–9.

Maron, B.J., Nishimura, R. a., McKenna, W.J., Rakowski, H., Josephson, M.E. & Kieval, R.S. (1999) Assessment of Permanent Dual-Chamber Pacing as a Treatment for Drug-Refractory Symptomatic Patients With Obstructive Hypertrophic Cardiomyopathy : A Randomized, Double-Blind, Crossover Study (M-PATHY). *Circulation* 99, 2927–2933.

Maron, B.J., Sato, N., Roberts, W.C., Edwards, J.E. & Chandra, R.S. (1979) Quantitative analysis of cardiac muscle cell disorganization in the ventricular septum. Comparison of fetuses and infants with and without congenital heart disease and patients with hypertrophic cardiomyopathy. *Circulation* 60, 685–96.

Maron, B.J., Shirani, J., Poliac, L.C., Mathenge, R., Roberts, W.C. & Mueller, F.O. (1996) Sudden death in young competitive athletes. Clinical, demographic, and pathological profiles. *JAMA* 276, 199–204.

Maron, B.J., Wolfson, J.K., Epstein, S.E. & Roberts, W.C. (1986) Intramural ("small vessel") coronary artery disease in hypertrophic cardiomyopathy. *Journal of the American College of Cardiology* 8, 545–57.

Maron, M.S., Hauser, T.H., Dubrow, E., Horst, T.A., Kissinger, K. V, Udelson, J.E. & Manning, W.J. (2007) Right ventricular involvement in hypertrophic cardiomyopathy. *The American journal of cardiology* 100, 1293–8.

Maron, M.S., Olivotto, I., Betocchi, S., Casey, S. a, Lesser, J.R., Losi, M. a, Cecchi, F. & Maron, B.J. (2003) Effect of left ventricular outflow tract obstruction on clinical outcome in hypertrophic cardiomyopathy. *The New England journal of medicine* 348, 295–303.

Maron, M.S., Olivotto, I., Maron, B.J., Prasad, S.K., Cecchi, F., Udelson, J.E. & Camici, P.G. (2009) The case for myocardial ischemia in hypertrophic cardiomyopathy. *Journal of the American College of Cardiology* 54, 866–75.

McGinn, A.L., White, C.W. & Wilson, R.F. (1990) Interstudy variability of coronary flow reserve. Influence of heart rate, arterial pressure, and ventricular preload. *Circulation* 81, 1319–30.

Mehta, P.K., Goykhman, P., Thomson, L.E.J., Shufelt, C., Wei, J., Yang, Y., Gill, E., Minissian, M., Shaw, L.J., Slomka, P.J., Slivka, M., Berman, D.S. & Bairey Merz, C.N. (2011) Ranolazine improves angina in women with evidence of myocardial ischemia but no obstructive coronary artery disease. *JACC. Cardiovascular imaging* 4, 514–22.

Meinders, J.M. & Hoeks, A.P.G. (2004) Simultaneous assessment of diameter and pressure waveforms in the carotid artery. *Ultrasound in medicine & biology* 30, 147–54.

Mitchell, A., West, N., Leeson, P. & Banning, A. (2008) *Cardiac Catheterisation and Coronary Intervention*. 1st ed. Oxford University Press.

Mordini, F.E., Haddad, T., Hsu, L.-Y., Kellman, P., Lowrey, T.B., Aletras, A.H., Bandettini, W.P. & Arai, A.E. (2014) Diagnostic accuracy of stress perfusion CMR in comparison with quantitative coronary angiography: fully quantitative, semiquantitative, and qualitative assessment. *JACC. Cardiovascular imaging* 7, 14–22.

Mundhenke M, Schwartzkopff B, S.B. (1997) Structural analysis of arteriolar and myocardial remodelling in the subendocardial region of patients with hypertensive heart disease and hypertrophic cardiomyopathy. *Virchows Arch.* 431, 265–73.

Nagueh, S.F., Bachinski, L.L., Meyer, D., Hill, R., Zoghbi, W.A., Tam, J.W., Quiñones, M.A., Roberts, R. & Marian, A.J. (2001) Tissue Doppler imaging consistently detects myocardial abnormalities in patients with hypertrophic cardiomyopathy and provides a novel means for an early diagnosis before and independently of hypertrophy. *Circulation* 104, 128–30.

Niki, K., Sugawara, M., Chang, D., Harada, A., Okada, T., Sakai, R., Uchida, K., Tanaka, R. & Mumford, C.E. (2002) A new noninvasive measurement system for wave intensity: evaluation of carotid arterial wave intensity and reproducibility. *Heart and vessels* 17, 12–21.

Noureldin, R.A., Liu, S., Nacif, M.S., Judge, D.P., Halushka, M.K., Abraham, T.P., Ho, C. & Bluemke, D.A. (2012) The diagnosis of hypertrophic cardiomyopathy by cardiovascular magnetic resonance. *Journal of cardiovascular magnetic resonance : official journal of the Society for Cardiovascular Magnetic Resonance* 14, 17.

O'Gara, P.T., Bonow, R.O., Maron, B.J., Damske, B.A., Van Lingen, A., Bacharach, S.L., Larson, S.M. & Epstein, S.E. (1987) Myocardial perfusion abnormalities in patients with hypertrophic cardiomyopathy: assessment with thallium-201 emission computed tomography. *Circulation* 76, 1214–23.

O'Hanlon, R., Grasso, A., Roughton, M., Moon, J.C., Clark, S., Wage, R., Webb, J., Kulkarni, M., Dawson, D., Sulaibeekh, L., Chandrasekaran, B., Bucciarelli-Ducci, C., Pasquale, F., Cowie, M.R., McKenna, W.J., Sheppard, M.N., Elliott, P.M., Pennell, D.J. & Prasad, S.K. (2010) Prognostic significance of myocardial fibrosis in hypertrophic cardiomyopathy. *Journal of the American College of Cardiology* 56, 867–74.

O'Mahony, C., Jichi, F., Pavlou, M., Monserrat, L., Anastasakis, A., Rapezzi, C., Biagini, E., Gimeno, J.R., Limongelli, G., McKenna, W.J., Omar, R.Z. & Elliott, P.M. (2014) A novel clinical risk prediction model for sudden cardiac death in hypertrophic cardiomyopathy (HCM risk-SCD). *European heart journal* 35, 2010–20.

Olivotto, I., Cecchi, F., Casey, S.A., Dolara, A., Traverse, J.H. & Maron, B.J. (2001) Impact of atrial fibrillation on the clinical course of hypertrophic cardiomyopathy. *Circulation* 104, 2517–24.

Olivotto, I., Cecchi, F., Gistri, R., Lorenzoni, R., Chiriatti, G., Girolami, F., Torricelli, F. & Camici, P.G. (2006) Relevance of coronary microvascular flow impairment to long-term remodeling and systolic dysfunction in hypertrophic cardiomyopathy. *Journal of the American College of Cardiology* 47, 1043–8.

Olivotto, I., Maron, M.S., Autore, C., Lesser, J.R., Rega, L., Casolo, G., De Santis, M., Quarta, G., Nistri, S., Cecchi, F., Salton, C.J., Udelson, J.E., Manning, W.J. & Maron, B.J. (2008) Assessment and significance of left ventricular mass by cardiovascular magnetic resonance in hypertrophic cardiomyopathy. *Journal of the American College of Cardiology* 52, 559–66.

Ommen, S.R., Shah, P.M. & Tajik, a J. (2008) Left ventricular outflow tract obstruction in hypertrophic cardiomyopathy: past, present and future. *Heart (British Cardiac Society)* 94, 1276–81.

Panting, J.R., Gatehouse, P.D., Yang, G.-Z., Grothues, F., Firmin, D.N., Collins, P. & Pennell, D.J. (2002) Abnormal subendocardial perfusion in cardiac syndrome X detected by cardiovascular magnetic resonance imaging. *The New England journal of medicine* 346, 1948–53.

Park, C.M., Korolkova, O., Davies, J.E., Parker, K.H., Siggers, J.H., March, K., Tillin, T., Chaturvedi, N. & Hughes, A.D. (2014) Arterial pressure: agreement between a brachial cuff-based device and radial tonometry. *Journal of hypertension* 32, 865–72.

Parker, K.H. (2009) An introduction to wave intensity analysis. *Medical & biological engineering & computing* 47, 175–88.

Parker, K.H. & Jones, C.J. (1990) Forward and backward running waves in the arteries: analysis using the method of characteristics. *Journal of biomechanical engineering* 112, 322–6.

Pasternac, A., Noble, J., Streulens, Y., Elie, R., Henschke, C. & Bourassa, M.G. (1982) Pathophysiology of chest pain in patients with cardiomyopathies and normal coronary arteries. *Circulation* 65, 778–89.

Pedone, C., Biagini, E., Galema, T.W., Vletter, W.B. & ten Cate, F.J. (2006) Myocardial perfusion after percutaneous transluminal septal myocardial ablation as assessed by myocardial contrast echocardiography in patients with hypertrophic obstructive cardiomyopathy. *Journal of the American Society of Echocardiography : official publication of the American Society of Echocardiography* 19, 982–6.

Pennell, D.J. (2010) Cardiovascular magnetic resonance. *Circulation* 121, 692–705.

Penny, D.J., Mynard, J.P. & Smolich, J.J. (2008) Aortic wave intensity analysis of ventricular-vascular interaction during incremental dobutamine infusion in adult sheep. *American journal of physiology. Heart and circulatory physiology* 294, H481–9.

Petersen, S.E., Jerosch-Herold, M., Hudsmith, L.E., Robson, M.D., Francis, J.M., Doll, H. a, Selvanayagam, J.B., Neubauer, S. & Watkins, H. (2007)a) Evidence for microvascular dysfunction in hypertrophic cardiomyopathy: new insights from multiparametric magnetic resonance imaging. *Circulation* 115, 2418–25.

Petersen, S.E., Jerosch-Herold, M., Hudsmith, L.E., Robson, M.D., Francis, J.M., Doll, H. a, Selvanayagam, J.B., Neubauer, S. & Watkins, H. (2007)b) Evidence for microvascular dysfunction in hypertrophic cardiomyopathy: new insights from multiparametric magnetic resonance imaging. *Circulation* 115, 2418–25.

Pijls, N.H., Van Gelder, B., Van der Voort, P., Peels, K., Bracke, F.A., Bonnier, H.J. & el Gamal, M.I. (1995) Fractional flow reserve. A useful index to evaluate the influence of an epicardial coronary stenosis on myocardial blood flow. *Circulation* 92, 3183–93.

Plehn, G., Vormbrock, J., Meissner, A. & Trappe, H.-J. (2004) Effects of exercise on the duration of diastole and on interventricular phase differences in patients with hypertrophic cardiomyopathy: relationship to cardiac output reserve. *Journal of nuclear cardiology : official publication of the American Society of Nuclear Cardiology* 16, 233–43.

Pries, A.R., Schönfeld, D., Gaehtgens, P., Kiani, M.F. & Cokelet, G.R. (1997) Diameter variability and microvascular flow resistance. *The American journal of physiology* 272, H2716–25.

Quail, M.A., Steeden, J.A., Knight, D., Segers, P., Taylor, A.M. & Muthurangu, V. (2014) Development and validation of a novel method to derive central aortic systolic pressure from the MR aortic distension curve. *Journal of magnetic resonance imaging : JMRI* 40, 1064–70.

Rader, F., Sachdev, E., Arsanjani, R. & Siegel, R.J. (2014) Left Ventricular Hypertrophy in Valvular Aortic Stenosis Mechanisms and Clinical Implications. *The American journal of medicine*.

Rajappan, K., Rimoldi, O.E., Dutka, D.P., Ariff, B., Pennell, D.J., Sheridan, D.J. & Camici, P.G. (2002) Mechanisms of coronary microcirculatory dysfunction in patients with aortic stenosis and angiographically normal coronary arteries. *Circulation* 105, 470–6.

Rickers, C., Wilke, N.M., Jerosch-Herold, M., Casey, S.A., Panse, P., Panse, N., Weil, J., Zenovich, A.G. & Maron, B.J. (2005) Utility of cardiac magnetic resonance imaging in the diagnosis of hypertrophic cardiomyopathy. *Circulation* 112, 855–61.

Rigo, F. (2005) Coronary flow reserve in stress-echo lab. From pathophysiologic toy to diagnostic tool. *Cardiovascular ultrasound* 3, 8.

Robinson, K., Frenneaux, M.P., Stockins, B., Karatasakis, G., Poloniecki, J.D. & McKenna, W.J. (1990) Atrial fibrillation in hypertrophic cardiomyopathy: a longitudinal study. *Journal of the American College of Cardiology* 15, 1279–85.

Rolandi, M.C., Nolte, F., van de Hoef, T.P., Remmelink, M., Baan, J., Piek, J.J., Spaan, J. a E. & Siebes, M. (2012) Coronary wave intensity during the Valsalva manoeuvre in humans reflects altered intramural vessel compression responsible for extravascular resistance. *The Journal of physiology* 590, 4623–35.

Rolandi, M.C., De Silva, K., Lumley, M., Lockie, T.P.E., Clapp, B., Spaan, J.A.E., Perera, D. & Siebes, M. (2014) Wave speed in human coronary arteries is not influenced by microvascular vasodilation: implications for wave intensity analysis. *Basic research in cardiology* 109, 405.

Rosing, D.R., Kent, K.M., Maron, B.J. & Epstein, S.E. (1979) Verapamil therapy: a new approach to the pharmacologic treatment of hypertrophic cardiomyopathy. II. Effects on exercise capacity and symptomatic status. *Circulation* 60, 1208–13.

Saito, M., Okayama, H., Yoshii, T., Hiasa, G., Sumimoto, T., Inaba, S., Nishimura, K., Inoue, K., Ogimoto, A., Shigematsu, Y., Funada, J., Hamada, M. & Higaki, J. (2011) Myocardial fibrosis attenuates the effect of cibenzoline on left ventricular diastolic function in patients with hypertrophic cardiomyopathy. *Journal of cardiovascular pharmacology* 57, 207–12.

Sato, Y., Taniguchi, R., Nagai, K., Makiyama, T., Okada, H., Yamada, T., Matsumori, A. & Takatsu, Y. (2003) Measurements of cardiac troponin T in patients with hypertrophic cardiomyopathy. *Heart (British Cardiac Society)* 89, 659–60.

Savitsky A, G.M. (1964) Smoothing and differentiation of data by simplified least squares fit procedures. *Anal Chem* 36, 1627–1639.

Savitzky, A. & Golay, M. (1964) Smoothing and differentiation of data by simplified least squares procedures. *Analytical Chemistry* 36, 1627–1639.

Sen, S., Asrress, K.N., Nijjer, S., Petraco, R., Malik, I.S., Foale, R.A., Mikhail, G.W., Foin, N., Broyd, C., Hadjiloizou, N., Sethi, A., Al-Bustami, M., Hackett, D., Khan, M.A., Khawaja, M.Z., Baker, C.S., Bellamy, M., Parker, K.H., Hughes, A.D., Francis, D.P., Mayet, J., Di Mario, C., Escaned, J., Redwood, S. & Davies, J.E. (2013)a) Diagnostic classification of the instantaneous wave-free ratio is equivalent to fractional flow reserve and is not improved with adenosine administration. Results of CLARIFY (Classification Accuracy of Pressure-Only Ratios Against Indices Using Flow Study. *Journal of the American College of Cardiology* 61, 1409–20.

Sen, S., Petraco, R., Mayet, J. & Davies, J. (2013)b) Sen WIA in the human coronary circulation in health and disease. *Curr Cardiol Rev* May 3., [ePub ahead of print].

Sen, S., Petraco, R., Mayet, J. & Davies, J. (2013)c) Wave Intensity Analysis in the Human Coronary Circulation in Health and Disease. *Current cardiology reviews* [Epub ahea.

Shah, J.S., Esteban, M.T.T., Thaman, R., Sharma, R., Mist, B., Pantazis, A., Ward, D., Kohli, S.K., Page, S.P., Demetrescu, C., Sevdalis, E., Keren, A., Pellerin, D., McKenna, W.J. & Elliott, P.M. (2008) Prevalence of exercise-induced left ventricular outflow tract obstruction in symptomatic patients with non-obstructive hypertrophic cardiomyopathy. *Heart (British Cardiac Society)* 94, 1288–94.

Shirani, J., Maron, B.J., Cannon, R.O., Shahin, S. & Roberts, W.C. (1993) Clinicopathologic features of hypertrophic cardiomyopathy managed by cardiac transplantation. *The American journal of cardiology* 72, 434–40.

Shirani, J., Pick, R., Roberts, W.C. & Maron, B.J. (2000) Morphology and significance of the left ventricular collagen network in young patients with hypertrophic cardiomyopathy and sudden cardiac death. *Journal of the American College of Cardiology* 35, 36–44.

De Silva, K., Foster, P., Guilcher, A., Bandara, A., Jogiya, R., Lockie, T., Chowiencyzk, P., Nagel, E., Marber, M., Redwood, S., Plein, S. & Perera, D. (2013) Coronary wave energy: a novel predictor of functional recovery after myocardial infarction.

*Circulation. Cardiovascular interventions* 6, 166–75.

Simonetti, O.P., Kim, R.J., Fieno, D.S., Hillenbrand, H.B., Wu, E., Bundy, J.M., Finn, J.P. & Judd, R.M. (2001) An improved MR imaging technique for the visualization of myocardial infarction. *Radiology* 218, 215–23.

Sipkema, P., Westerhof, N. & Hoogerwerf, N. (1997) Rate of the myogenic response increases with the constriction level in rabbit femoral arteries. *Annals of biomedical engineering* 25, 278–85.

Skalidis, E.I., Parthenakis, F.I., Patrianakos, A.P., Hamilos, M.I. & Vardas, P.E. (2004) Regional coronary flow and contractile reserve in patients with idiopathic dilated cardiomyopathy. *Journal of the American College of Cardiology* 44, 2027–32.

Sorajja, P., Ommen, S.R., Nishimura, R.A., Gersh, B.J., Berger, P.B. & Tajik, A.J. (2003) Adverse prognosis of patients with hypertrophic cardiomyopathy who have epicardial coronary artery disease. *Circulation* 108, 2342–8.

Spaan, J.A. (1995) Mechanical determinants of myocardial perfusion. *Basic research in cardiology* 90, 89–102.

Spaan, J.A., Breuls, N.P. & Laird, J.D. (1981)a) Diastolic-systolic coronary flow differences are caused by intramyocardial pump action in the anesthetized dog. *Circulation research* 49, 584–93.

Spaan, J.A., Breuls, N.P. & Laird, J.D. (1981)b) Forward coronary flow normally seen in systole is the result of both forward and concealed back flow. *Basic research in cardiology* 76, 582–6.

Spiewak, M., Malek, L.A., Misko, J., Chojnowska, L., Milosz, B., Klopotowski, M., Petryka, J., Dabrowski, M., Kepka, C. & Ruzyllo, W. (2010) Comparison of different quantification methods of late gadolinium enhancement in patients with hypertrophic cardiomyopathy. *European journal of radiology* 74, e149–53.

Spindler, M., Saupe, K.W., Christe, M.E., Sweeney, H.L., Seidman, C.E., Seidman, J.G. & Ingwall, J.S. (1998) Diastolic dysfunction and altered energetics in the alphaMHC403/+ mouse model of familial hypertrophic cardiomyopathy. *The Journal of clinical investigation* 101, 1775–83.

Spirito, P., Bellone, P., Harris, K.M., Bernabo, P., Bruzzi, P. & Maron, B.J. (2000) Magnitude of left ventricular hypertrophy and risk of sudden death in hypertrophic cardiomyopathy. *The New England journal of medicine* 342, 1778–1785.

Spirito, P. & Maron, B.J. (1990) Relation between extent of left ventricular hypertrophy and diastolic filling abnormalities in hypertrophic cardiomyopathy. *Journal of the American College of Cardiology* 15, 808–13.

Spirito, P., Seidman, C.E., McKenna, W.J. & Maron, B.J. (1997) The management of hypertrophic cardiomyopathy. *The New England journal of medicine* 336, 775–85.

Spoladore, R., Maron, M.S., D'Amato, R., Camici, P.G. & Olivotto, I. (2012) Pharmacological treatment options for hypertrophic cardiomyopathy: high time for evidence. *European heart journal* 33, 1724–33.

Sugihara, H., Taniguchi, Y., Ito, K., Terada, K., Matsumoto, K., Kinoshita, N., Azuma, A., Ushijima, Y., Maeda, T. & Nakagawa, M. (1998) Effects of diltiazem on myocardial perfusion abnormalities during exercise in patients with hypertrophic cardiomyopathy. *Annals of nuclear medicine* 12, 349–54.

Tanaka, M., Fujiwara, H., Onodera, T., Wu, D.J., Matsuda, M., Hamashima, Y. & Kawai, C. (1987) Quantitative analysis of narrowings of intramyocardial small arteries in normal hearts, hypertensive hearts, and hearts with hypertrophic cardiomyopathy. *Circulation* 75, 1130–1139.

Teare, D. (1958) Asymmetrical hypertrophy of the heart in young adults. *British heart journal* 20, 1–8.

Timmer, S.J., Knaapen, P., Germans, T., Dijkmans, P., Lubberink, M., Ten Berg, J.M., Ten Cate, F.J., Rüssel, I.K., Götte, M.J.W., Lammertsma, A. & van Rossum, A.C. (2011) Effects of alcohol septal ablation on coronary microvascular function and myocardial energetics in hypertrophic obstructive cardiomyopathy. *American journal of physiology. Heart and circulatory physiology* 301, H129–37.

Tonino, P.A.L., De Bruyne, B., Pijls, N.H.J., Siebert, U., Ikeno, F., van' t Veer, M., Klauss, V., Manoharan, G., Engstrøm, T., Oldroyd, K.G., Ver Lee, P.N., MacCarthy, P.A. & Fearon, W.F. (2009) Fractional flow reserve versus angiography for guiding percutaneous coronary intervention. *The New England journal of medicine* 360, 213–24.

Toyota, E., Ogasawara, Y., Hiramatsu, O., Tachibana, H., Kajiya, F., Yamamori, S. & Chilian, W.M. (2005) Dynamics of flow velocities in endocardial and epicardial coronary arterioles. *American journal of physiology. Heart and circulatory physiology* 288, H1598–603.

Tsybouleva, N., Zhang, L., Chen, S., Patel, R., Lutucuta, S., Nemoto, S., DeFreitas, G., Entman, M., Carabello, B.A., Roberts, R. & Marian, A.J. (2004) Aldosterone, through novel signaling proteins, is a fundamental molecular bridge between the genetic defect and the cardiac phenotype of hypertrophic cardiomyopathy. *Circulation* 109, 1284–91.

Udelson, J.E., Bonow, R.O., O'Gara, P.T., Maron, B.J., Van Lingen, A., Bacharach, S.L. & Epstein, S.E. (1989) Verapamil prevents silent myocardial perfusion abnormalities during exercise in asymptomatic patients with hypertrophic cardiomyopathy. *Circulation* 79, 1052–60.

Vaglio, J.C., Ommen, S.R., Nishimura, R., Tajik, J. & Gersh, B.J. (2008) Clinical characteristics and outcomes of patients with hypertrophic cardiomyopathy with latent obstruction. *American heart journal* 156, 342–7.

Varnava, a M., Elliott, P.M., Sharma, S., McKenna, W.J. & Davies, M.J. (2000) Hypertrophic cardiomyopathy: the interrelation of disarray, fibrosis, and small vessel disease. *Heart (British Cardiac Society)* 84, 476–82.

Varnava, A.M., Elliott, P.M., Mahon, N., Davies, M.J. & McKenna, W.J. (2001) Relation between myocyte disarray and outcome

in hypertrophic cardiomyopathy. *The American journal of cardiology* 88, 275–9.

Vlachopoulos, C., Aznaouridis, K. & Stefanadis, C. (2010) Prediction of cardiovascular events and all-cause mortality with arterial stiffness: a systematic review and meta-analysis. *Journal of the American College of Cardiology* 55, 1318–27.

Voci, P., Pizzuto, F. & Romeo, F. (2004) Coronary flow: a new asset for the echo lab? *European heart journal* 25, 1867–79.

Voges, I., Jerosch-Herold, M., Hedderich, J., Pardun, E., Hart, C., Gabbert, D.D., Hansen, J.H., Petko, C., Kramer, H.-H. & Rickers, C. (2012) Normal values of aortic dimensions, distensibility, and pulse wave velocity in children and young adults: a cross-sectional study. *Journal of cardiovascular magnetic resonance : official journal of the Society for Cardiovascular Magnetic Resonance* 14, 77.

Westerhof, N., Boer, C., Lamberts, R.R. & Sipkema, P. (2006) Cross-Talk Between Cardiac Muscle and Coronary Vasculature. *Physiol Review* 86, 1263–1308.

Woo, A., Williams, W.G., Choi, R., Wigle, E.D., Rozenblyum, E., Fedwick, K., Siu, S., Ralph-Edwards, A. & Rakowski, H. (2005) Clinical and echocardiographic determinants of long-term survival after surgical myectomy in obstructive hypertrophic cardiomyopathy. *Circulation* 111, 2033–41.

Yamada, M., Elliott, P.M., Kaski, J.C., Prasad, K., Gane, J.N., Lowe, C.M., Doi, Y. & McKenna, W.J. (1998) Dipyridamole stress thallium-201 perfusion abnormalities in patients with hypertrophic cardiomyopathy. Relationship to clinical presentation and outcome. *European heart journal* 19, 500–7.

Yang, E.H., Yeo, T.C., Higano, S.T., Nishimura, R. & Lerman, A. (2004) Coronary hemodynamics in patients with symptomatic hypertrophic cardiomyopathy. *The American journal of cardiology* 94, 685–7.

Zambanini, A., Cunningham, S.L., Parker, K.H., Khir, A.W., McG Thom, S.A. & Hughes, A.D. (2005) Wave-energy patterns in carotid, brachial, and radial arteries: a noninvasive approach using wave-intensity analysis. *American journal of physiology. Heart and circulatory physiology* 289, H270–6.

Zhang, Y., Liu, M., Wang, M., Zhang, L., Lv, Q., Xie, M., Xiang, F., Fu, Q., Yin, Y., Lu, C., Yan, T. & Huang, Y. (2010) Wave intensity analysis of carotid artery: a noninvasive technique for assessing hemodynamic changes of hyperthyroid patients. *Journal of Huazhong University of Science and Technology. Medical sciences = Hua zhong ke ji da xue xue bao. Yi xue Ying De wen ban = Huazhong keji daxue xuebao. Yixue Yingdewen ban* 30, 672–7.

Zipes, D.P., Camm, A.J., Borggrefe, M., Buxton, A.E., Chaitman, B., Fromer, M., Gregoratos, G., Klein, G., Moss, A.J., Myerburg, R.J., Priori, S.G., Quinones, M.A., Roden, D.M., Silka, M.J., Tracy, C., Smith, S.C., Jacobs, A.K., Adams, C.D., Antman, E.M., Anderson, J.L., Hunt, S.A., Halperin, J.L., Nishimura, R., Ornato, J.P., Page, R.L., Riegel, B., Blanc, J.-J., Budaj, A., Dean, V., Deckers, J.W., Despres, C., Dickstein, K., Lekakis, J., McGregor, K., Metra, M., Morais, J., Osterspey, A., Tamargo, J.L. & Zamorano, J.L. (2006) ACC/AHA/ESC 2006 Guidelines for Management of Patients With Ventricular Arrhythmias and the Prevention of Sudden Cardiac Death: a report of the American College of Cardiology/American Heart Association Task Force and the European Society of Cardiology Com. *Circulation* 114, e385–484.

Zografos, T., Kokladi, M. & Katritsis, D. (2010) Coronary artery ectasia and systolic flow cessation in a patient with hypertrophic cardiomyopathy: a case report. *International journal of cardiology* 145, e114–5.